

UNIVERSITÀ
DEGLI STUDI
DI PADOVA

University of Padova

Department of Chemical Sciences

DOCTORAL SCHOOL IN MOLECULAR SCIENCES

PHARMACEUTICAL SCIENCES CURRICULUM

XXX CYCLE

Development of new antibody-drug conjugates based on Fc binding moieties for therapeutic and diagnostic applications

Coordinator: Prof. LEONARD JAN PRINS

Supervisor: Prof. GIANFRANCO PASUT

PhD Student: KATIA MASO

TABLE OF CONTENTS

1	List of abbreviations	1
2	Abstract	3
3	Introduction.....	6
3.1	Targeted therapies	6
3.2	Brief history of Antibody-Drug Conjugates (ADCs).....	7
3.3	Design of an ADC	8
3.4	Monoclonal Antibodies (mAbs).....	9
3.5	Target antigens and antibody selection	12
3.6	Payload of ADCs.....	14
3.7	Linkers	15
3.8	Conjugation strategies.....	17
3.9	Pharmacokinetic and ADME considerations for ADCs	20
3.10	Clinical experience.....	22
3.10.1	Mylotarg	22
3.10.2	Adcetris.....	23
3.10.3	Kadcyla.....	24
3.11	Moving from ADCs to Antibody Drug Systems (ADSs)	25
3.12	Protein G.....	26
3.13	Secondary Antibodies.....	29
3.14	Fab	29
3.15	Polyethylene glycol (PEG).....	31
3.16	Tubulysin A	35
3.17	Drug conjugation via reversible disulphide linkages	36
3.18	Trastuzumab.....	37
3.19	Rituximab.....	39
3.20	Endothelium targeting	41
4	Materials and methods	44
4.1	Materials and instruments	44
4.2	Synthesis of PDP-PEG _{20kDa} -aldehyde.....	46
4.2.1	Synthesis of PDP-PEG _{20kDa} -COOH.....	46
4.2.2	Snyder-Sobocinsky TNBS essay for amino groups quantification	47

4.2.3	Pyridine-2-thione assay for the determination of PDP activation	48
4.2.4	Aldehyde functionalization of PDP-PEG-COOH.....	49
4.3	Synthesis of PEG _{20kDa} -Nter-Protein G and PDP-PEG _{20kDa} -Nter-Protein G.....	51
4.4	Synthesis of Cy5- and AlexaFluor488-PEG _{20kDa} -Nter-Protein G.....	51
4.5	Synthesis of Tubulysin A-PEG _{20kDa} -Nter-Protein G	52
4.6	Synthesis of AlexaFluor647-PEG _{5kDa} -maleimide	53
4.7	Synthesis of goat anti-human-Fc NEM-Fab, (PEG _{5kDa}) _n -Fab and (AlexaFluor647-PEG _{5kDa}) _n -Fab	53
4.8	PEGylation of Rituximab Fab' fragments	54
4.9	Cy5 and AlexaFluor647 conjugation to monoclonal antibodies	54
4.10	NMR analysis.....	55
4.11	Determination of protein concentration	55
4.11.1	UV-Vis spectroscopy.....	55
4.11.2	Bicinchoninic acid (BCA) assay	55
4.12	Sodium dodecyl sulphate polyacrylamide gel electrophoresis (SDS-PAGE)	56
4.13	Mass spectrometry	57
4.14	Circular dichroism analysis.....	57
4.15	Dynamic Light Scattering (DLS) measurements	58
4.16	Isothermal Titration Calorimetry (ITC)	59
4.17	Flow citometry	60
4.18	Tubulysin A-PEG-Protein G/ Trastuzumab cytotoxicity	61
4.19	Biodistribution studies	62
4.20	Cellular experiments using HUVECs.....	62
4.20.1	Binding experiment.....	63
4.20.2	Avidity experiment.....	63
4.20.3	Kinetic of binding experiment.....	63
4.20.4	Internalization mechanism of Alexa488-PEG-Protein G/aICAM	63
4.20.5	Internalization and lysosomal trafficking of Alexa488-PEG-Protein G/aICAM ...	64
4.20.6	Statistics	65
5	Results.....	66
5.1	Characterization of PDP-PEG-diethylacetal 20 kDa	66
5.2	Protein G characterization	68
5.3	Characterization of PEG _{20kDa} -Nter-Protein G and PDP-PEG _{20kDa} -Nter-Protein G	69
5.4	Characterization of Cy5- and Alexa488-PEG _{20kDa} -Protein G	71

5.5	Characterization of Tubulysin A-PEG _{20kDa} -Nter- Protein G	73
5.6	Characterization of Alexa647-PEG _{5kDa} -maleimide	75
5.7	Characterization of goat anti-human-Fc NEM-Fab, (PEG _{5kDa}) _n -Fab and (Alexa647-PEG _{5kDa}) _n -Fab	76
5.8	Fab PEGylation pattern of Rituximab Fab	81
5.9	Dye conjugation to monoclonal antibodies	83
5.10	Circular dichroism.....	84
5.11	Dynamic light scattering.....	87
5.12	Isothermal titration calorimetry.....	88
5.13	Analysis of interaction of ADS with target cancer cell lines	90
5.14	Evaluation of <i>in vitro</i> tumor growth inhibition activity of ADS	100
5.15	Evaluation of ADS biodistribution in an animal model	102
5.16	Binding of Alexa488-PEG-Protein G/aICAM ADS to HUVECs	103
5.17	Internalization mechanism of Alexa488-PEG-Protein G/aICAM	107
5.18	Kinetic of internalization and lysosomal trafficking	108
6	Discussion.....	110
7	References.....	118

1 LIST OF ABBREVIATIONS

Ab	antibody
ADC	antibody-drug conjugate
ADCC	antibody-dependent cellular cytotoxicity
ADCP	antibody-dependent cellular phagocytosis
aICAM	anti ICAM-1 antibody
ALCL	anaplastic large-cell lymphoma
AML	acute myeloid leukemia
ADS	antibody-drug system
ASCT	autologous stem-cell transplantation
ALCL	anaplastic large cell lymphoma
BCA	bicinchoninic acid assay
β -MA	β -mercaptoethylamine
β -ME	β -mercaptoethanol
BSA	bovine serum albumin
CDC	complement-dependent cytotoxicity
CDR	complementary determining region
CHO	chinese hamster ovary cells
DAR	antibody-drug ratio
DCC	N,N'-dicyclohexylcarbodiimide
DLS	dynamic light scattering
DM1	emtansine
DTT	dithiothreitol
Fab	antigen binding fragment
F(ab') ₂	two Fab linked by disulphide bonds
FACS	Fluorescence-activated cell sorting
Fc	fragment crystallisable
FcBM	Fc binding moiety
FcR	Fc receptor
FcRn	neonatal Fc receptor
FDA	Food and drug administration
FUV-CD	far UV circular dichroism
Gly-gly	glycyl-glycine
HACAs	human anti-chimeric antibodies
HAMAs	human anti-mouse antibodies
HER2	human epidermal growth factor receptor 2
HSA	human serum albumin
HOBt	hydroxybenzotriazole
HUVECs	human umbilical vein endothelial cells
ICAM-1	Intercellular adhesion molecule-1
Ig	immunoglobulin
ITC	isothermal titration calorimetry
mAb	monoclonal antibody
NEM	N-ethylmaleimide
NHL	non-Hodgkin's lymphoma
NHS	N-hydroxysuccinimide

List of abbreviations

NK	natural killer
PDP	3-(2-pyridyldithio)-propionate
PFA	paraformaldehyde
SDS	sodium dodecyl sulfate
SMCC	succinimidyl-4-[N-maleimidomethyl]-cyclohexane-1-carboxylate
SPDP	succinimidyl 3-(2-pyridyldithio)propionate
TCEP	tris-(2-carboxyethyl) phosphine
T-DM1	Ado-trastuzumab emtansine
TGase	transglutaminase
TNBS	2,4,6-trinitrobenzenesulfonic acid
TNF	tumour necrosis factor
TubA	Tubulysin A

2 ABSTRACT

Monoclonal antibodies (mAbs) are extensively used in several therapeutic fields and in particular are used against cancer as therapeutic entity and/or targeting agents. The last application belongs to the several strategies to promote selective drug delivery in order to spare healthy tissues from unspecific toxicities of invasive therapies, as anticancer treatments, and to improve final clinical outcomes. Among all, targeted therapy includes antibody-drug conjugates (ADCs) approach, which exploit the synergic action of potent cytotoxic agents conjugated to a monoclonal antibody (mAb) coupled by specific linkers. The antibody acts as drug-carrier and targeting agent, and eventually also as a drug *per se*, in order to selectively kill cancer cells. As single therapeutic agents, both mAbs and highly cytotoxic drugs present critical issues in their clinical use. mAbs usually have to be used in combination therapy with other drugs because the majority of them show an insufficient, although specific, clinical response. On the other hand, chemotherapeutic drugs, especially the very potent ones, have a narrow therapeutic window and, therefore, their therapeutic doses are close to the maximum tolerated dose. Consequently, they present heavy side effects owing to the lack of tumour cells selectivity. The bright idea to combine mAbs and cytotoxic drugs in a unique entity offers the possibility to overcome their limitations. Traditionally, drugs have been coupled in a random way to lysine or cysteine residues, and the final product heterogeneity unfortunately has relevant impact on ADC activity, characterization and manufacturing, thus affecting the efficacy of the therapy. In an era in which product homogeneity and batch-to-batch reproducibility are essential pre-requisites for pharmaceuticals, the development of new technologies for site-directed coupling have become a primary focus. New methodologies for site-specific conjugation are now widely investigated, and some example are the introduction of cysteine residues using site-directed mutagenesis, the use of enzymes, the insertion of unnatural amino acids and the conjugation to Fc N-Glycans. Nevertheless, such approaches require a specific development of each new ADC, thus offering few opportunities of know-how

List of abbreviations

sharing between different projects, in fact these are often limited to the linker stability and the drug activity.

In this work, a new construct for the delivery of active drugs has been proposed based on mAbs non-covalently interacting with a Fc-binding moiety (FcBM) that carries also the drugs. The aim is to achieve a higher degree of homogeneity and create a versatile and adaptable drug delivery system. Drug is not linked directly to the FcBM but through a linker constituted of a linear PEG chain. The drug-PEG-FcBM/antibody systems, from here called Antibody-Drug Systems (ADSs), present some advantages with respect to ADCs: they can be a versatile platform with which different mAbs can be used by simple mixing on demand with a drug-Fc binding module on the basis of the target tumour/disease to be treated. FcBM is the core of the system and must present unique binding properties for the Fc of antibodies. In this work, Protein G (22.8 kDa), a bacterial Fc binding receptor, and a goat Fab' (≈ 50 kDa) against human Fc were tested as FcBM candidate, while a PEG chain was selected as linker for drug/dye attachment. Protein G was selectively PEGylated at the N-terminus with a PEG 20kDa, while Fab' was mono-, bi- and tri-PEGylated with a PEG 5 kDa after the reduction of the sulfhydryl bridges at the hinge region of the progenitor F(ab')₂. Circular dichroism studies showed that the conjugates preserved protein secondary structure and isothermal titration calorimetry experiments determined that their affinity for Fc is about 10^7 - 10^8 M⁻¹. After the complexation with a model mAb (Trastuzumab or Rituximab), NIR labelled ADSs were tested in vitro by cytometry analysis showing a high selectivity for antigen expressing cells. Furthermore, when a FcBM is conjugated to labelling molecule instead of a drug it would allow the switch from therapeutic application to diagnosis purposes.

Tubulysin A (TubA), a potent inhibitor of tubulin polymerisation, was selected as drug model and tethered to the free end of PEG through a disulphide bond. TubA-PEG-Protein G/Trastuzumab ADS showed a preferential cytotoxic activity against the HER2+ cell line (SKBR-3), thus supporting the approach for both diagnostic and therapeutic purposes in cancer. A preliminary biodistribution study was performed in immunodeficient NSG mice, inoculated via subcutaneous injection with IGROV-1 (HER2-) and SKOV-3 (HER2+) tumour cells. Total body scanning showed a very rapid accumulation of Cy5-PEG-Protein G/Trastuzumab within 8 hours from ADS injection.

Finally, uptake and intracellular trafficking of an ADS composed by a mouse IgG2a against ICAM-1 and Protein G as FcBM were evaluated in human umbilical vein endothelial cells (HUVECs). HUVECs were stimulated with TNF α to promote the expression of ICAM-1 receptor toward which the ADS was targeted. Fluorescence microscopy was used to follow ADS internalization by endothelial cells. The results disclosed that mechanism of uptake was based

on CAM-mediate endocytosis, which relies in the binding between the receptor and anti ICAM-1 antibody. After internalization, the ADS followed the classical pathway toward the lysosomes to be degraded. This proves the possibility to achieve a selective intracellular delivery of active agents through ADS approach and open the way of new applications of this technology.

3 INTRODUCTION

3.1 Targeted therapies

The term “targeted therapy” refers to all those approaches which seek to specifically interfere with molecular targets and pathways that are important for the proliferation of diseased cells¹. Although this concept may be generically adapted to different pathologic states, its major application remains cancer treatment. Cancer is a major public health problem worldwide and is the second leading cause of death in the United States with 1,688,780 new cases in 2017². In this context, anticancer targeted therapy can be defined as a therapeutic with a focused mechanism that specifically acts on a well-defined target or biologic pathway that, when inactivated, causes regression or destruction of the tumour³.

The ideal targets are preferentially expressed on the surface or in the cytoplasm of cancer cells, with any or minimal expression in vital organs and tissues. In this way, therapeutic agents can be selectively cytotoxic to tumour (or in general to other type of diseased tissues), while systemic toxicity is reduced, and a wider therapeutic window is obtained. In many cases, these markers are cell surface proteins, glycoproteins or carbohydrates selectively expressed, over-expressed or presented in a mutated form.

The progresses made in tumour biology at cellular and subcellular levels have permitted the identification of pathways that are unique for cancer cells, and the development of innovative anticancer therapies that present advantages respect to conventional cancer treatment. Traditional chemotherapy is based on the observation that malignant cells grow more rapidly than normal cells. For example ionizing radiation induces DNA damage that results in cell death due to errors in transcription and translation upon cell division, while cytotoxic chemotherapy may interfere with microtubule formation that is essential during mitosis. Despite the benefits derived from conventional anticancer drugs, the quality of life of patients may be substantially reduced by treatment-related toxicity. In fact, these drugs also target rapidly dividing cells in certain normal tissues, such as hair, gastrointestinal epithelium, bone marrow, and, as a result, many patients experience the classic toxicities of alopecia,

gastrointestinal symptoms, and myelosuppression. These side effects, along with reducing the quality of life, also limit dose intensification and ultimately therapeutic antitumor activity.

In order to overcome these issues, many researchers are now focusing on the development of new targeted therapy strategies. The major areas of targeted therapy in cancer treatment include small targeting-molecule drug conjugates (for example folate–vinca alkaloid conjugates), inhibitors of tyrosine kinases receptors, antisense and siRNA technologies, monoclonal antibodies and antibody–drug conjugates (ADCs). In particular, ADCs have been aroused a great interest for their ability to combine the potent cytotoxic action of small anticancer drugs to the targeting activity of monoclonal antibodies in a unique therapeutic entity.

3.2 Brief history of Antibody-Drug Conjugates (ADCs)

The first seed of the concept of “targeted medicine” was planted in 1913 by Paul Ehrlich, a German physician and scientist who coined the term “magic bullet” to indicate a selective delivery of cytotoxic drugs to target cells⁴. Forty five years later, the fruits of this idea were collected into the form of an Antibody-Drug Conjugate (ADC) in which methotrexate was attached to a leukaemia cell-targeting antibody⁵. This system combined the cytotoxic properties of the antitumoral drug methotrexate to the targeting activity of a monoclonal antibody with the aim to selectively hit disease cells without any damage of healthy tissues. The antibody acted as a vehicle to bring drugs to specific tissues improving activity and selectivity of cytotoxic agents while systemic toxicity decreases. As a result, the therapeutic index of the payload increases⁶ and, for this reason, many of the cytotoxic drugs that are too toxic for use in traditional chemotherapy can be utilized in the construction of ADCs⁷. Overall, this antibody-based platform could improve efficacy, reduce systemic toxicity and ensure a preferable pharmacokinetics and biodistribution compared to traditional chemotherapy⁵.

The first clinical trial with an ADC having a human antibody was conducted in 1983 by Ford and colleagues: they used an anti-carcinoembryonic antigen antibody conjugated to vindesine (a vinca alkaloid) in patients with advanced metastatic carcinoma (colorectal or ovarian) and promising results were obtained achieving conjugate localization at tumour site⁸. From that moment, ADCs have aroused an increasing interest and many efforts have been made for their development, leading to FDA approval of three ADCs: gentuzumab ozogamicin (Mylotarg, Pfizer/Wyeth-Ayerst Laboratories, 2000)^{9, 10}, brentuximab vedotin (Adcetris, Seattle Genetics, 2011)¹¹ and ado-trastuzumab emtansine (Kadcyla, Genentech, 2013)¹². Despite the initial promising clinical outcomes of Mylotarg, Pfizer withdrawn the drug from the market in 2010

Introduction

because, in post-marketing follow-up clinical trials, it failed to meet the efficacy targets required as a condition of its accelerated approval by the FDA. However, the run of ADCs to gain their share of the market has never stopped and, boosted by the successes of Adcetris and Kadcyła, about 60 ADCs entered clinical trials last year⁵. On September 1st 2017, FDA approved again Mylotarg with a lower recommended dose, a different schedule in combination with chemotherapy or on its own, and a new patient population.

The main clinical application of ADCs still remains chemotherapy, although new approaches have been recently investigated.

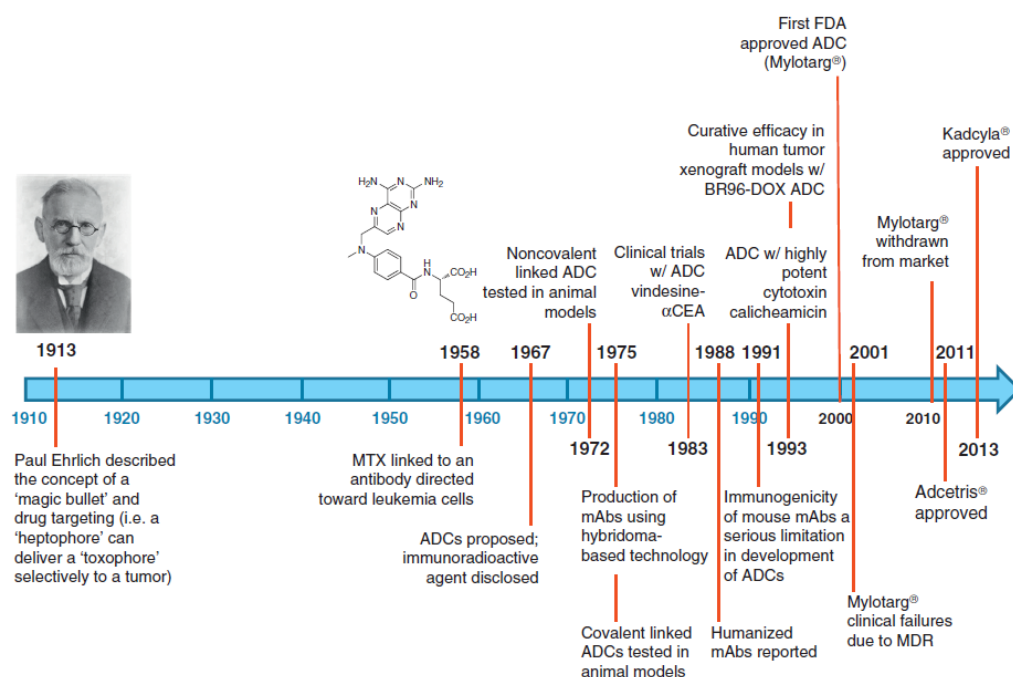


Figure 1. ADCs timeline⁴.

3.3 Design of an ADC

The structure of an ADC is simple to be described: it is formed by a monoclonal antibody, highly cytotoxic small molecules (payloads) and the chemical linker connecting them. Although the minimal structural concept, developing an ADC into a therapeutically effective format still remains an art since it is a delicate balance of multiple factors and an optimization of each building block. Only recently, important results in this field have been achieved thanks to significant advances in conjugation techniques and linker strategies¹³. In fact, initial attempts using approved drugs, such as doxorubicin and methotrexate, suffered from a series of shortcomings. The following paragraphs provide an insight into ADCs components and the parameters that must be carefully considered during the construction of an ADC.

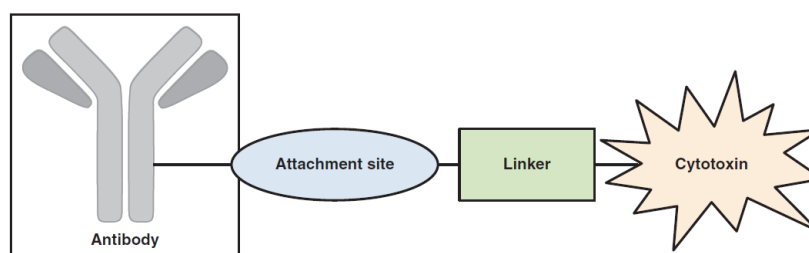


Figure 2. Schematic structure of an ADC⁴.

3.4 Monoclonal Antibodies (mAbs)

Antibodies (Abs) or immunoglobulins (Igs) are glycoproteins (82–96% protein and 4–18% carbohydrate) produced by B lymphocytes in form of soluble proteins circulating in the bloodstream, where they account for about 10–20% of plasma proteins, or in form of membrane-attached receptors¹⁴. They are roughly Y-shaped molecules (or a combination of such molecules) and their structure can be divided into two regions: the variable region (the “arms” of the Y) and the constant region (the “stem” of the Y)¹⁵. The variable (V) part of antibodies consists of two antigen binding regions called Fab and covers approximately the first 110 amino acids, whereas the constant (C) portion is called Fc (fragment crystallisable). Based on C region, immunoglobulins are divided into five different classes, IgA, IgD, IgE, IgG and IgM. IgAs and IgMs are present in multimeric form: IgAs can be dimers and IgM are pentamers or hexamers.

Table 1. Characteristics of the human immunoglobulin isotypes¹⁶.

	IgA	IgD	IgE	IgG	IgM
Molecular weight	160 kDa, 400 kDa	175 kDa	190 kDa	150 kDa	950 kDa, 1150 kDa
Molecular form	Monomer, dimer	Monomer	Monomer	Monomer	Pentamer, hexamer
Valence	2, 4	2	2	2	10, 12
Serum concentration (mg/mL)	1.5–2.6	0.04	0.0003	9.5–12.5	0.7–1.7
Serum half-life (days) ^a	6	3	2.5	23	5

IgGs are the most abundant and widely used for therapeutic purposes. An IgG molecule is composed of four polypeptide chains: two identical 50 kDa heavy (H) chains and two identical 25 kDa light (L) chains, linked together by inter-chain disulphide bonds and non-covalent interactions, for a total molecular weight of about 150 kDa. Each heavy chain presents a variable N-terminal domain (VH) and three constant domains (CH1, CH2 and CH3), with a hinge region between CH1 and CH2. Moreover, in the CH2 domain an oligosaccharide is covalently attached at asparagine 297. The part of the antibody including CH2 and CH3 domains forms

Introduction

the Fc. The light chains are made of one variable N-terminal domain (VL) and one constant domain (CL). There are two types of light chains, lambda (λ) and kappa (κ), and the average of κ to λ ratio in humans is 2:1. The variable chains plus CH1 and CL forms the Fab.

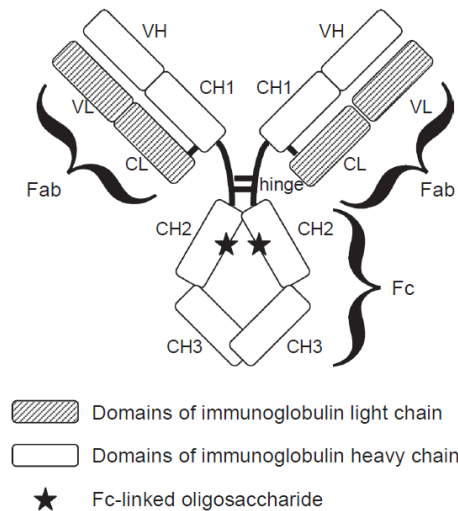


Figure 3. Schematic structure of an antibody¹⁷.

According to heavy chain type, IgGs are further divided into four subclasses: IgG1, IgG2, IgG3 and IgG4. Healthy adults have the highest concentration in blood of IgG1 (5-12 mg/ml), followed by IgG2 (2-6 mg/ml), IgA1 (0.5-2 mg/ml), IgM (0.5-1.5 mg/ml), IgG3 (0.5-1.0 mg/ml), IgG4 (0.2-1.0 mg/ml), IgA (0-0.2 mg/ml), IgD (0-0.4 mg/ml) and IgE (0-0.002 mg/ml)^{18, 19}. IgGs share over 95% homology in primary sequence with differences at the hinge region and at N-terminal sequences of both heavy and light chains that determine antigen-binding specificity. V regions are further divided into three hypervariable sequences called complementarity determining regions (CDR1, CDR2, and CDR3).

As already reported, IgGs have two functional areas, the constant and the variable region. The variable region comprehends two identical antigen-binding sites (two Fab) that recognize and interact with antigens through the CDRs. The binding of the two Fab can be independent of each other and does not seem to depend on the constant region (Fc)²⁰. The latter possess three main effector functions: complement-dependent cytotoxicity (CDC), antibody-dependent cellular cytotoxicity (ADCC) and antibody-dependent cellular phagocytosis (ADCP)²¹. ADCC and ADCP occur when antibodies bind to antigens presented on pathogen surface through Fab, while Fc domains engages interaction with receptors (FcR) on immune effector cells, such as granulocytes, natural killer (NK) cells, monocytes and macrophages. Immunoglobulins can also activate the complement system resulting in CDC²². Upon the formation of antigen-antibody complexes, multiple binding sites in close proximity on the CH2 domains are unlocked and can

interact with C1q, a component of the complement. C1q–IgG interaction triggers a cascade of events involving a series of other proteins of the complement and leads to the proteolytic release of effector-cell chemotactic/activating agents and the formation of a membrane attack complex, which creates pores in the pathogen cell membrane. IgG subclasses display different capacity in promoting the effector properties: IgGs1 have the highest effector activity, while IgGs2 and IgGs4 lack some of the effector functions.

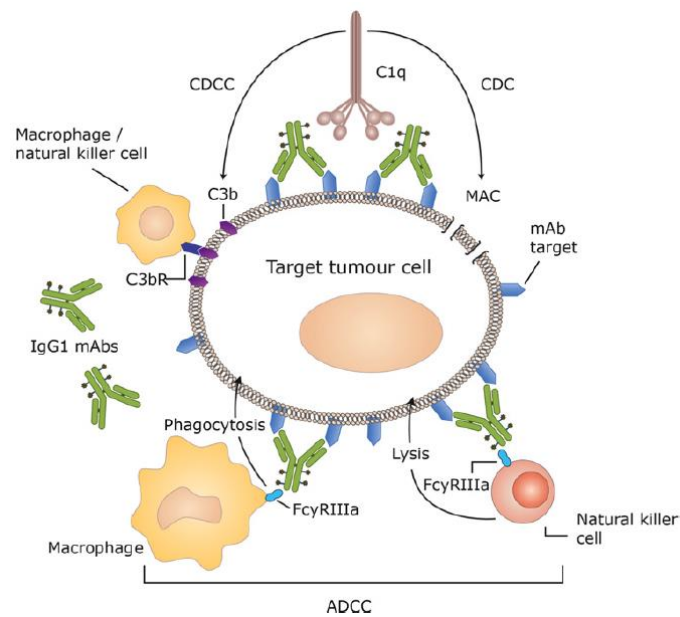


Figure 4. Mechanism of ADCC, ADCP and CDC²³.

Serum antibodies are polyclonal since the exposure to an antigen leads to stimulation, diversification, and propagation of a large number of genetically distinct B-cells that produce antibodies with different affinities and specificities. However, it is possible to generate monoclonal antibodies from a single clone of B cells, which have a unique structure and a unique affinity for a specific epitope of the antigen. The pioneers in mAbs production were Kohler and Milstein who, in 1975, developed a method based on the fusion of a lymphocyte with a myeloma cell to generate murine monoclonal antibodies²⁴. The hybrid cell they created was called hybridoma, and possessed the immortal growth properties of myeloid cells and the ability to secrete antibodies of B lymphocytes. However, murine monoclonal antibodies obtained with hybridoma technology have limited use as therapeutic agents because of the short serum half-life and the capacity to evoke a strong immune response in humans, with production of human anti-mouse antibodies (HAMAs)²⁵. Despite this, in 1986 FDA approved the first mouse monoclonal antibody, orthoclone OKT3, for clinical use in prevention of organ graft rejection²⁶. In order to reduce immunogenicity, genetic engineering techniques were

Introduction

applied to generate chimeric antibodies with human constant regions and mouse variable regions²⁷. However, also in this case an immune response with the production of human anti-chimeric antibodies (HACAs) was observed. A further minimization of the murine component of antibodies was achieved grafting murine CDRs into the human IgG framework, and humanized antibodies were so produced. Finally, the isolation of genes encoding human variable regions, their successful expression in *E.Coli* and the introduction of phage-display technology allowed the production of fully human mAbs. Another possible approach is to use transgenic mice for the human Ig locus, that produce human antibodies after immunization²⁸. Monoclonal antibodies are not enough potent to be therapeutically active on their own in anticancer therapy and are used in combination therapy with other active substances. Alternatively, they can directly bind more potent drugs as happens in ADCs.

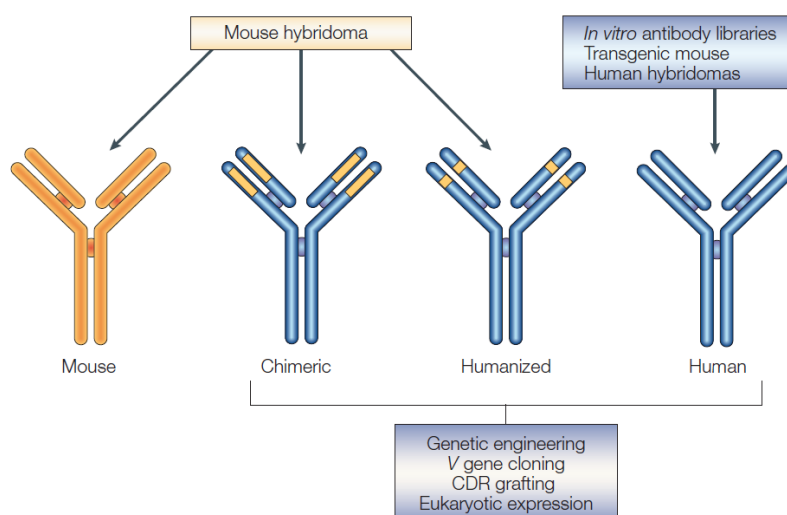


Figure 5. A schematic representation of mouse (0% human sequence), chimeric ($\approx 70\%$), humanized ($\approx 90\%$), and human antibodies (100 %)²⁵.

3.5 Target antigens and antibody selection

Ideally, the mAb component of an ADC should bind antigens that are highly expressed on tumour or diseased tissue ($>10^5$ /cell) with minimal expression on normal cells, thus maximizing efficacy and minimizing toxicity⁴. Those antigens are usually receptors over-expressed on tumour cells and should be well-internalized upon ADC binding so that drug molecules are then released inside the cell. Antibodies recognize antigens with a high affinity. However the proper binding affinity of an ADC is still under debate because a very high affinity ($K_D < 1$ nM) may ensure good tumour localization, but some in vivo studies have suggested that antibodies with lower binding affinity may be able to penetrate solid tumours to a greater extent¹. In fact,

if affinity is extremely high, a low solid tumour penetration can occur according to the so-called “binding site model”²⁹. High-affinity antibodies have a limited diffusion into solid tumour because the slow rate of dissociation from the antigen leads to a decrease in the concentration of the diffusible, free antibody. In other words, as the strength of antibody-antigen interaction increases, the amount of free antibody able to diffuse decreases and binding sites closest to the vasculature are occupied before further penetration occurs.

Moreover, the efficacy of an ADCs cannot be predicted on the basis of antigen expression level: several studies suggested that the correlation between efficacy and antigen density depend on the internalization rate of each antigen after complex formation⁵. Ideally, the ADC-antigen complex is internalized in a rapid and efficient manner but various factors can influence internalization rate, such as the epitope of the target antigen, the affinity of ADC-antigen interaction and the intracellular trafficking pathway³⁰. For example, Owen *et al.* demonstrated that anti-HER2 antibodies directed against different epitopes of HER2 receptor presented different downstream trafficking and lysosomal accumulation³¹. Anyway, upon ADC-antigen binding, the complex is internalized through a receptor-mediated endocytosis and undergoes lysosomal processing⁵. After antibody degradation inside lysosome vesicles, the cytotoxic payload is liberated in the cytoplasm and can hit its pharmacological target inducing cell death.

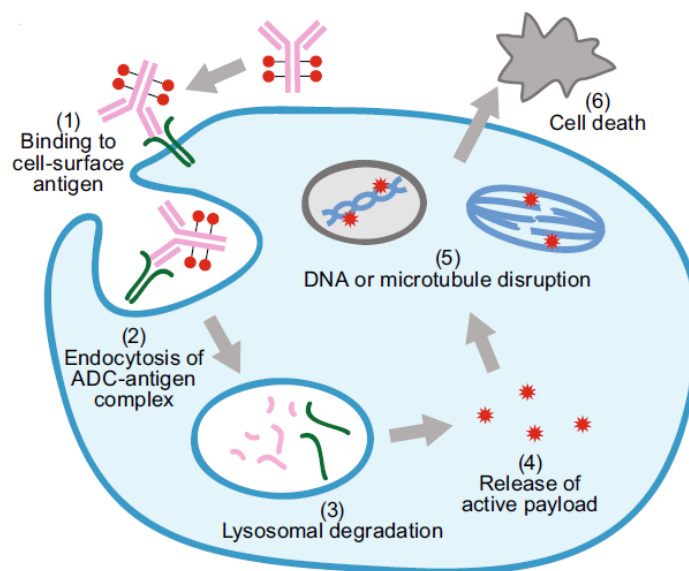


Figure 6. Internalization and mechanism of action of an ADC.⁵

Sometime, ADCs produce a bystander killing effect for which free drugs released intracellularly are able to permeate plasmatic membrane, efflux outside the cell and enter neighbouring

Introduction

cells³². Potentially, this effect represents an advantage for the treatment of solid tumours but the possibility to damage normal cells puts a warning on systemic toxicity that could be a serious issue.

In addition, mAbs may possess intrinsic anti-tumour activity resulting from direct modulation of the biological activity of the target antigen and/or via immune effector functions such as ADCC, CDC and CDCC²³. These inherent effector functions could be beneficial increasing antitumor activity, as in the case of Kadcylla that was demonstrated to activate ADCC in preclinical models³³. Adcetris, however, was shown to retain minimal ADCC activity and any detectable CDC activity despite being an IgG1⁴. The lack of effector can turn into an advantage since ADCs binding to effector cells could reduce tumour localization, prevent internalization and cause off-target toxicity³⁴. Overall, the contribution of effector functions to the efficacy, selectivity and toxicity of ADCs is not yet well understood. All human IgG isotypes, except for IgG3, are currently used for ADCs in clinical trials and IgG1 is the most commonly exploited format. For example, Mylotarg is composed by an IgG4, whereas Adcetris and Kadcylla contain an IgG1. In early ADCs, murine mAbs were employed arising a strong, acute immune response in humans that resulted in formation of human anti-mouse antibodies within 2 weeks of a single dose³⁵. Since then, murine mAbs have been replaced with chimeric, humanized or human antibodies: most ADCs currently in use or in clinical development employ either humanized or fully human antibodies³⁶. Moreover, conversion to human mAbs prolongs retention in systemic circulation thanks to recognition by the human neonatal Fc receptor (FcRn)⁴.

3.6 Payload of ADCs

It is estimated that only 1-2% of the administered ADC dose will reach tumour site³⁷. For this reason, drugs must be highly efficacious at very low concentration (nanomolar or picomolar range, 100–2000 fold more potent than doxorubicin, vinca alkaloids or taxanes). Moreover, compared to parent free drug, conjugation often led to a potency decrease that can be imputed to the different mechanism of cellular uptake between free and conjugate drug¹. A free hydrophobic drug can diffuse inside cells and concentrate at its intracellular target causing cell death. The number of a moderately potent drug necessary to promote cell kill could be very high ($> 10^6$ molecules/cell). When drug is attached to an antibody, its delivery is limited by the moderate number of antigens on cell surface (typically 10^5 receptors/cell) and by possible inefficient mechanisms of internalization or intracellular release of the active drug. The failure

of the first generation of ADCs was imputable to these limitations: classical chemotherapy drugs such as doxorubicin and methotrexate were used with the benefit of a well-known toxicity profiles, but were not enough potent to be therapeutically active¹³. Drugs that are too toxic for traditional chemotherapy have become necessary components of ADCs. In addition, drugs have to be stable and soluble in the aqueous milieu of the antibody and should be chemically modifiable for the attachment to antibodies. Site and type of modifications must be carefully optimized to preserve drug potency. Nowadays, two main categories of cytotoxic drugs are used in ADC development: tubulin polymerization inhibitors and DNA-damaging agents. The first class comprehends drugs that disrupt the microtubule apparatus, yielding G2/M phase cell cycle arrest, such as auristatin analogs (Adcetris, MMAE free drug display $IC_{50} = 0.01\text{--}0.1\text{ nM}$)³⁸ and maytansinoids (Kadcyla, DM1 alkylated derivative displays $IC_{50} = 0.01\text{--}0.04\text{ nM}$)³⁹. The second class includes active molecules that target DNA, such as calicheamicin analogs (Mylotarg) that bind the minor groove of DNA double helix causing its cleavage⁴⁰. Drug loading or drug-antibody ratio (DAR) is a key parameter for the success of an ADC since it profoundly impacts on the pharmacokinetics, stability and therapeutic index⁴¹. A higher DAR is associated with increased systemic clearance, reduction of therapeutic efficacy, lower stability, protein aggregation and immunogenicity^{42, 43}. Several studies demonstrated that an optimal threshold for ADCs therapeutic activity is obtained with a DAR of 2-4⁴⁴.

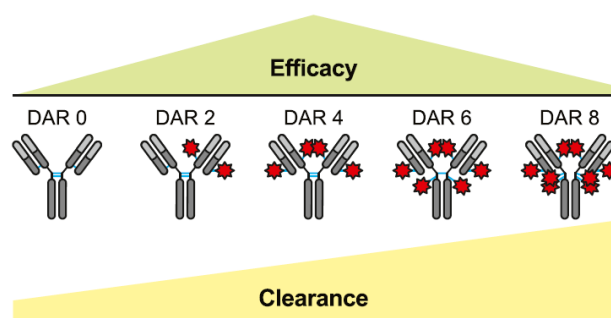


Figure 7. Relationship between drug-antibody ratio (DAR), antitumor activity (efficacy), and elimination of antibody from blood (clearance)⁴⁴.

3.7 Linkers

The linker should preserve its stability (i.e. retention of drugs by the antibody) during systemic circulation and should release drugs upon ADC internalization into cells. In general, linkers can be divided into two broad categories, cleavable and non-cleavable^{4,42}. The former category, in turn, comprehends three different subtypes according to the mechanism of drug release.

Introduction

- ❖ Acid-labile linkers take advantage of the low pH inside lysosomal vesicles to trigger hydrolysis of an acid labile group. An example is hydrazone linker which undergoes hydrolysis in endosomes (pH 5–6.5) and lysosomes (pH 4.5–5) environments. This linker is used in Mylotarg, whose first withdrawal from the market was attributed to toxicities related to linker instability⁴⁵.
- ❖ Protease cleavable linkers: this strategy exploits lysosomal proteases that recognize and cleave dipeptide bonds inside the linker⁴⁶. For example, Adcetris contains a valine-citrulline dipeptide linker that can be cleaved by cathepsin B, a cysteine protease, in lysosomal acidic environment.
- ❖ Glutathione sensitive linkers exploit the higher concentration of thiols, such as glutathione, inside cells. Disulphide bonds of linker are relatively stable in circulation and are reduced once inside the cell. To increase plasma stability, they can be protected with methyl groups that sterically hinder premature cleavage⁴⁷.

Non-cleavable linkers possess higher blood stability and their success depends on the complete degradation of the antibody after ADC internalization, resulting in the release of the free drug with the linker attached to an amino acid residue from the mAb. This strategy can be applied to drugs that are able to exploit their action despite being chemically modified. To date, the majority of non-cleavable linkers have utilized thioether bonds⁴⁸. This is the case of Kadcyra in which the bifunctional crosslinking agent SMCC (succinimidyl-4-[N-maleimidomethyl]-cyclohexane-1-carboxylate) was used to introduce a maleimido group on the antibody to enable linkage of the maytansinoid via a non-reducible thioether bond. Lysosomal degradation of the mAb liberates the linker-drug moiety attached to a lysine residue. Because of net charge, it does not readily cross lipid bilayers and remains sequestered inside cells abating the bystander killing effect⁴⁹. On the contrary, cleavable linkers produce neutral drug molecules that could cross plasmatic membranes and could kill surrounding cells, such as tumour stromal cells and tumour blood vessels, enhancing anti-tumour effect⁶, but also normal cells.

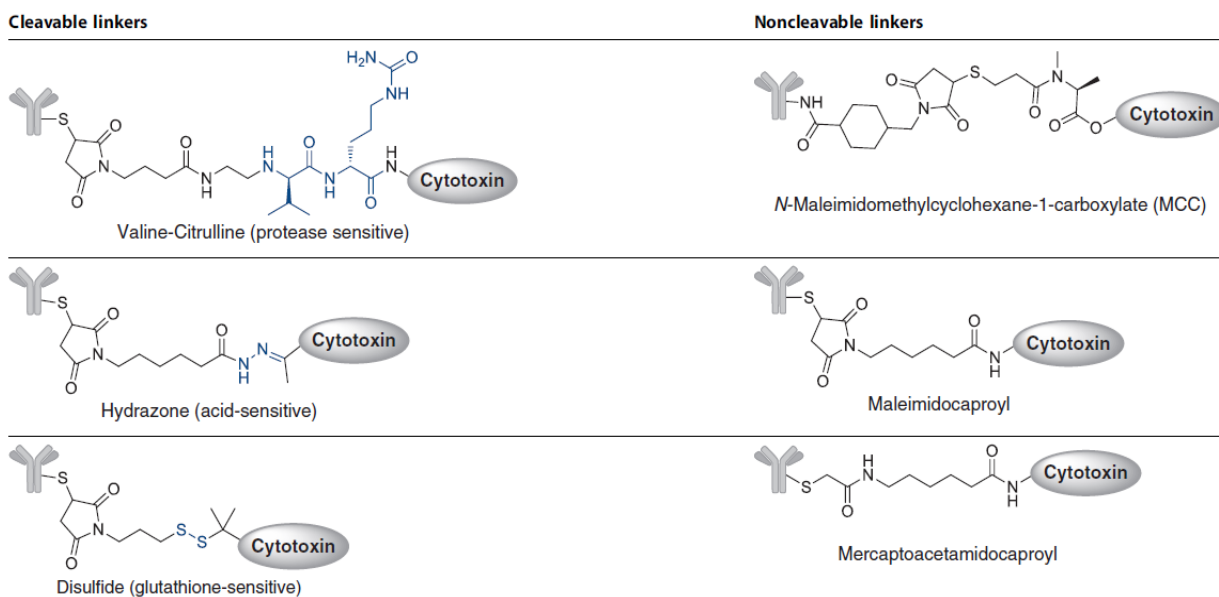


Figure 8. Examples of ADCs drug linkers⁴.

3.8 Conjugation strategies

There is an inter-dependency between linker and conjugation chemistry and the choice of linker-conjugation chemistry affects ADCs efficacy, stability, pharmacokinetics, pharmacodynamics and homogeneity¹.

The most exploited conjugation sites have involved lysine or cysteine residues belonging to the native amino acidic composition of the antibody. The relative conjugation methods are based on the acylation of lysines and on the alkylation of reduced inter-chain cysteine disulfides⁷.

Lysine residues are usually exposed on antibody surface and therefore are easily accessible. Antibodies contain up to 80 lysines⁵⁰ available for the reaction with carboxylic acid derivatives of drugs (such as N-hydroxysuccinimide [NHS] derivatives)⁵. Optimized conjugation conditions give an average DAR value of 3.5–4, with a distribution between 0–7.

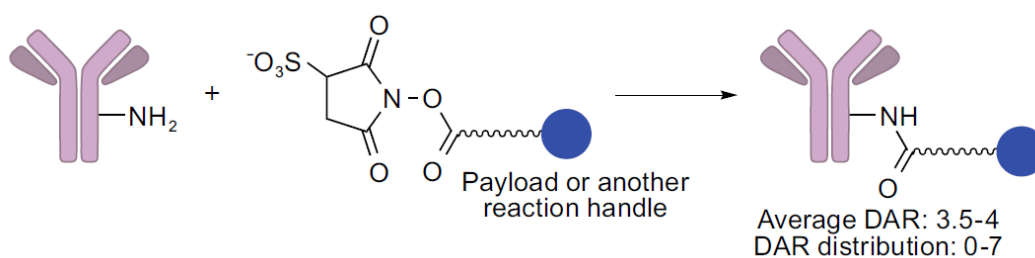


Figure 9. Lysine coupling. An activated carboxylic acid moiety reacts with a lysine residue, which results in amide bond linkage between mAb and the payload⁵.

Introduction

Lysine-coupling was used in Mylotarg production: a semi-synthetic calicheamicin derivative was activated with NHS and then randomly tether to the lysines of gentuzumab, forming stable amide bonds. Also Kadcyra was generated by lysines modification, but in this case a two-step process was employed. In fact, lysines were first modified to introduce a maleimido group and then were conjugated to a drug-linker containing a thiol reactive function.

The second strategy is based on the controlled reduction of mAb inter-chain disulphide bonds accomplished by mild reducing agents, such as dithiothreitol (DTT) or tris-(2-carboxyethyl) phosphine (TCEP), that liberate free cysteine residues able to react with the maleimido group of the drug-linker moiety. Controlling reducing conditions is fundamental to maintain intact intra-chain disulphide bonds and minimize mAb structural disruption. In a human IgG1, there are four inter-chain and 12 intra-chain disulphide bonds. The 4 inter-chain disulphides, which are not critical to preserve IgG structural stability, can be selectively reduced and exploited as potential conjugation sites, allowing to conjugate up to 8 drug molecules per mAb⁵. Adcetris was produced by conjugating a maleimide-functionalized drug to inter-chain cysteine residues of brentuximab.

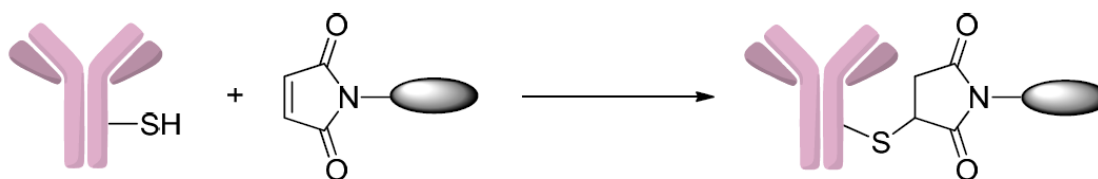


Figure 10. Cysteine coupling. A maleimide containing moiety reacts with a cysteine residue, with results in a stable thioether bonds between mAb and the payload⁷.

Both these approaches provide a heterogeneous mixture of ADCs with variable DARs and tethering sites (i.e. ADCs with a different number of drug molecules and isomers of antibodies with the same DARs but different sites of conjugation). Broad distribution of DARs and presence of multiple isomers can lead to reduced efficacy and, for this reason, research is now oriented versus the development of site-specific conjugation techniques²³. Homogenous products permit a better control over pharmacokinetic and safety profiles, along with an improved batch to batch reproducibility⁵¹. Moreover, drugs should ideally be linked far from CDRs in order to not affected ADC's capacity to recognize its targets.

Currently, there are three most explored pathways of site-directed conjugation: insertion of an unnatural amino acid in mAb scaffold, introduction of cysteine residues and enzymatic approaches.

Incorporation of non-natural amino acids, such as para-acetylphenylalanine (pAF) and para-azidophenylalanine (pAZ), can provide sites for bio-orthogonal conjugation chemistries^{52, 53}. An alternative of unnatural amino acids may be selenocysteine that is naturally present as a component of selenoproteins. Selenocysteine contains selenium in place of sulphur which makes it more reactive towards electrophiles in acidic conditions and this property is exploited to selectively couple maleimide and iodoacetamide containing agents to the antibodies⁵⁴.

In THIOMAB strategy, two cysteine residues are inserted using site-directed mutagenesis in the constant domains of Fab region which is not involved in antigen binding⁵⁵. These ADCs are produced by global reduction of the naturally occurring inter-chain disulphide bonds and the inserted cysteine residues, which are blocked, followed by oxidation (with CuSO_4 or dehydroascorbic acid) to regenerate the inter-chain disulphides. Conjugation of the reactive cysteine thiol to maleimide reagents is then performed and involved only the inserted cysteines. This method generated site specifically modified ADCs with a DAR of 2.

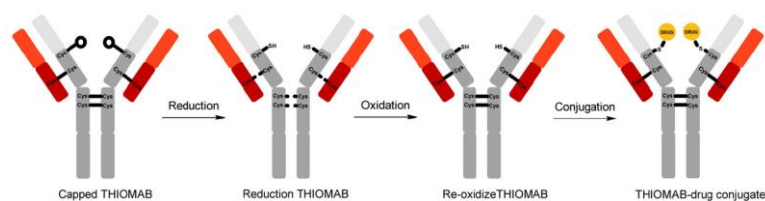


Figure 11. Schematic mechanism of drug conjugation to THIOMABs.⁵⁴

In another approach, solvent-accessible cysteines that form the inter-chain disulphide bonds are replaced with serines, to reduce the potential conjugation sites down to 4 or 2. The Cys→Ser variants are then employed to generate homogeneous ADCs with defined sites and stoichiometries⁵⁶.

Chemoenzymatic approaches have been largely investigated and include also the use of transglutaminases (TGases) that catalyse acyltransfer reactions between the γ -carboxamide group of a glutamine and the primary ϵ -amino group of a lysine, forming a stable isopeptide bond. The enzyme can be used for the conjugation of amino-containing drugs to a glutamine residue on the antibody^{57, 58}. Glutamine residues can act as substrates if are both located in a flexible region of the protein and flanked by specific amino acids, giving selectivity to the conjugation. Moreover, engineered glutamine or consensus sequences, such as LLQG, can be inserted at different sites on the antibody to obtain site-directed conjugation via TGase. Another enzyme, sortase A (SrtA), is used for drug conjugation to antibodies tagged with an LPXTG (X: any amino acid) motif. Sortase A catalyzes hydrolysis of the threonine–glycine bond to form a new peptide bond between the exposed C-terminus of threonine and the N-terminal

Introduction

of an oligoglycine containing molecule⁵⁹. Another example of enzymatic strategy is given by “aldehyde tag technology” where a short consensus sequence, CXPXR (X: any amino acid), is insert in the mAb⁶⁰. This sequence is recognized by formyl glycine generating enzyme (FGE) that converts the consensus cysteine to a formyl glycine containing a reactive aldehyde group which acts as a chemical handle for bio-orthogonal conjugation.

Many other site-directed conjugation techniques are now under examination, such as the “glyco-engineering method”. A human IgG1 is *N*-glycosylated with a biantennary oligosaccharide chain in the CH2 domain of the Fc fragment at the conserved Asn297^{61, 62}. This *N*-linked glycan can be modified by several methods, making it possible to conjugate a drug at this site. For example, glycosyltransferases can be exploited to attach sugars with a chemical handle to mAb glycans.

Table 2. Examples of site-specific conjugation methods⁵⁴.

Company/institution	Conjugation strategy	Antibody engineering	Chemistry (non-enzymatic reactions)	DAR
Genentech Seattle Genetics	Conventional lysine and cysteine conjugation Lewis Phillips et al. (2008) and Senter and Sievers (2012)	Not required	Thiol-melamide Primary amine-NHS-ester (coupling linker-drug to a native antibody)	3-4
Sutro Biopharma Ambrx	Incorporation of unnatural amino acids into antibodies Axup et al., 2012 and Zimmerman et al., 2014	Required	Click chemistry oxime ligation (coupling linker-drug to an incorporated unnatural amino acid)	2
National Cancer Institute	Incorporation of selenocysteine into antibodies Hofer et al. (2009)	Required	Selenol-maleimide Selenol-iodoacetamide (coupling linker-drug to an incorporated selenocysteine)	2
Rinat-Pfizer	<i>Streptococcus pneumoniae</i> transglutaminase (mTG) Specifically recognizes and modifies genetically introduced glutamine tag (LLQGA) with a primary amine-containing linker-drug module Strop et al. (2013)	Required	-	1.8-2
Sanofi-Genzyme	Glycoengineering Site-specific introduction of sialic acid with the use of galactosyl- and sialyltransferases Zhou et al. (2014a)	Not required	Oxime ligation (coupling linker-drug to a modified Fc glycans)	~1.6
Innate Pharma	Microbial transglutaminase (MTGase) Enzymatic conjugation of a primary amine-containing linker/linker-drug module to glutamine specifically recognized by MTGase Dennler et al. (2014)	Required	Thiol-maleimide Click chemistry (coupling drug to linker-antibody)	2
Redwood Bioscience	Formylglycine generating enzyme (FGE) Converts cysteine located in the CXPXR consensus sequence to formylglycine (FGly) Drake et al. (2014)	Required	Hydrazino-iso-Pictet-Spengler ligation (coupling linker-drug to FGly)	2
UCL Cancer Institute	Next generation maleimides (NGMs) Rebridge reduced interchain disulfide bonds of a native antibody Schumacher et al. (2014)	Not required	Reaction between thiols and leaving groups of the NGM linker-drug (coupling linker-drug to a native antibody)	1 2 3 4
PolyTherics	Bis-alkylating reagents Rebridge reduced interchain disulfide bonds of a native antibody Badescu et al. (2014)	Not required	Micheal addition and elimination reactions (coupling linker-drug to a native antibody)	2 4

3.9 Pharmacokinetic and ADME considerations for ADCs

A major benefit of ADCs respect to small anticancer molecules is their favorable pharmacokinetics with low clearance and long half-lives⁶³. ADCs are administered via intravenous injections to prevent the destruction of mAb mediated by proteolytic enzymes and gastric acids. Once an ADC is in the bloodstream, it can distribute into diseased tissues

either via extravasation through pores in the endothelium or via pinocytosis mediated by endothelium cells²³. Unlike normal blood vessels presenting a monolayer of endothelial cells united by tight junctions, tumour endothelium is characterized by a fenestrated monolayer that permit extravasation⁶⁴. However, ADCs distribution in diseased tissues can be limited by the size of the antibody that structurally accounts for approximately 98% of the total ADC molecular mass. In addition, solid tumour often lack functioning lymphatic vessels due to their uncontrolled growth, and lymph drainage is thus impaired increasing interstitial hydrostatic pressure. The increased pressure reduces the rate of fluid movement from blood to tumour tissue and thereby reduces the rate of antibody delivery to tumour cells¹⁶.

The large size of ADCs minimizes the distribution into metabolizing and eliminating organs such as liver, intestines, muscle and skin, extending their half-life to 3 weeks (except for IgG3 that have an half-life of 1 week)^{65, 66}. An additional mechanism which prolonged ADC half-life in plasma is the binding of the Fc portion to neonatal Fc receptors (FcRn) in endosomal vesicles of endothelial cells⁶⁷. Immunoglobulines may be taken up into cells by nonspecific pino- or endocytosis. Intracellularly, FcRn receptors protect IgGs against degradation by binding to the Fc region in a pH dependent manner: binding occurs in acidic (pH 6.0-6.5) but not in neutral (pH 7.0-7.5) conditions⁶⁸. The IgG-FcRn complex is formed in the slightly acidic environment of the endosomes and is then transported back into systemic circulation. In contrast, the unbound fraction of IgG is degraded to amino acids. This protection mechanism is present in a wide variety of tissue types, mainly in endothelial cells but also in renal epithelial cells, and creates a reservoir system recycling ADCs in the bloodstream. Therefore, a strategy to prolong circulatory half-life could rely in the improvement of ADCs binding to endothelial FcRn receptors.

The mAb moiety allows the ADC to circulate in the bloodstream until it binds the specific targets on cells; in fact, the distribution volume of mAbs is very low (3-5 l)⁶⁶. ADME properties of ADCs are very similar to the unconjugated antibodies, however, ADCs consist of two pharmacologically distinct components -the mAb and the drugs- and it is necessary to understand the in vivo fate of both components. Moreover, drugs conjugation may affect mAb pharmacokinetic behaviour increasing clearance: ADCs with higher DARs tend to have a faster clearance than ADCs with lower DARs. Because of the large molecular weight, little intact immunoglobulin is filtered by the kidney and excreted in the urine, instead the vast majority is eliminated by catabolism¹⁶. ADCs catabolic products occur by two concurrent processes: deconjugation and catabolism. In deconjugation, cytotoxic agents are released via enzymatic or chemical processes with preservation of the antibody backbone. Instead, the catabolism

Introduction

process involves antibody degradation and the formation of drug-containing catabolites (free drug or drug-amino acid conjugates) that can retain cytotoxicity. As endogenous IgGs, monoclonal antibodies are metabolized in the vascular compartment by endothelial cells that assimilate them either through receptor-mediated endocytosis or fluid-phase pinocytosis. Then, ADCs are moved to lysosomes where they are degraded. The pharmacologic activity of the catabolites may not be limited to diseased tissues, as they may diffuse in plasma and exhibit systemic effects. Moreover, their size and structure are similar to small molecule therapeutics and they can be subject to metabolism and elimination processes associated with them, being also engaged in drug-drug interactions. However, the concentrations of cytotoxic drugs released from ADCs are very low so the risk of interaction is presumably irrelevant. ADCs efficacy can also be limited when drug resistance mechanisms evolve. Little is known about the clinical manifestations of drug resistance to this class of biotherapeutics. Recent preclinical studies has revealed that there are several emerging mechanisms of ADC resistance, such as antigen down-regulation, drug transporter protein over-expression, defects in ADC trafficking pathways and alterations⁶⁹.

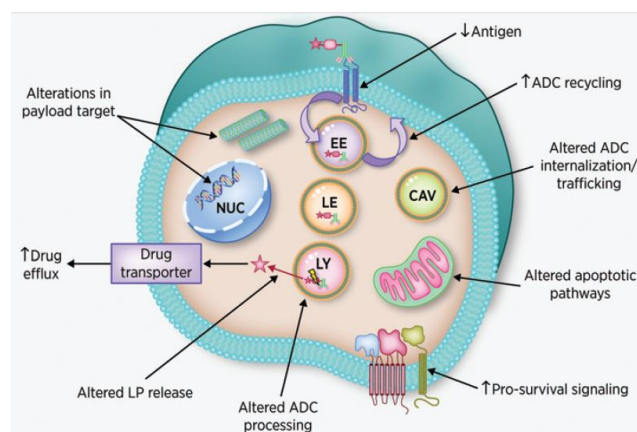


Figure 12. Emerging mechanisms of ADC resistance⁶⁹.

3.10 Clinical experience

3.10.1 Mylotarg

In gemtuzumab ozogamicin (Mylotarg, Pfizer/Wyeth-Ayerst Laboratories) the antitumor antibiotic calicheamicin- γ_1 (N-acetyl- γ_1 -calicheamicin dimethyl hydrazide) is attached to a recombinant humanised IgG4 anti-CD33 via a hydrolyzable bifunctional linker⁷⁰. About 50% of the antibody is linked to the drug with an average loading of four to six molecules of calicheamicin for antibody, while the remaining antibody is unconjugated. Mylotarg is now

approved for the treatment of adults with newly diagnosed acute myeloid leukemia whose tumors express the CD33 antigen (CD33-positive AML) and for the treatment of patients aged 2 years and older with CD33-positive AML who have experienced a relapse or who have not responded to initial treatment (refractory). Originally, Mylotarg received accelerated approval by FDA in 2000 as a stand-alone treatment for older patients with CD33-positive AML who had experienced a relapse. Then, it was withdrawn from the market due to the failure of the trials to verify clinical benefit and due to safety concerns, including a high number of early deaths.

CD33 is a 67 kDa transmembrane cell surface glycoprotein, belonging to the superfamily subset of sialic acid binding immunoglobulin-related lectins. Its natural ligand and its biologic function are unknown. Mylotarg's half-life is 67 h, and a 2-week interval between doses was chosen to prevent drug accumulation⁷¹. The approved dose is 9 mg/m² infused intravenously over 2 h⁷². Anti-CD33 monoclonal antibody rapidly accumulates in the marrow of AML patients. CD33–Mylotarg complex is rapidly internalized and translocated into lysosomes where the acid environment cleaves the linker, releasing the drugs. Calicheamicin- γ_1 is a potent cytotoxic enediyene antibiotic, originally isolated from *Micromonospora echinospora* ssp. *Calichensis*. It is reduced to a highly reactive 1,4-dehydrobenzene-diradical species, presumably through the action of glutathione. The diradical species locates within the minor groove of DNA causing site-specific double-stranded cleavage and cell death.

Toxic effects of gemtuzumab are myelosuppression and hepatotoxicity⁷². Although CD33 is not expressed on pluripotent progenitor cells, more differentiated multipotent hematopoietic cells are CD33-positive and may be a target for the antibody, causing thrombocytopenia and neutropenia.

3.10.2 Adcetris

Brentuximab vedotin (Adcetris, Seattle Genetics) is formed by a chimeric anti CD30 IgG1 (cAC10) that is conjugated to the antitubulin agent monomethyl auristatin E (MMAE), an analogue of the natural product dolastatin 10, through an enzyme-cleavable valine–citrulline dipeptide⁷³. On average four molecules of MMAE are attached to cAC10 interchain cysteine residues.⁷⁴ In 2011, FDA approved brentuximab vedotin for patients with relapsed Hodgkin lymphoma and relapsed systemic anaplastic large-cell lymphoma (ALCL)⁷⁵. Classical Hodgkin lymphoma and ALCL are hematologic malignancies that highly and uniformly expressed the cell surface protein CD30, a marker of lymphocyte activation. CD30 is a membrane glycoprotein that belongs to the TNF receptor superfamily and the interaction with its ligands activates a

Introduction

variety of adaptor proteins that promote cellular proliferation and survival. Moreover, a soluble CD30 is present in elevated concentration in the serum of patients with Hodgkin lymphoma and other CD30-expressing tumours, as well as in inflammatory conditions with a strong T- or B-cell activation. Adcetris binds the extracellular domain of CD30 and is internalized by clathrin-mediated endocytosis. Then, it travels to lysosomes where proteases cleave the peptide linker releasing MMAE. The drug binds to tubulin and inhibits microtubule polymerization, causing G2–M phase growth arrest and apoptosis. MMAE can also diffuse into the microenvironment, exerting a bystander effect on the surrounding cells.

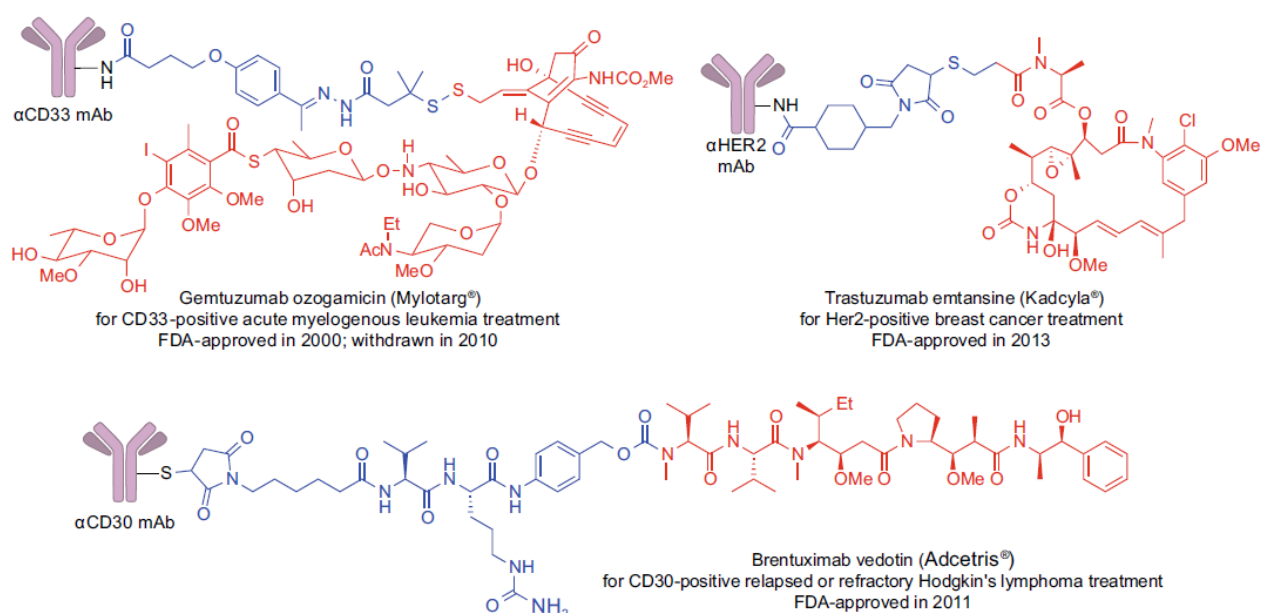


Figure 13. Structures of ADCs that have received FDA approval: Mylotarg (withdrawn in 2010), Adcetris and Kadcyla (pink: mAb, blue: linker, red: payload)⁵.

3.10.3 Kadcyla

In ado-trastuzumab emtansine (T-DM1) targeting and antitumoral properties of trastuzumab are combined with the high cytotoxic activity of emtansine (DM1). An average of 3.6 DM1 molecules are connected to the antibody via a stable thioether linker⁷⁶. T-DM1 received FDA approval in 2013 for the treatment of refractory human epidermal growth factor receptor 2 (HER2) positive metastatic or locally advanced breast cancer, becoming the first ADC therapeutically used for a solid malignancy. The approved dosage is a 3.6 mg/kg intravenous injection every 3 weeks. DM1 is a derivative of maytansine, isolated from the Ethiopian plant *Maytenus ovatus*, which acts as a potent microtubule-disrupting agent. HER2 receptor is over-expressed in about 20-25% of human breast cancer and it is a marker of high tumour

aggression and poor clinical outcomes. It is a 185 kDa transmembrane glycoprotein having a tyrosine kinase activity. Trastuzumab recognizes HER2 and, after the binding, ADC-HER2 complex is internalized via receptor-mediated endocytosis. An active derivative of DM1 (lysine- N^{ϵ} -MCC-DM1) is subsequently released by proteolytic degradation of the antibody moiety within the lysosomes⁴⁹. The most common adverse effects of T-DM1 are thrombocytopenia and elevation in liver transaminases.

3.11 Moving from ADCs to Antibody Drug Systems (ADSs)

Nowadays, the research in the field of ADCs is mainly focused in developing site specific approaches of drug conjugation to mAbs in order to improve the final ADC activity, homogeneity, characterization, manufacturing and therapeutic index. Although innovative, these new technologies might face the problem of increased costs of ADC production since mAbs themselves are already complex structures characterized by a high cost and the additional steps required for an ADC production risk to make these drugs unaffordable for many countries. In this project, we proposed a new approach in ADC development that consists in a class of ADCs based on a non-covalent interaction between the targeting moiety, a mAb, and a moiety carrying the anticancer drugs. The latter, that can be termed Fc binding moiety (FcBM), must present unique binding properties for the Fc region of mAbs avoiding affecting its antigen binding properties. Being this class characterized by a non-covalent conjugation, is from here referred as Antibody Drug Systems (ADSs).

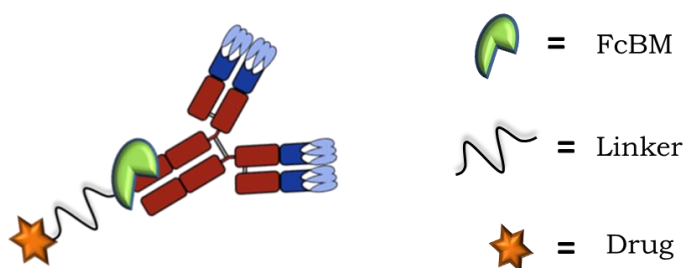


Figure 14. Schematic representation of an Antibody-Drug System (ADS).

The core of the ADS design is the FcBM that has to be selected and optimized to achieve a very high affinity toward the Fc region, the constant region shared between all IgGs. The FcBM/mAb interaction has to be stable in order to avoid a premature release of drugs and the exchange of the mAb with circulating antibodies of the patient. Moreover, FcBM has the role

Introduction

to carry drugs respecting the desired DAR. The linker between the FcBM and drugs plays a fundamental role in determining ADS selectivity, pharmacokinetic, therapeutic index and efficacy as it happens for ADCs. In fact, it must be stable in systemic circulation and labile enough to ensure efficient drug release inside tumor/disease cells.

ADS may prove to be a versatile platform since Fc region is the constant portion of an antibody and therefore the FcBM can strongly interact with most of the mAb present on the market, that are chimeric and humanized. With this feature, different ADSs can be prepared by simply mixing the FcBM-drugs conjugate with the mAb that is chosen on the basis of the tumour/disease to be treated.

Beside the therapeutic application of ADSs, this technology may also find an application in other fields, such as: in diagnosis as a tool for bioimaging when FcBM is coupled with a labelling molecule, in laboratory research when essays involving antibodies are employed (e.g. ELISA kits and FACS) or in biosensor technology.

Moreover, the overall cost of an ADS could be reduced respect to the cost of an ADC since an optimized FcBM may be suitable for different drugs and diagnostic agents generating a family of different ADSs.

In this project, we have investigated two possible FcBM: Protein G and an anti-human-Fc Fab fragment.

3.12 Protein G

Protein G is a cell wall receptor of some *Streptococci* C and G strains, whose function is to protect bacteria from host immune system during infections. The protein binds selectively to Fc of antibodies and this unique property has been exploited for a variety of immunochemical applications, including detection and purification of antibodies by affinity chromatography⁷⁷. Protein G is able to bind all human IgG subclasses, as well as a number of other mammalian antibodies (mouse, rat, rabbit, bovine, sheep, goat, horse)⁷⁸. It also interacts with Fab at CH1, that is the most highly conserved site inside Fab region; however, its binding affinity for Fab is only about 10% of its affinity for Fc (some authors reported a K_a of about 10^5 M^{-1})⁷⁹. During past decades, several Protein G genes have been cloned and sequenced; for this region, literature reports different molecular weights and domains designation. Protein G from *Streptococcus* G148 strain was the most studied^{80, 81, 82, 83, 84}. Akerstrom and Bjorck found that Protein G has an elongated shape and reported an affinity for IgG of about 10^{10} M^{-1} ^{78, 85}.

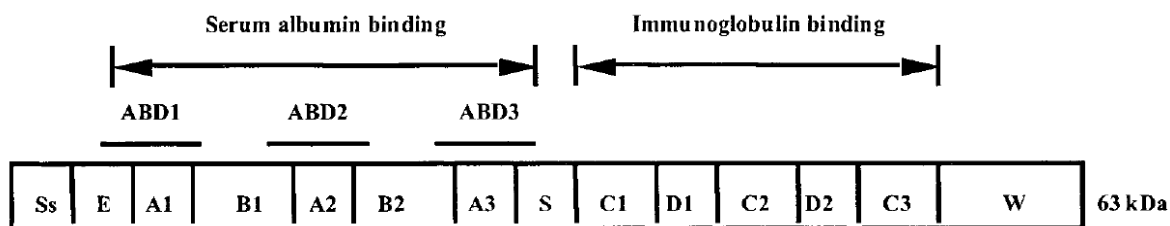


Figure 15. An overview on the structure of streptococcal protein G⁸⁶.

In its entire and complete form, Protein G is a ≈ 60 kDa receptor formed of about 600 amino acids, part of which are arranged in three repeated domains of about 55 amino acids, called C1, C2 and C3, which are responsible for Fc-binding. Two 15-amino acids linker regions, called D1 and D2, separate the three Fc-binding repeats. The IgG-binding domains are highly homogeneous with only two differences between C1 and C2 and six differences between C1 and C3. Those repeats are located at the C-terminus of the molecule. The C-terminus forms also a hydrophilic anchor necessary for the attachment to cell-wall, and is followed by M region that is the transmembrane portion. The N-terminal part contains the albumin-binding site which consists of three homologous 46-residues triple α helical domains^{80, 86}.

NMR spectroscopy and X-ray crystallography have been extensively used to determine the structure of the complex between protein G and the Fc^{87, 88, 89, 90, 91}. According to these results, IgG-binding domains consist of a α -helix diagonally positioned across a four stranded β -sheet with the secondary-structure elements connected by short loop regions. It has been proposed that Protein G interacts with the hinge region connecting the second and third constant domains of the heavy chains (CH2 and CH3). Protein G-Fc complex is based on an intricate network of hydrogen bonds and salt links, involving mainly charged and polar residues. The crystal structure of C2 fragment of Protein G in complex with the Fc domain of a human IgG outlined that there are three residues of the CH2 domain (Ile253, Ser254 and Gln311) and two areas in CH3 domain (Glu380 and Glu382, and the residues His433-Gln438) involved in interfacial interactions. The residues in Protein G that were found to participate in the interaction are the following: Glu27, Lys28, Lys31, Gln32, Asn35, Asp40, Glu42 and Trp43.

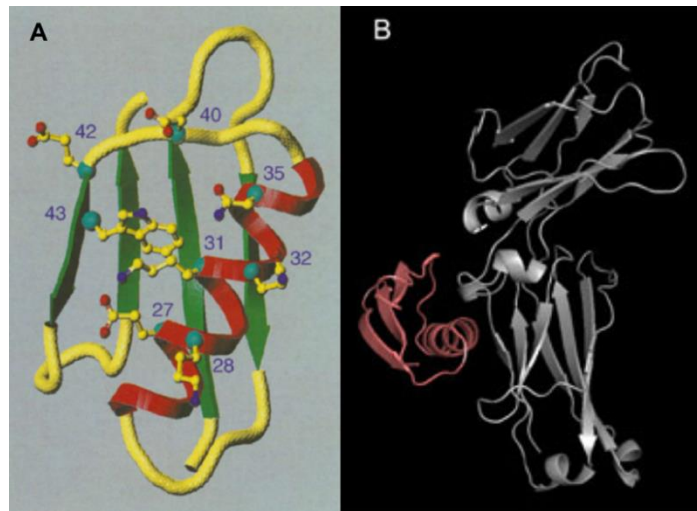


Figure 16. A) Schematic representation of an IgG-binding domain of Protein G with the residues most involved in Fc binding and B) its complex with the Fc region⁷⁹.

The interfacial interactions between Protein G and Fc can be divided in three different regions. The first region comprises a large hydrogen bonding network that involves residues Lys28 and Gln32 of protein G (situated in the center of the α -helix) and the following residues of Fc: Lys248, Glu380, Glu382, Ser426 and Gln438. In particular, Lys28 bridges between the carboxyl groups of Glu380 and Glu382, while Gln32 forms a hydrogen bond with Gln438. In the second region of the interface, there are two charged residues of protein G, Glu27 and Lys31, that are situated in the central part of the α -helix, with their side chains extend from the opposite side of the helix relative to those of Lys28 and Gln32. Glu27 forms a salt link with Lys31 and hydrogen bonds with Ile253 and Ser254 of Fc, while Lys31 does not interact directly with Fc. The third interface region involves Protein G's residues Asn35 (situated at the C-terminal part of the α -helix), Asp40 (located in the loop region connecting the α -helix and the third β -strand) and Glu42/Trp43 (positioned at the N terminus of the third β -strand). Val39 also contributes to Fc binding. Residues from Fc are His433, Asn434 and Tyr436.

In Protein G-Fab complex the binding is predominantly mediated by hydrogen-bonds through the pairing of two β -strands: the second β -strand of Protein G forms an antiparallel sheet with the last β -strand of the CH1 domain of Fab⁹².

In this work, we used a truncated form of Protein G of about 22.8 kDa that comprehends C1, C2 and C3 domains, while all other regions included HSA binding domain were deleted. The protein was selectively PEGylated at the N-terminal using a methoxy-PEG-aldehyde 20 kDa.

3.13 Secondary Antibodies

Antibodies are extremely useful in laboratory and industrial applications for the detection of biomarkers involved in some diseases such as cancers. Depending on their function inside the specific assay and the binding activity, antibodies are classified into primary and secondary. Primary antibodies target the antigen or biomarker through Fab regions exposing the Fc domain that can be recognized by secondary antibodies. This system is used in many laboratory essays such as ELISA, western blot, flow cytometry and cell imaging. Secondary antibodies reduce experiment costs since Fc portion is constant within the same class and species, so the same secondary antibody can be used to label different primary antibody instead of directly labelling various type of primary antibodies. In order to permit the detection of primary antibodies, secondary antibodies are usually tethered to fluorescent dyes (FITC, AlexaFluor, etc), or conjugated to enzymes (peroxidase, alkaline phosphatase) or biotin. Secondary antibodies are usually produced in species such as rabbit, goat, sheep or donkey. In particular, goat is the host species most easily and frequently used by manufacturers. Goats have two IgG subclasses, IgG1 and IgG2, with IgG1 accounting for the 55% of total IgG content⁹³. It was shown that interchain disulphide bridge arrangement of a goat IgG is the following: there is one disulphide bond between the two heavy chains and one disulphide bond between the heavy and light chains⁹⁴. This arrangement is similar to that proposed for rabbit immunoglobulin G⁹⁵.

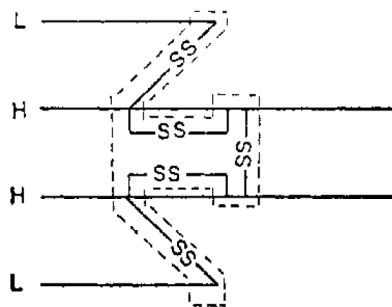


Figure 17. Arrangement of disulphide bonds in goat IgG⁹⁴.

3.14 Fab

Recently, there has been increasing interest in the use antibody fragments, such as Fab, as therapeutic entities. From a mere economic perspective, Fab manufacturing is much less expensive respect entire IgG since Fab can be also produced in microbial expression host such

Introduction

as *E. coli*. Most importantly, Fab' has some interesting properties: monovalent antigen binding, lack of innate effector functions and higher tumour penetrating capacity. However, the reduced molecular size that makes Fab subject to renal filtration and the lack of Fc function that allows the receptor-mediated recycling are also the causes of the very short serum half-life. It was reported that in mouse models Fab fragment is cleared from the body 35 times faster than entire IgG⁹⁶. The short circulation time in vivo can be overcome by conjugation to PEG⁹⁷. The circulating half-life increases proportionally respect to PEG size and it was shown that the conjugation to a 40 kDa PEG confers to Fab a serum half-life very similar to that of an IgG⁹⁸. It is fundamental that the Fab affinity for its antigen is preserved after PEGylation. Random conjugation often results in loss of protein activity due to interference or steric hindrance of the antigen-binding site⁹⁹. For this reason, site-specific PEGylation strategies involving Fab sites located far away from antigen-binding sites have been developed. One of these is directed to the solvent accessible cysteine residues and is based on the use of a PEG-maleimide¹⁰⁰. The hinge region of immunoglobulin is composed by a variable number of disulphide bonds, ranging from two to fifteen. Those cysteine residues can be reduced by mild reduction agents such as DTT (dithiothreitol), β -mercaptoethylamine (β -MA), β -mercaptoethanol (β -ME), glutathione or cysteine. The activate cysteines can be modified with PEG-maleimide through a simple and efficient reaction. Moreover, Fab can be engineered in order to have a single cysteine that can be selectively PEGylated.

Certolizumab pegol, marketed as Cimzia, is a recombinant, humanized antibody Fab fragment manufactured in *E. coli* and conjugated to PEG¹⁰¹. Certoluzimab recognizes human tumour necrosis factor α (TNF α), which is partly responsible for the inflammatory effect of several autoimmune disorders. In 2008, Cimzia was approved by FDA for the treatment of adult patients with moderate-to-severe Crohn's disease who have not responded to conventional therapies, and it is the only commercially available PEGylated antibody or antibody fragment. In this bioconjugate, Fab has been engineered to contain a free cysteine residue in the hinge region and this modification have not affected the affinity for TNF α ¹⁰². PEG has a total molecular weight of 40 kDa and is formed by two branches of 20 kDa each.

Well-established techniques to obtain Fab, Fab' or F(ab')₂ fragments from an entire IgG are based on the use of proteolytic enzymes such as pepsin and papain¹⁰³. When an IgG is digested by papain, two Fab (50 kDa each) and one Fc fragments (50 kDa) are obtained. F(ab')₂ is produced by pepsin digestion and is formed by two Fab' fragments linked together through the disulphide bonds of the hinge region. F(ab')₂ is divalent with a molecular weight of about 110 kDa and can generate two Fab' fragments with free cysteine when undergoes a mild reduction process in presence of reducing agents such as DTT or β -MA.

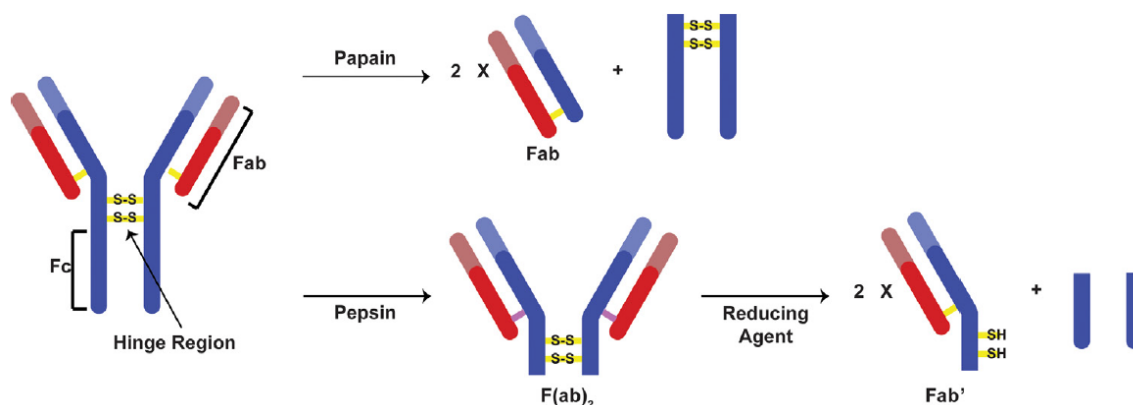


Figure 18. Proteolytic fragments obtained from IgG digestion mediated by pepsin or papain¹⁰⁴.

3.15 Polyethylene glycol (PEG)

In this work, a polyethylene glycol chain was used as linker between the drug (or the dye) and the FcBM. Polyethylene glycol is a synthetic polymer with a linear or branched structure, made of repetitive units of ethylene oxide which gives amphiphilic properties to the polymer^{105, 106}.

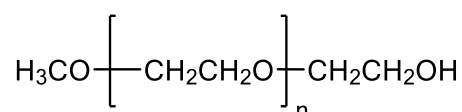


Figure 19. General structure of polyethylene glycol (PEG).

PEG is synthesized by anionic ring opening polymerization of ethylene oxide, a reaction initiated by nucleophilic attack of a hydroxide ion on the epoxide ring. The polymer is available in a variety of molecular weights and different end groups can be prepared by using suitable initiator and/or termination reagents. In this way, numerous functionalities can be introduced, and it is also possible to obtain heterobifunctional products. PEG has a relatively narrow polydispersity (Mw/Mn) in the range of 1.01 for low molecular weight PEGs (< 5 kDa) and of 1.1 for high molecular weight PEGs (> 5 kDa). The polymer is soluble in most organic solvents and in water; each ethylene oxide unit typically binds 2-3 water molecules. For this and for the high flexibility of the backbone chain, a PEG molecule acts as if it were five to ten times as large as a soluble protein of comparable molecular weight. PEG is considered a non biodegradable polymer, however, low molecular weight oligomers (< 400 Da) have been shown to be degraded in vivo by alcohol dehydrogenase generating toxic metabolites¹⁰⁷. PEGs with a molecular weight above 1000 Da are non toxic and cleared in vivo without structural

Introduction

change. Clearance rate depends on the molecular weight: PEGs with MW < 20 kDa are rapidly cleared in urine, while higher MW PEGs are cleared more slowly in urine and feces. PEGs with MW > 40 kDa remain in the blood stream for long time and accumulate in the liver.

Thanks to its non toxicity and biocompatibility, PEG has received FDA approval for use in pharmaceutical and cosmetic formulations. In particular, it is one of the most exploited polymers in drug delivery applications. PEGylation, the covalently attachment of PEG to proteins or small drug molecules, was first described in the 1970s by Davies and Abuchowsky^{108, 109}. This modification gives active conjugates with improved chemical-physical, pharmacokinetic and pharmacodynamic properties: low immunogenicity, low antigenicity, increased serum lifetimes, increased solubility of hydrophobic molecules, reduced clearance rate, prevention of degradation by cells and enzymes, and reduced aggregation and absorption¹¹⁰.

Table 3. Polyethylene glycol (PEG)-modified proteins approved by FDA¹¹¹.

Drug	Protein	Protein Size (kDa)	PEG Size (kDa)	Functional Group on PEG	Site of Attachment	Site-Specific	Year of Approval	Use
Adagen®	Adenosine deaminase	40	5	Succinimidyl ester	Lysines, serines, tyrosines, histidines	No	1990	Severe combined immunodeficiency disease
Oncaspar®	Asparaginase	31	5	Succinimidyl ester	Lysines, serines, tyrosines, histidines	No	1994	Leukemia
PegIntron®	Interferon- α -2b	19.2	12	Succinimidyl ester	Lysines, serines, tyrosines, histidines, cysteines	No, but 47.8% one isomer	2000	Hepatitis C
Pegasys®	Interferon- α -2a	19.2	40	Succinimidyl ester	Lysines	No	2001	Hepatitis C
Neulasta®	Granulocyte colony-stimulating factor (G-CSF)	18.8	20	Aldehyde	N-Terminal amine	Yes	2002	Neutropenia
Somavert®	Human growth hormone (hGH)	22	5	Succinimidyl ester	Lysines, N-terminus, phenylalanine	No	2003	Acromegaly
Mircera®	Erythropoietin (18 unglycosylated)	30	40	Succinimidyl ester	Lysines	No	2007	Anemia
Cimzia®	Anti-tumor necrosis factor (TNF) α Fab'	51	40	Maleimide	C-Terminal cysteine	Yes	2008	Rheumatoid arthritis, Crohn disease, psoriatic arthritis
Krystexxa®	Urate oxidase	34	10	p-Nitrophenyl carbonate ester	Lysines	No	2010	Gout
Omontys	Synthetic, dimeric peptide (erythropoiesis stimulating agent)	4.9	40 (2 20 kDa chains)	Succinimidyl ester (added during chemical synthesis of the peptide)	Lysines	Yes	2012 (Recalled 2014)	Anemia in chronic kidney disease

Although PEG has been traditionally considered only weakly immunogenic, some recent studies have suggested that PEG conjugates are able to induce anti-PEG antibodies associated with the rapid clearance of subsequent doses of PEGylated therapeutics¹¹². In addition, it has been shown that the PEGylated liposomal formulation of doxorubicin, Doxil, can activate the complement system and potentially cause hypersensitivity reactions in animal models. Those

recent observations have focused researchers' attention on PEG immunogenicity and further investigations are in current advancement.

In the first generation of PEGylated proteins, the most common reactive groups involved in coupling were amino groups of lysine residues because they are the most represented groups in proteins, generally exposed to the solvent and modifiable with a wide selection of chemical strategies^{113, 114}. A lot of PEG derivatives have been used for this modification, including PEG-dichlorotriazine, PEG-tresylate, PEG-succinimidyl carbonate, PEG-benzotriazole carbonate, PEG-p-nitrophenyl carbonate, PEG-trichlorophenyl carbonate, PEG-carbonylimidazole and PEG-succinimidyl succinate. The obtained products were heterogeneous mixtures of conjugated isomers, such as in the case of PEG–asparaginase and PEG–adenosine deaminase, differing in the number of coupled polymer chains and in the tethering site. Product heterogeneity complicates downstream purification, and characterization and batch-to-batch reproducibility are difficult to be achieved. The evolution of PEGylation chemistry has allowed site-specific protein modification that has also permitted to better preserve the native protein activity in the conjugate.

An example of selective conjugation is N-terminal PEGylation, that takes advantage of the different pKa values between the ϵ -amino residue of lysines (about 9.3–9.5) and the α -amino group at the N-terminus (about 7.6–8). The reaction is performed in mildly acidic buffers (pH 4.5–6) since in this condition the lysines will be protonated and consequently non reactive, while a significant fraction of free α -amino groups will be non protonated and available for coupling. This strategy employed PEGylating agent with a low reactivity, such as PEG-aldehyde, differently, a high reactive PEG will yield substantial degrees of lysine coupling. PEGylation at N-terminus is a two-step reaction. Initially, a *Shiff* base is formed between the aldehyde group of PEG and the α -amino group of protein. Then, *Shiff* base is converted into a stable secondary amino group by adding a reducing agent¹¹⁵.

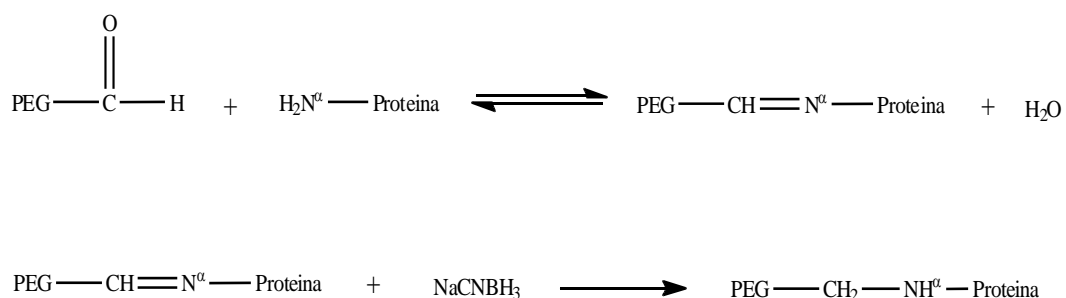


Figure 20. Reaction mechanism for the N-terminal PEGylation of a protein.

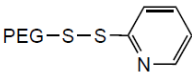
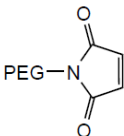
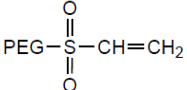
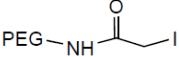
Introduction

This strategy was employed for the preparation of numerous PEGylated proteins such as Neulasta, the N-terminal PEGylated form of G-CSF (granulocyte colony-stimulating factor), that has gained a great therapeutic success after FDA approval in 2002.

Another site-specific PEGylation approach exploits the reactivity of thiol groups of cysteines that are not engaged in disulphide bridges, since cysteines in reduced form are rarely present in proteins or peptides. Unfortunately, cysteines are often buried inside hydrophobic cleft and therefore are only partially accessible to reagents. A simple alternative strategy, although less specific, relies on the reduction of protein disulphide bridges with the aim of exposing new thiol groups. This strategy has been used for the PEGylation of antibodies and their Fab fragments because the conjugation sites are localized far from the antibodies recognition region. Moreover, thanks to genetic engineering, cysteine residues can be introduced almost anywhere in the protein sequence giving new sites for protein PEGylation. PEG maleimide is the most commonly used reactive PEGylating agent to achieve cysteine modification. According to the mechanism of reaction, thiol group of cysteine and the double bond of the maleimide ring undergo a Michael's addition and form a thioether bond. The optimal pH of the reaction solution is 6.5-7.5, since at more alkaline pH values protein's amino groups can also react with maleimide. There are two main causes of instability of these conjugates. First, the maleimide ring tends to open forming an inactive derivative. Second, cases of retro Michael's addition involving substitution of the protein coupled to PEG-maleimide with albumin or glutathione have been reported *in vivo*¹¹⁶.

Another strategy for thiol PEGylation exploits orthopyridyl disulphide PEGs, creating a disulphide link between the polymer and the protein, which might be reduced *in vivo* in certain intracellular compartments⁴⁷.

Table 4. Some selective thiol PEGylating agents¹¹⁴.

Structure	Thioreactive PEGs	Properties
	PEG-pyridyldisulphide	The most specific towards thiol but yields a cleavable linkage by a reducing agent also <i>in vivo</i> .
	PEG-maleimide	Gives stable linkage by double bond addition but can also react with amines at pH >8.
	PEG-vinylsulfone	
	PEG-iodo acetamide	Less reactive, not much used

With the evolution of PEGylation chemistry, many heterobifunctional PEGs have been synthesized. PEGs bearing dissimilar terminal groups may be used to link two entities where a hydrophilic, flexible, and biocompatible spacer is needed. Nowadays, heterobifunctional PEG are used in a variety of ways including macromolecules binding to surfaces (for immunoassays, biosensors, etc), targeting of drugs, liposomes and, and many others.

3.16 Tubulysin A

Tubulysins are a novel class of therapeutics discovered by Höfle and co-workers, that originally isolated these compounds from the broth of myxobacteria strains in 2000^{117, 118}. Two different species of myxobacteria were identified to produce tubulysins, *Archangium gephyra* and *Angiococcus disciformis*. From a structural and biosynthetic point of view, tubulysins are related to dolastatin 10, which was isolated from the sea hare *Dolabella auricularia*¹¹⁹. They are linear tetrapeptide made of unusual amino acids; in particular, Tubulysin A (TubA) is formed by N-methyl pipecolic acid, L-isoleucine (Ile), a novel amino acid named tubuvaline (Tuv), and a novel chain-extended tyrosine analogue named tubutyrosine (Tut)^{120, 121}. The hydroxyl group of tubuvaline is acetylated, and the amino group forms an N,O-acetal, which is O-acylated with 3-methyl butyric acid. To date, 14 different tubulysins were identified.

Tubulysins are potent inhibitors of tubulin polymerization with IC50 values between 0.01 and 10 nM. The great interest they have aroused is due to their high cytotoxicity against a wide range of human cancer cells lines, including multi-drug resistant carcinoma models.

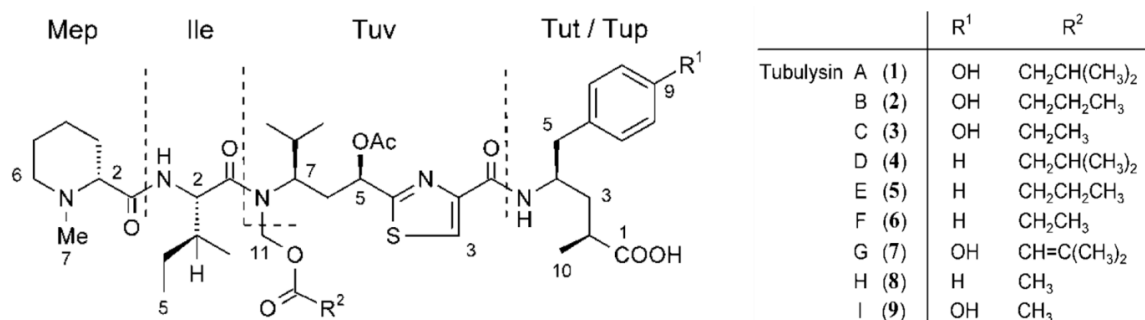


Figure 21. General chemical structure of tubulysins¹¹⁸.

Microtubular apparatus plays a crucial role in cellular life, especially for growth, mitosis and cell morphology. For these reasons, microtubules are attractive targets for anticancer therapies. They are dynamic structures made of α - and β - tubulin heterodimers that rapidly polymerise and depolymerise. Inhibitors of tubulin polymerization, such as Tubulysin A, cause a depletion of cell microtubules that leads to cell cycle arrest at the metaphase/anaphase (G2/M phase) transition and finally induce apoptosis.

Nowadays, microtubules are a well-established target in anticancer therapy. However, tubulin-binding agents are generally limited by poor therapeutic indices, emerging mechanisms of drug resistance, suboptimal pharmacokinetics due to poor aqueous solubility and severe toxicity. Like other microtubule inhibitors, tubulysins have not shown promise as stand-alone agents because of the extreme toxicity but, after Kadcylla and Adcetris approval, they have become attractive payloads for selective targeting of cancer via ADCs^{122, 123, 124}. In fact, Kadcylla and Adcetris carry as payloads tubulin binding agents, maytansinoid and auristatin, and now there is strong interest in the development of additional similar agents that may offer advantages over existing payloads.

In ADCs, drugs require a suitable “handle” to tether the linker, for this reason, we used a Tubulysin A modified with a 3-pyridyldithio propionate at C1. The introduction of a disulphide bridge has permitted to attach the drug to the linker through a thiol-disulphide exchange reaction.

3.17 Drug conjugation via reversible disulphide linkages

A disulphide bond (S-S) is a covalent linkage resulting from the oxidation of two sulphhydryl (SH) groups. This type of bond has been largely exploited in the design of drug delivery systems thanks to its relative stability in plasma and its reversibility in reducing environments as the cellular cytoplasm. The high redox potential difference between the oxidizing extracellular

space and the reducing intracellular space makes possible to achieve the cleavage of disulphide bonds upon cell entry and obtain a control over drugs site of release. In the cytosol, disulphide bond formation is prevented by the presence of small redox molecules and redox proteins, whose active site is regenerated by the previous ones or by some enzymes. Glutathione is the most abundant non-protein reducing agent in mammalian cells where it reaches a concentration in the millimolar range¹²⁵. The redox state of glutathione is based on the ratio between the reduced form, GSH, and the oxidized form, GSSG, which is typically greater than 100 due to the activity of glutathione reductase and NADPH. On the opposite, GSH concentration in plasma is typically $\approx 10 \mu\text{M}$. In addition, the enzymes of the thioredoxin family catalyze reducing reactions and are regenerated by the thioredoxin reductase that maintains their active site in the reduced state. As a result, the cytoplasmic environment prevents disulphide bonds formation. Reduction is also considered an essential component in the antigen-processing pathway subsequent to internalization in order to facilitate the proteolytic degradation of proteins¹²⁶. It is believed that lysosomal environment is kept in a reducing state by cysteine¹²⁷. Cysteine transporters are present on lysosomes membranes and produce a net influx of cysteine inside them. In nature, this mechanism is exploited by several potent toxins such as diphtheria toxin, ricin and abrin that become active after the cleavage of their interchain disulphide bonds.

3.18 Trastuzumab

Trastuzumab and rituximab have been here chosen as active targeting moiety for ADSs because they specifically bind to two of the most validated and well known cancer targets, they are used in clinic and Trastuzumab is also already approved as part of an ADC in adotrastuzumab-emtansine.

Trastuzumab is a recombinant humanized immunoglobulin G1 kappa produced by Genentech (South San Francisco, CA) and present on the market with the brand name of Herceptin¹²⁸. In 1998, it obtained FDA approval for patients with invasive breast cancers that overexpress human epidermal growth factor receptor type 2 (HER2, also referred to as HER2/neu or ErbB2), becoming the first monoclonal antibody used in the treatment of a solid tumour¹²⁹. Trastuzumab is produced by chinese hamster ovary (CHO) cell culture and contains human framework regions with murine CDRs that bind with high affinity -in nanomolar range- the extracellular domain of human HER2. The HER2 gene encodes a 185-kD transmembrane/kinase receptor that is over-expressed in 20 to 30% of invasive breast carcinomas and in other

Introduction

human malignancies. HER2 over-expression leads to a faster cells division and growth, and is associated with poor clinical prognosis (recurrences, metastasis, reduced survival). HER2 is part of the HER/ErbB2/Neu family of receptors which also includes HER1/EGFR, HER3 and HER4. They are glycoprotein receptors formed by an extracellular domain that permits ligand binding, a transmembrane region and a cytoplasmic tyrosine kinase domain¹³⁰. HER receptors exist as monomers, but they form dimers upon ligand binding thanks to the higher stability of the complex between a ligand and two receptors. The dimers can be both homodimers between the same receptors type (e.g. HER3-HER3) and heterodimers between different receptors types (HER2-HER3). The HER family is involved in the transmission of signals that control normal cell growth and differentiation. A range of growth factors serve as ligands, but none is specific for the HER2 receptor that is considered an orphan receptor¹³¹. HER1 is activated by six ligands, such as epidermal growth factor (EGF) and transforming growth factor α (TGF α), whereas HER3 and HER4 bind neuregulins (NGFs). Even in absence of a specific ligand, HER2 receptor is able to participate in heterodimers formation for signal transduction. In fact, it results to be the favourite partner for dimerization among HER receptors and HER2 containing heterodimers generate a more potent signal than the other dimer combinations. The most potent combination is HER2-HER3 that is the predominant in carcinoma cells. HER2-containing heterodimers have an increased potency because of the relative slow rate of ligand dissociation and the slow rate of receptors internalization, that give a prolonged activation of signaling pathways. In fact, these receptor complexes phosphorylate a variety of substrates triggering various signal transduction cascades, which are essential to the development and progression of cancer cells.

Trastuzumab's mechanism of action has not been fully elucidated, even if literature reports several proposed mechanisms including down-regulation of HER2 receptor by accelerating endocytic degradation, and inhibition of HER family dimerization^{128, 132}. In addition, Trastuzumab induces a host immune response via antibody-dependent cell cytotoxicity (ADCC) mechanisms and complement activation. In ADCC mechanism, Trastuzumab activates natural killers cells that express the Fc gamma receptor, inducing the lysis of cancer cells bound to Trastuzumab.

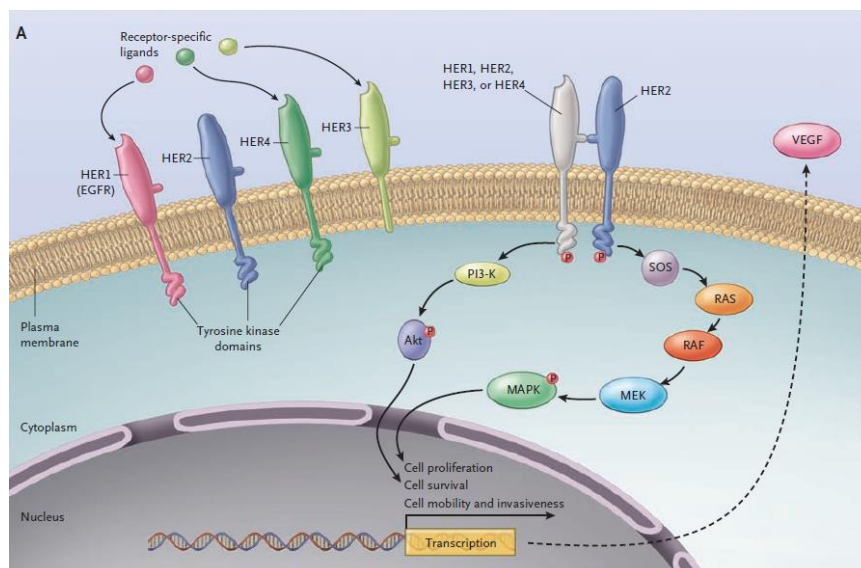


Figure 22. Pathways involved in downstream signaling after HER2 activation¹²⁸.

Some molecular mechanisms of Trastuzumab resistance have been reported¹³³. A potential mechanism of resistance is associated with increased expression of the membrane glycoprotein MUC4 that was shown to bind and sterically hinder HER2 receptor, preventing the interaction with the antibody. Trastuzumab resistance has also been associated with increased signaling from the insulin-like growth factor-I receptor (IGF-IR) that reduces Trastuzumab-mediated growth arrest of HER2-overexpressing breast cancer cells. In addition, constitutive PI3K/Akt activity was shown to inhibit cell-cycle arrest and apoptosis mediated by Trastuzumab.

Trastuzumab therapy is generally well tolerated and, during clinical trials, the most common side effects were mild to moderate chills and fever, associated primarily with the first infusion¹³⁴.

3.19 Rituximab

Rituximab is an engineered chimeric monoclonal antibody with human IgG1 and *k* constant regions linked to murine light-chain and heavy-chain variable sequences¹³⁵. It is produced by mammalian CHO cell suspension culture and sold under the brand name of Rituxan or MabThera. In 1997, FDA approved Rituximab for the treatment of indolent B-cell non-Hodgkin's lymphoma (NHL) and it became the first monoclonal antibody approved for clinical use in cancer therapy. NHL is the most common hematologic cancer in adults and approximately 85% of the cases are of B cell origin¹³⁶. NHL patients receive Rituximab either as

Introduction

a single agent or more often in combination with chemotherapy. Rituximab's use has now expanded to virtually any CD20-positive NHL, including marginal-zone lymphoma, lymphoplasmacytic lymphoma, small lymphocytic lymphoma, and to other areas such as immune-related diseases (immune thrombocytopenic purpura, systemic lupus erythematosus, myasthenia gravis, rheumatoid arthritis and post-transplant lymphoproliferative disease)¹³⁷.

Rituximab recognizes with high affinity (K_d 5×10^{-9} M) the CD20 antigen through the Fab regions of murine 2B8 antibody. CD20 is a 35 kDa transmembrane protein present on pre-B and mature B lymphocytes. It is first expressed on pre-B cells and persists until later in differentiation but is absent on terminally differentiated plasma cells, stem cells or other normal tissues. The binding of rituximab to CD20 leads to a depletion of both CD20 positive normal B cells and tumour cells in the peripheral blood and bone marrow. Despite the absence of normal B cells for approximately six months, there are only mild a reduction of IgM and IgG serum levels and any significant increase in infectious risk.

CD20 represents the ideal target: it is expressed at high levels and in a heterogeneous manner in many lymphoma types, is not down-regulated after the binding to the antibody, and is not shed or secreted into the circulation. The receptor is made of four transmembrane regions with two extracellular loops, a larger one between the third and fourth transmembrane regions and a smaller one between the first and the second ones. Rituximab is able to recognize and bind the larger loop. Three different mechanisms have been proposed for the elimination of B cells after rituximab's binding: stimulation of the apoptotic pathway, ADCC and CDC.

The function of CD20 remains unclear; it acts as a calcium channel either directly or activating another calcium channel^{138, 139}. The receptor is associated with a number of tyrosine kinases, including lyn, fyn, lck and p75/85 kinase, and its engagement leads to the activation of phospholipase C γ . The stimulation of this complex signaling pathway results in cell cycle arrest or apoptosis. Resistance to rituximab might be due to alterations in intracellular signals.

Common side effects correlated with rituximab therapy consist of fevers, chills, rigor, orthostatic hypotension and bronchospasm. During the infusions, patient can experience other adverse events including headache, nausea, vomiting, rhinitis and mild hypotension.

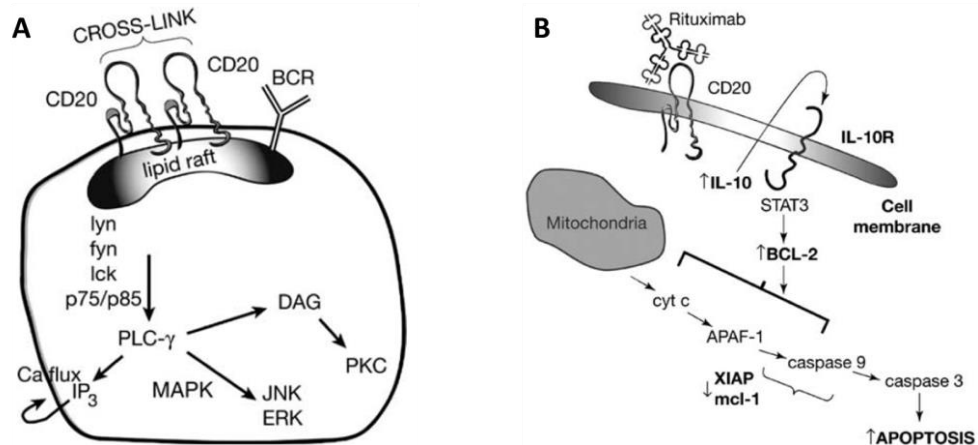


Figure 23. A) Intracellular signaling pathways activated by crosslinking of CD20 and B) apoptotic control pathways involved in Rituximab-induced apoptosis¹³⁸.

3.20 Endothelium targeting

The endothelium is a specialized tissue constituted of different endothelial cells (ECs) subtypes and associated with a wide variety of pathological conditions such as ischemia, thrombosis, inflammation and vascular oxidative stress. Therefore, the endothelium and, in particular, the monolayer of EC, that line the luminal surface of blood vessels, represent a promising target for the pharmacological treatment of some acute and chronic conditions, including cardiovascular and pulmonary diseases and diabetes¹⁴⁰. Moreover, ECs are highly accessible to drugs circulating in the bloodstream. ECs in the lung vessels represent a privileged vascular target since approximately 30% of total endothelial surface is contained in lung and lung endothelium experiences a relatively slow perfusion rate which favors the binding of ligands to ECs.

One of the most studied ECs surface determinants is the intercellular adhesion molecule-1 (ICAM-1), that was first identified by Springer and co-workers in 1986¹⁴¹. ICAM-1 belongs to the immunoglobulin (Ig) supergene family and is a transmembrane glycoprotein that contains five IgG-like binding domains followed by a hydrophobic transmembrane domain and a cytoplasmatic tail, for a total of 505 amino acids and a molecular weight of 110 kDa¹⁴¹. The IgG-like domains have a β sheet structure stabilized by disulphide bonds between cysteine residues, except for the fourth domain.

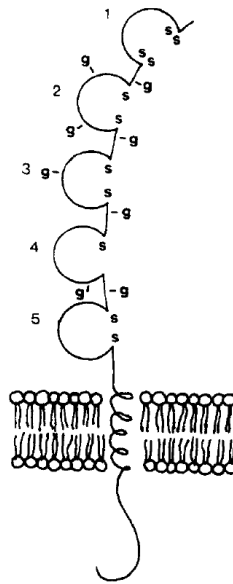


Figure 24. ICAM-1 structure¹⁴¹.

ICAM-1 is expressed constitutively at low levels on ECs and on some lymphocytes and monocytes, however its expression can be induced by cytokines and proinflammatory factors such as tumor necrosis factor- α (TNF α), interleukin-1 (IL-1) and interferon- γ (INF γ), also on other cell types including fibroblasts, epithelial cells, neurons and some cancer cells¹⁴². Adhesion molecules mediate the interaction between cells. In the case of ICAM-1, the receptor mediates the interaction between ECs and leukocytes. ICAM-1 plays an important role in the migration of leukocytes to the site of inflammation because it binds two β 2 integrin molecules present on the surface of these immune cells: LFA-1 through the first IgG-like binding domain and MAC-1 through the third domain. The cytoplasmic tail of ICAM-1 interacts with the cytoskeleton protein α -actinin¹⁴³.

Other ICAM-1 ligands are CD34 (leukocytes and platelets), fibrinogen, hyaluronan, rhinovirus and *Plasmodium falciparum* malaria-infected erythrocytes. ICAM-1 may also participate in signal transduction across cell membranes activating specific kinases and giving as final results cytokine production, cell membrane protein expression, reactive oxygen species production and cell proliferation. The fact that ICAM-1 is over expressed in pathologic and inflammatory condition makes this adhesion molecule a useful target for the delivery of therapeutics to endothelial tissue. Vascular immunotargeting can be achieved using antibodies that recognize the extracellular portion of ICAM-1. In addition to acting as delivery vehicles, antibodies can block ICAM-1 and suppress leukocyte adhesion to ECs, providing an anti-inflammatory benefit to the effects of drugs. Anti-ICAM-1 conjugates internalization by endothelial cells has been studied by Koval and co-workers¹⁴⁴. According to their studies, ICAM-1 endocytic pathway,

called cellular adhesion molecule (CAM)-mediated endocytosis, is clathrin- and caveolar independent and is shown to traffic anti-ICAM-1 nanoparticles to lysosomes for degradation.

4 MATERIALS AND METHODS

4.1 Materials and instruments

Recombinant Protein G was purchased from ProSpec-Tany TechnoGene Ltd. (Israel), while secondary goat F(ab')₂ anti human IgG was obtained from Thermo Fisher Scientific (Waltham, MA, USA). Trastuzumab, rituximab and bevacizumab were gently provided by Veneto Institute of Oncology (IOV-IRCCS). Murine monoclonal antibodies against human ICAM-1 were provided by Robert Rothlein (Boehringer-Ingelheim, Ridgefield, CN). Control murine IgG and fluorescently labelled secondary antibodies were purchased from Jackson ImmunoResearch (West Grove, PA, USA). HUVECs were from Clonetics (San Diego, CA, USA) and M199 medium from Thermo Fisher Scientific (Waltham, MA, USA). Cy5-maleimide and Cy5-NHS ester were acquired from GE Healthcare (Uppsala, Sweden), while AlexaFluor dyes were purchased from Thermo Fisher Scientific (Waltham, MA, USA). N-succinimidyl-3-(2-pyridyldithio)-propionate (SPDP) was from Proteochem (Loves Park, IL, USA). BCA Protein Assay Kit for protein concentration quantification, trifluoroacetic acid, sinapinic acid, D₂O and all other reagents including salts and solvents were acquired from Sigma-Aldrich s.r.l. (Milan, Italy). H₂N-PEG20kDa-COOH was obtained from JenKem Technology USA and all other PEGs were from NOF Corporation (Tokyo, Japan). Precast gels for SDS-PAGE were purchased from Thermo Fisher Scientific (Waltham, MA, USA) and Bio-Rad (Milan, Italy). Pierce™ Dye Removal Columns for the elimination of unconjugated Cy5 was from Thermo Fisher Scientific (Waltham, MA, USA).

Spectrophotometric UV-Vis determinations were made on a Thermo Scientific Evolution 201 spectrophotometer (Waltham, MA, USA). Aqueous solutions were filtered with Millipore 0.22 µm cellulose acetate filter (Billerica, MA USA). pH measurement were made using a Metrom (Herisau, Svizzera) 794 Basic Titrino. Solvents and buffers were sonicated in a Branson-Emerson 5210 Ultrasonic Cleaner (Danbury, CT, USA). Samples were centrifuged using a D3024 High Speed Micro-Centrifuge (Scilogex LLC, Rocky Hill, CT, USA) or a Sorvall™ ST 16 Centrifuge (Thermo Scientific). Samples were lyophilized using a Hetosic HETO lyophilizator (Allerød,

Denmark) or a CentriVap Benchtop Vacuum Concentrators (Labconco, Kansas City, MO, USA) connected to a Heto cooling trap. Far-UV circular dichroism spectra were measured on a Jasco J-810 spectropolarimeter equipped with a Peltier temperature (Easton, MD, USA). Mass spectra were obtained with an Ab Sciex 4800 Plus MALDI TOF/TOF instrument (Framingham, MA, USA), an Applied Biosystems Mariner ESI–TOF instrument (Monza, MI, Italy) or a Xevo G2-S Q-ToF instrument (Waters Corporation, Milford, MA, USA). NMR spectra were obtained using a Brüker Avance 400 spectrometer (Rheinstetten, Germany). operating at 400.132 MHz and the spectra were processed with MestReNova software. Hydrodynamic diameters were determined using a Malvern Instrument Ltd. Zetasizer Nano ZS apparatus (Worcestershire, United Kingdom). Isothermal calorimetric experiments were performed with GE Healthcare VP-ITC MicroCalorimeter provided with a ThermoVac accessory (Uppsala, Sweden). Reactions were incubated in a water bath SCANVAC SHC 2000 Chillsafe™ (Labogene, Lynge, Denmark) or in an Eppendorf ThermoMixer C (Hamburg, Germany). Solutions were dried under vacuum using a Buchi R II Rotavapor (Flawil, Switzerland).

The used HPLC systems were the following:

- HPLC Jasco composed of two PU-1580 pumps and a UV-Vis 1575 detector (Oklahoma City, OK, USA);
- HPLC Shimadzu composed of two LC-10AD and a UV-Vis SPD-10AV detector (Kyoto, Japan);
- HPLC Agilent Technologies, 1260 Infinity model (Santa Clara, CA, USA).

For chromatographic separations, an AKTApurifier (GE Healthcare, Uppsala, Sweden) was also used. Electrophoretic runs were made using an Electrophoresis Power Supply 300 (Pharmacia, New Jersey, USA). During flow cytometry experiments cells were analysed using a flow cytometer FACS-CALIBUR (Becton Dickinson, Erembodegem, Belgium).

NGs mice were obtained from Charles River Laboratories International (Wilginton, MA, USA). Fluorescent images of cells were captured with Slidebook™ 4.2 software (Intelligent Imaging Innovation, Denver, CO, USA), ORCAER camera (Hamamatsu, Bridgewater, NJ, USA), a 60x objective (Olympus Uplan F LN; Olympus, Inc., Center Valley, PA), and DAPI, FITC and/or Texas Red filters (1160A-OMF, 3540B-OMF, 4040B-OMF; Semrock, Inc., Rochester, NY). Images were analysed using Image Pro 6.3 (Media Cybernetics, Silver Spring, MD, USA).

4.2 Synthesis of PDP-PEG_{20kDa}-aldehyde

The starting polymer is a linear heterobifunctional PEG 20 kDa with an amino group at one end and a carboxylic group at the other end (NH₂-PEG-COOH). First, the polymer was modified at the amino group with succinimidyl 3-(2-pyridyldithio)propionate (SPDP), a linker containing a disulphide bond that can be reduced to a thiol group aiming to provide a reactive chemical handle for the conjugation of a drug or a dye. SPDP contains a N-hydroxysuccinimide (NHS) group that rapidly reacted with the amino group of the PEG, forming a stable amide bond. Then, the carboxylic end group of PEG was tether to an acetal moiety whose hydrolysis permitted to obtain an aldehyde group that was exploited for the N-terminal PEGylation of protein G.

4.2.1 Synthesis of PDP-PEG_{20kDa}-COOH

500 mg of the heterobifunctional H₂N-PEG-COOH 20 kDa were dissolved in acetonitrile/0.2 M sodium borate buffer pH 8 1:2 v/v to reach the final concentration of 10% w/v. Then 3 equivalents of SPDP (MW 312.36 Da) were added in portions within an hour. The reaction solution was stirred at room temperature overnight. The unreacted amino groups of PEG were blocked by adding 100-fold molar excess of acetic anhydride with respect to the mmols of PEG. Before adding acetic anhydride, the degree of 3-(2-pyridyldithio)-propionate (PDP) activation was established by Snyder-Sobocinsky TNBS assay¹⁴⁵. PEG was dialyzed against water for 48 hours using a 3.5 kDa cut-off membrane and the dialyzed product was finally lyophilized. The percentage of PDP linkage was established also by pyridine-2-thione assay¹⁴⁶ and ¹H-NMR. PDP-PEG-COOH (D₂O, δ ppm): 3.68 (m, 1818.18 H, -O-[CH₂-CH₂-O]_n- PEG chain), 7.30 (dd, 1 H, C3 pyridyl ring), 7.80 (dt, 2 H, C4-C5 pyridyl ring), 8.40 (dd, 1 H, C6 pyridyl ring).

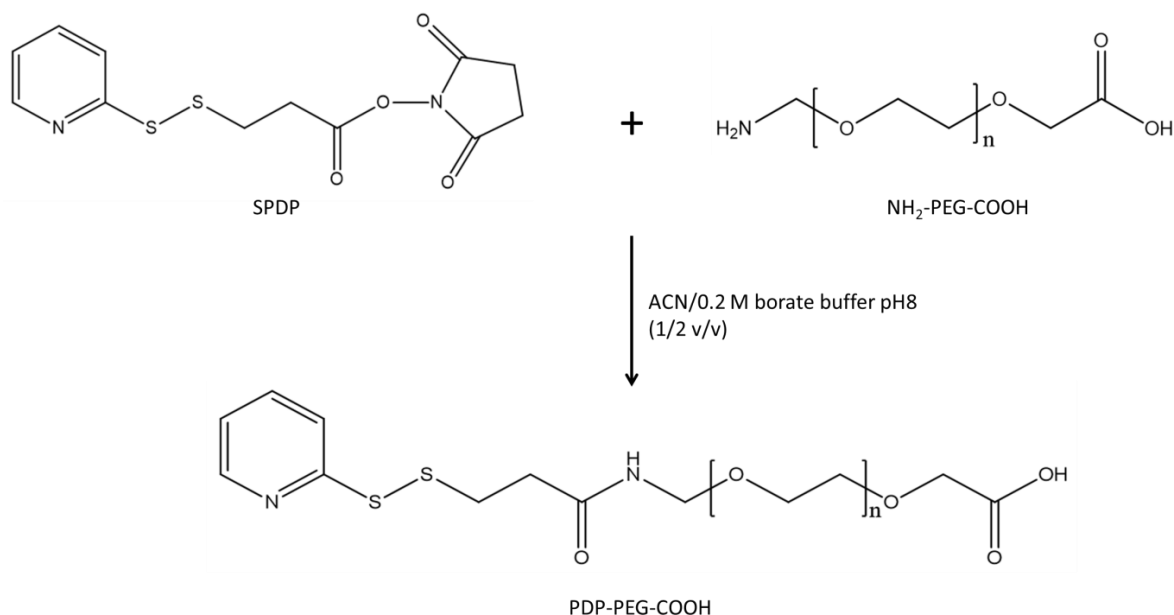


Figure 25. Synthesis of PDP-PEG-COOH.

4.2.2 Snyder-Sobocinsky TNBS assay for amino groups quantification

TNBS assay was exploited for the determination of the amount of SPDP tethered to PEG. In this assay a 0.285 mg/ml solution of the dipeptide glycyl-glycine (Gly-Gly, MW 132.12 Da) was used as reference together with an equimolar solution (47.47 mg/ml) of the starting NH₂-PEG-COOH 20kDa polymer. PDP-PEG-COOH was dissolved at a final concentration of 47.47 mg/ml to respect amino groups equimolarity between all the solutions. The samples were dissolved in 0.2 M borate pH 8.

The assay is based on the reaction between 2,4,6-trinitrobenzenesulfonic acid (TNBS) and primary amino groups. The product of this reaction is a chromophore with maximum absorption at 420 nm.

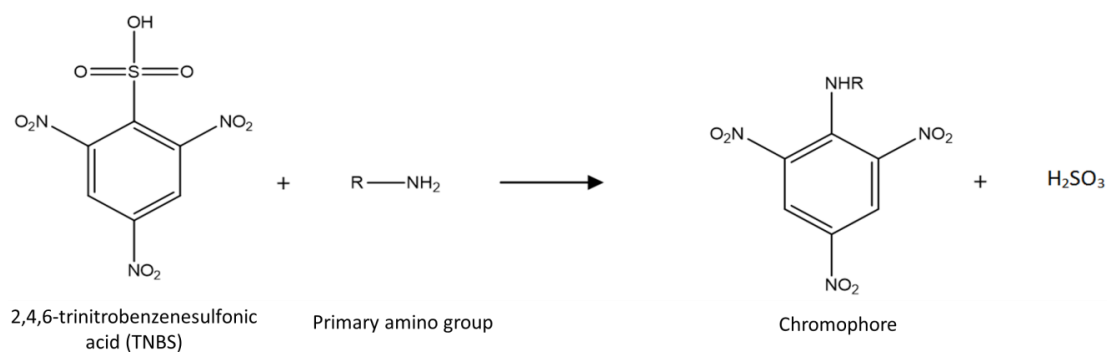


Figure 26. Chromophore formation after the reaction between TNBS and a primary amino group.

Materials & Methods

The assay was prepared as followed:

Blank	950 μ l of 0.2 M borate buffer pH 9.3
	25 μ l of 0.2 M borate buffer pH 8
	25 μ l of TNBS
Gly-Gly	950 μ l of 0.2 M borate buffer pH 9.3
	25 μ l of Gly-Gly 0.285 mg/ml
	25 μ l of TNBS
Polymers	950 μ l of 0.2 M borate buffer pH 9.3
	25 μ l of polymer solution 47.47 mg/ml
	25 μ l of TNBS

Reactions were incubated at room temperature for 30 minutes. Then, absorbance at 420 nm was measured. The percentage of free amino groups was calculated as:

$$\text{Abs}_{420} \text{ sample} : \text{Abs}_{420} \text{ reference} = x : 100$$

From the percentage of free amino groups, the percentage of SPDP linkage can be obtained:

$$\% \text{ SPDP activation} = 100 - x.$$

4.2.3 Pyridine-2-thione assay for the determination of PDP activation

The assay exploited the release of the chromophore pyridine-2-thione after the reduction of the disulphide bond. The aromatic ring of pyridine-2-thione is liberated with a 1:1 stoichiometry respect to PDP moles linked to the polymer, and presents a maximum absorbance at 343 nm. Measuring absorbance before and after the reductive step permitted to determine the degree of PDP activation. Absorbance at 343 nm of a 0.2 mg/ml solution of SPDP-PEG-COOH in PBS was measured and, then, DTT was added at a final concentration of 10 mM. After 15 minutes, absorbance at 343 was measured again.

PDP degree of activation was calculated as:

$$\Delta A = (\text{Abs}_{343} \text{ after DTT}) - (\text{Abs}_{343} \text{ before DTT})$$

$$(\Delta A / 8080) \times (\text{MW polymer} / \text{polymer concentration}) = \text{mols SPDP} / \text{mols polymer}$$

where 8080 is the molar extinction coefficient of pyridine-2-thione at 343 nm ($8080 \text{ M}^{-1} \text{ cm}^{-1}$).

4.2.4 Aldehyde functionalization of PDP-PEG-COOH

The activation of the carboxylic groups of PDP-PEG-COOH was carried out as follows: the intermediate was solubilized in dichloromethane at a final concentration of 10% w/w and 2 equivalents of *N,N'*-dicyclohexylcarbodiimide (DCC, MW 206.33 Da) and 2 equivalents of hydroxybenzotriazole (HOBT, MW 135.12 Da) were added.

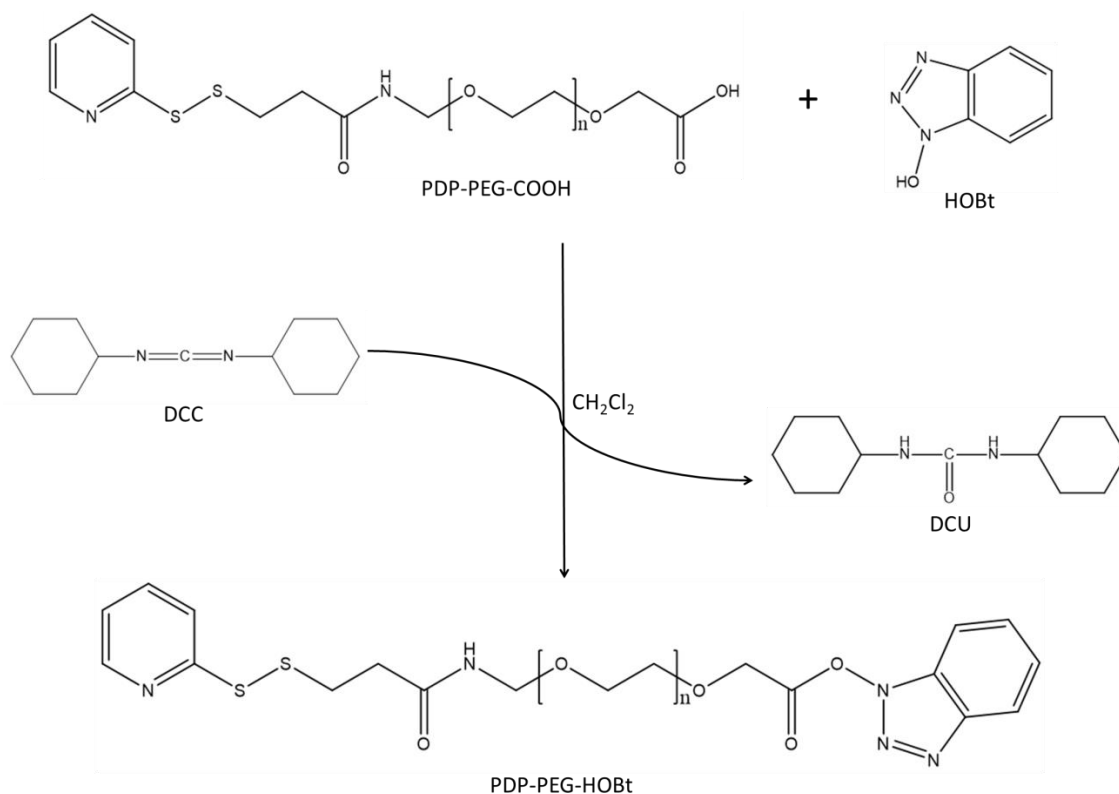


Figure 27. Activation of PDP-PEG-COOH carboxylic groups via DCC/HOBT.

After 1 h, 3 equivalents of 4-aminobutyraldehyd-diethylacetal (MW 161.24 Da) were added. If necessary, pH was adjusted to 8 with triethylamine. The reaction was let to proceed under stirring at room temperature overnight. The by-product *N,N*-dicyclohexylurea was removed by filtration and the solution was dropped in diethyl-ether to obtain the precipitation of the product. After 1 h at -20°C the product was recovered by filtration and dried under vacuum. The degree of diethylacetal derivatization was determined by $^1\text{H-NMR}$.

PDP-PEG-diethylacetal (D_2O , δ ppm): 3.68 (m, 1818.18 H, $-\text{O}-[\text{CH}_2-\text{CH}_2-\text{O}]_n-$ PEG chain), 1.15 (t, 6 H, $-(\text{OCH}_2\text{CH}_3)_2$).

Materials & Methods

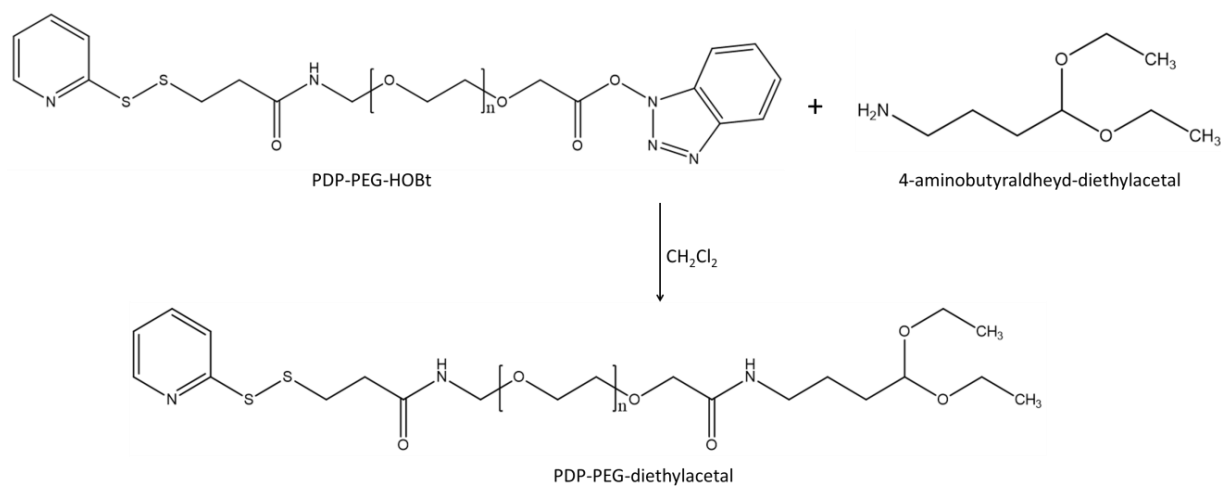


Figure 28. Synthesis of PDP-PEG-diethylacetal.

The acetal was hydrolysed at high temperature in acidic conditions to obtain the aldehyde group: PEG was dissolved in 25 mM phosphate pH 2.15 at the final concentration of 50 mg/ml and maintained at 60°C for 2 h. This solution was then added to Protein G solution in order to conjugate PEG to the N-terminus of the protein.

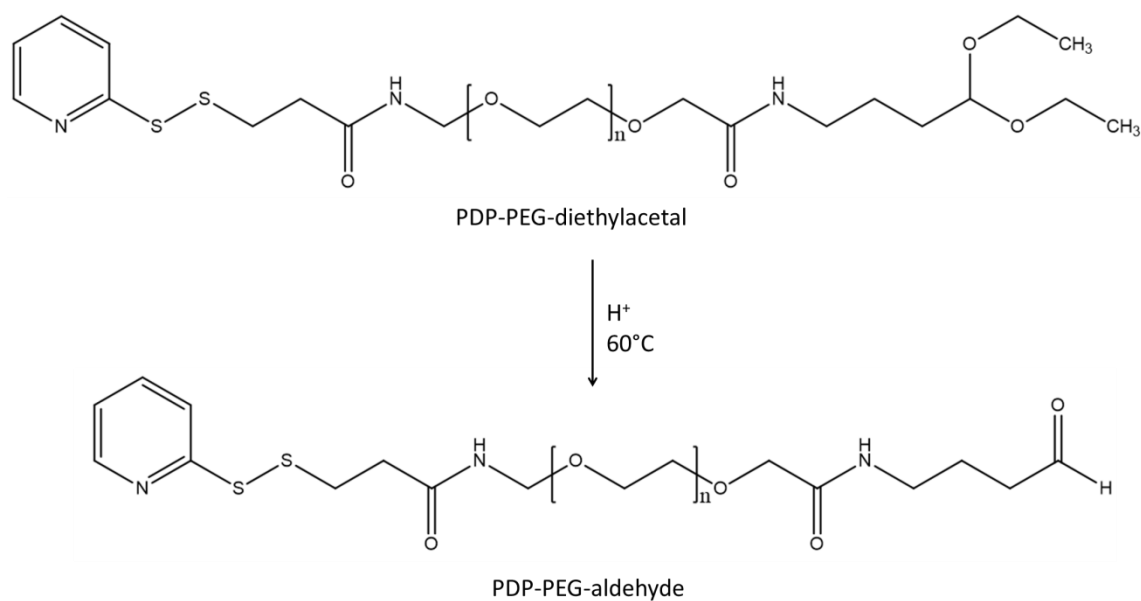


Figure 29. Hydrolysis of PDP-PEG-diethylacetal to PDP-PEG aldehyde in acidic conditions and at high temperature.

4.3 Synthesis of PEG_{20kDa}-Nter-Protein G and PDP-PEG_{20kDa}-Nter-Protein G

The N-terminal PEGylation of proteins takes advantage of the different pKa between the ϵ -amino groups of lysines (pKa = 9.5-10.2) and the N-terminal α -amino group (pKa = 7.6-8): at a slight acidic pH (pH 4.5-6) lysines amines are protonated while the N-terminus can still act as a nucleophile. Using a PEG-aldehyde, it is possible to obtain a *Shiff base*, between the polymer aldehyde group and the protein N-terminal amino group, which is then reduced to a secondary amino group by adding NaCNBH₃.

5 equivalents of PEG-aldehyde 20kDa (mPEG-aldehyde or PDP-PEG-aldehyde) and, after 1 h, 150 equivalents of NaCNBH₃ were added to a 1.6 mg/ml solution of Protein G (22.8 kDa) in 0.1 M sodium acetate buffer pH 4.5. The reaction mixture was stirred at room temperature for 48 h. Analysis of the reaction mixture were performed using a Jupiter C18 column (250 × 4.6 mm, 300 Å, 5 μ m; Phenomenex, USA) eluting with H₂O + 0.1% TFA (eluent A) and ACN + 0.1% TFA (eluent B) at 1.0 ml/min flow-rate (gradient B%: 0' 10%, 25' 60%, 28' 90%, 30' 10% B). The effluent was monitored at 226 nm. The purification of the conjugate was carried out with a DEAE-Toyopearl 650M column (1.6 × 4.5 cm) working at a flow-rate of 1.0 ml/min and registering the absorbance at 280 nm (buffer A: 10 mM Tris-HCl pH 8 and buffer B: 10 mM Tris-HCl, 0.1 M NaCl pH 8; gradient B%: 0' 0%, 10' 0%, 80' 100%, 105' 100%, 110' 0%). Before the injection, the buffer of the reaction solution was exchanged with the eluting buffer A. The peak of the conjugated protein was pooled and concentrated with Amicon Ultra Centrifugal filters. mPEG-Protein G was dialyzed against PBS and used for in vitro characterization and ITC binding studies with mAbs, while PDP-PEG-Protein G was conjugated to Cy5, AlexaFluor488 or TubA to perform cells and in vivo experiments.

4.4 Synthesis of Cy5- and AlexaFluor488-PEG_{20kDa}-Nter-Protein G

Cy5 and AlexaFluor488 are fluorescent dyes largely employed for conjugation to proteins or to polymers and used in a broad range of applications. Cy5 is a far-red-fluorescent dye with maximum excitation at 649 nm and maximum emission at 666 nm, while AlexaFluor488 is a green-fluorescent dye with maximum excitation at 493 nm and maximum emission at 525 nm. Both the dyes contain a maleimide group for the conjugation to the thiol group of HS-PEG-

Materials & Methods

Protein G. The optimal pH for the reaction is about 7-7.5: in these conditions thiol groups are sufficiently nucleophilic to react with the maleimide, whereas amino groups are mostly protonated and non reactive. The reaction was performed in PBS pH 7.4.

A 1.2 mg/ml solution of PDP-PEG-Protein G in DEAE eluting buffers was added of 100 equivalents of DTT and stirred for 1 h at room temperature in order to obtain HS-PEG-Protein G. DTT was removed by SEC chromatography using a Superdex® 200 Increase 10/300 GL column (30 cm × 10 mm, 8.6 µm particle size, GE Healthcare) eluting with PBS and 5 mM EDTA pH 7.4 at 0.5 ml/min and measuring absorbance at 280 nm. The purified peak of HS-PEG-Protein G was added of 3 equivalent of Cy5-maleimide (MW 817 Da) or AlexaFluor488-maleimide (MW 720.66 Da). The reactions were let to proceed overnight at room temperature and in the dark. Unreacted dye was removed using Pierce™ Dye Removal Columns and dye removal was confirmed by SEC-HPLC. The solution was dialysed against PBS and dye coupling was quantified by UV-Vis spectrophotometer analysis following the manufacturer instructions. The molar absorption coefficient of Cy5 at 650 nm is 250000 M⁻¹ cm⁻¹ and the absorbance of the conjugate at 280 nm was corrected for dye contribution, approximately the 5% of the absorbance at 650 nm. Similarly, the molar absorption coefficient of AlexaFluor488 at 493 nm is 72000 M⁻¹ cm⁻¹ and its contribution at 280 nm is approximately the 11% of the absorbance at 493 nm.

4.5 Synthesis of Tubulysin A-PEG_{20kDa}-Nter-Protein G

HS-PEG-Protein G was obtained as previously described. Methanol was added to the collected peak from Superdex column in order to have a final concentration of 30% v/v, that was necessary to guarantee TubA solubility. 3 equivalents of the toxin were added to HS-PEG-Protein G solution and the reaction was stirred overnight at room temperature. Then, reaction mixture was dialyzed against PBS and the insoluble TubA was removed by filtering the solution through a 0.22 µm filter. Reaction was monitored using a Jupiter C18 column (250 × 4.6 mm, 300 Å, 5 µm; Phenomenex, USA) working at a flow-rate of 1.0 ml/min and registering the absorbance at 254 nm (eluent A: 10 mM ammonium bicarbonate pH 7 and eluent B: ACN; gradient B%: 0' 40%, 10' 52%, 15' 70%, 18' 90%, 25' 40%). The sample was concentrated in Amicon and the loading of TubA was quantified by HPLC analysis using a calibration curve of standard toxin solutions.

4.6 Synthesis of AlexaFluor647-PEG_{5kDa}-maleimide

AlexaFluor647 has equivalent spectroscopic properties to Cy5 but is generally brighter and more stable. Alexa647-cadaverine contains an amino group that was exploited for the conjugation to the activate ester of the heterobifunctional polymer NHS-PEG-maleimide 5kDa. The maleimide group of the polymer was then reacted with cysteine residues a goat Fab' against the Fc of human IgGs.

A 4 mg/ml solution of Alexa647-cadaverine (MW 1000 Da) in 0.2 M borate, 25% DMF pH 8 was added of 1.15 equivalents of NHS-PEG-maleimide 5kDa and the reaction was monitored by SEC-HPLC reading absorbance at 649 nm (the polymer does not absorb at this wavelength). After 24 h of incubation in the dark, AlexaFluor647-PEG-maleimide 5kDa was dialyzed overnight against Milli-Q water in the dark and at room temperature.

4.7 Synthesis of goat anti-human-Fc NEM-Fab, (PEG_{5kDa})_n-Fab and (AlexaFluor647-PEG_{5kDa})_n-Fab

A 1.3 mg/ml solution of secondary goat anti-human-Fc F(ab')₂ in PBS pH 7.6 was treated with 10 mM cysteamine for 30 minutes at room temperature in order to obtain Fab'. The product was purified by gel filtration using Superdex column (buffer: 50 mM sodium phosphate, 150 mM sodium chloride, 10 mM EDTA, pH 5; 0.5 ml/min; 280 nm), and the collected peak of Fab' was immediately added of 50 equivalents of N-ethylmaleimide (NEM, MW 125.13 Da), or 20 equivalents of mPEG-maleimide or 8.15 equivalents of Alexa647-PEG-maleimide. Then, pH was brought up to 7 with sodium hydroxide. The reaction was let to proceed overnight at room temperature (and in the dark when AlexaFluor647 was present). NEM-Fab was then dialyzed against PBS using a 3.5 kDa cut-off membrane, while the reaction solutions between the protein and the polymers were purified by gel filtration eluting with PBS pH 7.4 and using the previous conditions. NEM-Fab and the collected peaks of the conjugates were analysed by SEC-HPLC, SDS-PAGE, MALDI-TOF and circular dichroism. Dye/Fab ration in (AlexaFluor647-PEG_{5kDa})_n-Fab was quantified by UV-Vis spectrophotometer analysis following the manufacturer instruction. The molar absorption coefficient of AlexaFluor647 at 650 nm is 239000 M⁻¹ cm⁻¹ and the absorbance of the conjugate at 280 nm was corrected for dye contribution, approximately the 3% of the absorbance at 650 nm.

4.8 PEGylation of Rituximab Fab' fragments

Rituximab was used as model IgG in order to compare its PEGylation pattern to goat Fab' PEGylation. As previously reported, Rituximab is a chimeric IgG1 and has a human hinge region with two disulphide bridges. The reduction of Rituximab F(ab')₂ is expected to provide two Fab' molecules each presenting two thiol group that can be PEGylated using a PEG-maleimide.

Rituximab was dialyzed against 0.1 M acetate pH 3.8 and digested by pepsin using an enzyme/substrate ratio of 1:50 (w/w) in order to obtain F(ab')₂. Digestion was performed incubating the solution at 37°C for 4 hours, then pepsin was quenched with 2 M Tris-HCl pH 8.2. F(ab')₂ was purified by gel filtration (Superdex column eluting with PBS pH 7.4 at 0.5 ml/min, 280 nm) and the collected peak was treated with 10 mM cysteamine for 30 minutes at room temperature. Cysteamine was removed by gel filtration (Superdex column; buffer: 50 mM sodium phosphate, 150 mM sodium chloride, 10 mM EDTA, pH 5; 0.5 ml/min; 280 nm) and Fab' peak was immediately added of 20 equivalents of mPEG-maleimide 5kDa and pH was adjusted up to 7. Reaction proceeded under stirring overnight at room temperature and was purified by gel filtration (Superdex column eluting with PBS pH 7.4 at 0.5 ml/min, 280 nm). The collected peaks were analysed by SDS-PAGE and MALDI-TOF.

4.9 Cy5 and AlexaFluor647 conjugation to monoclonal antibodies

Trastuzumab (145531 Da), Rituximab (143859.7 Da) and Bevacizumab (MW 149000 Da) were labelled with Cy5 or AlexaFluor647 to be used as positive or negative control in cells and in vivo studies. Fluorescent dyes have a NHS group that in basic conditions rapidly reacts with amino groups of lysine residues forming a stable amide bond between the dye and the antibody.

To a 1-2 mg/ml solution of antibody in PBS pH 8, 5-10 equivalents of Cy5-NHS (MW 791.99 Da) or AlexaFluor647-NHS (MW 1250 Da) were added and the reaction mixture was stirred in the dark overnight at room temperature. Unreacted dye was removed with Pierce™ Dye Removal Columns and dye removal was confirmed by gel filtration chromatography. The solution was dialyzed against PBS and dye coupling was quantified by UV-Vis spectrophotometer analysis.

4.10 NMR analysis

The degree of SPDP and diethylacetal derivatization of PEG was determined recording ^1H NMR spectra in a Brüker Avance 400 spectrometer (Rheinstetten, Germany) operating at 400.132 MHz. Samples were prepared dissolving the polymer in D_2O at a concentration between 5 and 10 mg/ml. The recorded spectra were processed with MestReNova software.

4.11 Determination of protein concentration

4.11.1 UV-Vis spectroscopy

Protein concentrations were determined spectrophotometrically measuring the absorbance at 280 nm and using the following extinction coefficients:

Protein	ϵ ($\text{mL cm}^{-1} \text{mg}^{-1}$)
Protein G	0.90
Goat Fab'	0.81
Rituximab	1.63
Trastuzumab	1.43
Bevacizumab	1.70

Extinction coefficients at 280 nm for PEG-proteins were considered unvaried respect to the unmodified protein.

4.11.2 Bicinchoninic acid (BCA) assay

BCA method is a colorimetric assay for the determination of total protein concentration in solution. It is based on the ability of peptide bonds to reduce Cu^{2+} ions from the copper (II) sulfate (a green solution) to Cu^+ , in basic condition and in a temperature dependent manner. After copper reduction, two molecules of bicinchoninic acid chelate a Cu^+ ion. The resulting complex is purple-coloured and has a maximum absorbance at 562 nm. The colour change of the sample solution from green to purple is proportional to protein concentration. The linear relationship between absorbance at 562 nm and protein concentration is preserved in a 0.1-1 mg/ml range of protein concentration.

Materials & Methods

The assay is performed as here described using a commercial kit from Sigma Aldrich. Standards were prepared dissolving bovine serum albumin (BSA) at different concentrations ranging from 0.1 to 1 mg/ml. Working reagent was prepared mixing bicinchoninic acid solution with CuSO_4 solution at a ratio of 50:1 v/v. 20 μl of each standard and of sample were added of 450 μl of working reagent and incubated at 37°C for 30 minutes. Then, absorbance at 562 nm was measured and a calibration curved was made using the standards, permitting to calculate the protein concentration of the sample.

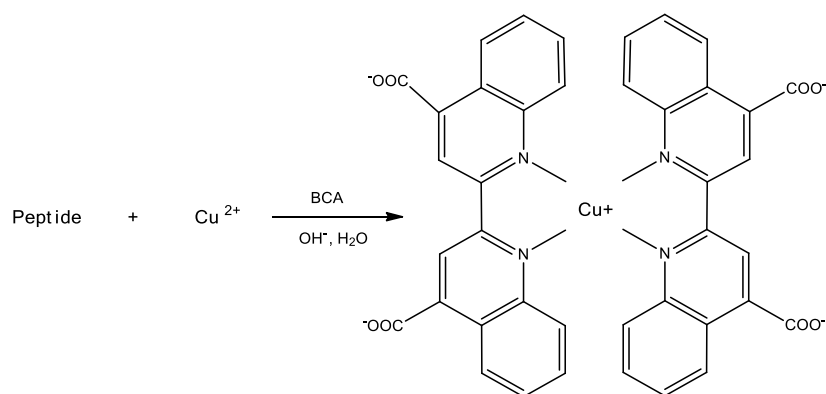


Figure 30. Complex between two molecules of bicinchoninic acid and a Cu^+ ion.

4.12 Sodium dodecyl sulphate polyacrylamide gel electrophoresis (SDS-PAGE)

Electrophoresis SDS-PAGE was performed according to Laemmli method¹⁴⁷ using precast gels with a gradient of polyacrylamide percentage (4-15% or 8-16%). After the run, the gel was stained with Coomassie Brilliant Blue R250 for protein detection, and with iodine and barium chloride for PEG visualization. Briefly, the gel was first pretreated with perchloric acid 0.1 M and then PEG bands were stained with a iodine and barium chloride solution (in acidic conditions). Iodine staining was removed using ascorbic acid. Finally, protein bands were colored with Coomassie. Unspecific staining of polyacrylamide was removed with a destaining solution (40% methanol, 7% acetic acid v/v). 5-10 μg of protein were dissolved in reducing or non reducing loading buffer according to the necessity and heated at 100°C for 5 minutes to favour protein denaturation. Non reducing loading buffer was composed of SDS, glycerol, bromophenol blue in TRIS-glycine pH 6.8 buffer. In addition reducing loading buffer contained DTT to reduce protein disulphide bonds. TRIS 0.0248 M, glycine 0.2 M, SDS 0.1% w/v buffer pH

8.3 was used as running buffer. During electrophoretic runs, voltage and amperage were set at 160 V and 40 A, respectively, and were maintained constant.

4.13 Mass spectrometry

ESI–TOF mass spectra (ESI-MS) were recorded on an Applied Biosystems Mariner ESI–TOF instrument (Monza, MI, Italy) or on a Xevo G2-S Q-ToF (Waters Corporation, Milford, MA, USA) instrument, operating in positive ion mode. Samples were dissolved in MilliQ water or methanol and from 2 to 10 µg of sample were injected in the mass spectrometer.

Mass spectra of PEG and PEGylated proteins were obtained using a MALDI spectrometer with a REFLEX time-of-flight (4800 Plus MALDI TOF/TOF, AB Sciex, Framingham, MA, USA) equipped with a SCOUT ion source, operating in positive linear mode. A pulsed UV laser beam (nitrogen laser, λ 337 nm) generates ions that are accelerated to 25 kV. Matrix (a saturated solution of sinapinic acid in water/ACN (1:1, v/v) + 0.1% TFA (v/v)) was mixed with an equal volume of sample and 1 µl of this mixture was loaded on the plate.

4.14 Circular dichroism analysis

Circular dichroic analyses were performed in order to assess if polymer conjugation caused a modification in protein secondary structure that could lead to a potential loss of biological activity. Far-UV circular dichroism spectra were measured on a Jasco J-810 spectropolarimeter equipped with a Peltier temperature control unit at 25°C. The samples were dissolved in PBS pH 7.4 at a protein concentration of 0.08-0.1 mg/ml. The spectra were collected between 200 and 250 nm with an average of 3 scans and the data at each wavelength were averaged for 8 s. The sample cell path length was 1 mm. CD data were converted to mean residue ellipticity, expressed in $\text{deg cm}^2 \text{dmol}^{-1}$ by applying the following formula:

$$\Theta = \Theta_{\text{obs}} (\text{MRW})/10L[\text{C}]$$

where Θ is the observed ellipticity in degrees, MRW is the mean residue weight of the protein (molecular weight divided by the number of amino acids), [C] is the protein concentration in mg/mL, and L is the optical path length in centimeters.

Protein G is a highly stable bacterial receptor. In order to establish if the protein could recover the secondary structure after thermal stress, Protein G was denatured gradually bringing the

temperature to 90°C. A thermal stability analysis was made increasing temperature from 25° to 90°C at a rate of 2°C/minute and wavelength was set at 209 nm. Then, temperature was brought down to 25°C and CD spectrum between 200 and 250 nm was registered again.

4.15 Dynamic Light Scattering (DLS) measurements

DLS was used to determine the size of unmodified proteins, PEGylated proteins and the complexes between FcBMs and antibodies. Hydrodynamic diameters were measured with a Zetasizer Nano ZS apparatus (Malvern Instruments Ltd., Worcestershire, United Kingdom) at 25°C with an average of three measurements. The instrument irradiates the sample with a 675 nm beam.

A series of solutions in PBS pH 7.4 with different antibody/FcBM molar ratios (1:0.25, 1:0.5, 1:1 and 1:2) were prepared maintaining fixed antibody concentration and varying protein concentration. The solutions were let to equilibrate for 1 h at room temperature and filtered with a 0.22 µm cellulose acetate centrifuge tube filter before analysis.

Three set of complexes between FcBM and Trastuzumab (Trs) were analysed, using the following FcBM: the complex between mPEG-protein G (mPEG-PG), PDP-PEG-Protein G (PDP-PEG-PG) and goat mPEG₂-Fab. Samples were prepared as reported in Table 5.

Table 5. Solutions of the complexes between FcBM and trastuzumab for DLS analysis.

Molar ratio Ab/FcBM	Set I		Set II		Set III	
	Trs (µM)	mPEG-PG (µM)	Trs (µM)	PDP-PEG-PG (µM)	Trs (µM)	mPEG ₂ -Fab (µM)
1:4	3.33	13.3	5.68	22.70	-	-
1:2	3.33	6.67	5.68	11.35	6.87	13.74
1:1	3.33	3.33	5.68	5.68	6.87	6.87
1:0.5	3.33	1.67	5.68	2.84	6.87	3.44
1:0.25	3.33	0.83	5.68	1.42	-	-

4.16 Isothermal Titration Calorimetry (ITC)

Affinity constants and binding stoichiometry between FcBM and antibodies were determined by isothermal titration calorimetry using a VP-ITC MicroCalorimeter (GE Healthcare, Uppsala, Sweden) provided with a ThermoVac accessory for thermostating and degassing samples. Samples were dissolved in PBS pH 7.4 and degassed before running the experiment. Sample cell was filled with antibody solution that was titrated with FcBM solution loaded in the injector syringe. Reference cell was filled with PBS. FcBM concentrations ranged from 6 to 14 μM , whereas antibody concentration was 0.7-2 μM . The first injection was of 1 μl , and all the subsequent of 10 μl every 240 seconds. The injection duration was 20 seconds and the stirring speed was set at 307 rpm. At every injection, some heat was developed due to the exothermic interaction between FcBM and antibody and the temperature in the sample cell became higher than in the reference cell. The amount of heat (q_i) is proportional to the amount of ligand that binds to the antibody in a specific injection ($v \times \Delta L_i$) and to the characteristic binding enthalpy (ΔH) for the reaction:

$$q_i = v \times \Delta H \times \Delta L_i$$

where v is the volume of the reaction cell and ΔL_i is the increase in the concentration of bound ligand after the i_{th} injection. For the case in which there is only one binding site, the equation becomes:

$$q_i = v \times \Delta H \times [P] \times \left(\frac{K_a [L]_i}{1 + K_a [L]_i} - \frac{K_a [L]_{i-1}}{1 + K_a [L]_{i-1}} \right)$$

where K_a is the binding constant and $[L]$ is the concentration of free ligand.

The instrumental response (measured signal) is the amount of power (microcalories per second) necessary to maintain constant the temperature difference between sample and reference cells.

Experiments were conducted at 30°C with a reference power of 9 $\mu\text{Cal}/\text{sec}$. The data were elaborated with Origin 7.0, MicroCal LLC ITC and fitted to “one set of sites” model to obtain the stoichiometry (n), the thermodynamic association constant (K_a) and enthalpy energy (ΔH°). The performed experiments were reported in Table 6.

Table 6. ITC experiments for the determination of affinity constant and binding stoichiometry between FcBM and antibodies.

Exp#	Sample cell	Injector syringe
1	Trastuzumab, 2 μ M	Protein G, 13.63 μ l
2	Trastuzumab, 1 μ M	mPEG-Protein G, 10.14 μ M
3	Trastuzumab, 1.05 μ M	Cy5-PEG-Protein G, 10.67 μ M
4	Trastuzumab, 2 μ M	Goat NEM-Fab
5	Trastuzumab, 2 μ M	(mPEG _{5kDa}) ₃ -Fab
6	Trastuzumab, 2 μ M	mPEG _{5kDa} -Fab

4.17 Flow cytometry

The capacity of an ADS to selectively bind the target antigen expressed on cells surface was assessed by flow cytometry analysis. Flow cytometry experiments were carried out in the laboratory of Prof Antonio Rosato at Istituto Oncologico Veneto. Trastuzumab and Rituximab were used as models to prepared the following ADSs:

- Cy5-PEG-Protein G/Trastuzumab,
- Alexa647-PEG-Fab/Trastuzumab
- (Alexa647-PEG)₂₋₃-Fab/Trastuzumab
- Alexa647-PEG-Fab/Rituximab
- (Alexa647-PEG)₂₋₃-Fab/Rituximab

During ADS preparation, the antibody was simply mixing to FcBM solution according to an FcBM/antibody molar ratio of 1:1. Solutions were then diluted with PBS in order to have a final antibody concentration of 0.2, 0.1 or 0.002 mg/ml.

The following human tumor cells lines were used for ADCs of Trastuzumab: IGROV-1 (HER2-) and SKOV-3 (HER2+) are ovarian adenocarcinoma cell lines; MDA/MB-231 (HER2-) and SKBR-3 (HER2+) are breast cancer cell lines. Trastuzumab-Cy5 or Trastuzumab-AlexaFluor647 were used as positive controls, while the ADCs of Rituximab was used as negative control since the antibodies does not recognize HER2 antigen.

The following cells lines were used for ADCs of Rituximab: LCL (CD20+) is a lymphoblastoid cell line generated by EBV infection of PBMC and A375 (CD20-) is a malignant skin melanoma cell line. In this case, Rituximab-Cy5 or Rituximab-Alexa647 were used as positive controls,

while the ADCs of Trastuzumab was used as negative control since it does not recognize CD20 antigen.

The samples were prepared in order to maintain constant the dye/targeting antibody ratio between ADS and antibodies controls (adding unconjugated antibody if necessary). Dye-PEG-FcBM was also tested in absence of the targeting antibody to verify if some non-specific binding to cell surface occurred.

ADSs stability was also tested incubating the system in human plasma at 37°C for 30 min. In this case, the ADS was diluted in plasma in order to reproduce Trastuzumab blood concentration about 0.044 mg/ml during therapy with Kadcyła®.

A further competition experiment was performed for the ADS Cy5-PEG-Protein G/Trastuzumab in order to verify if the complex was stable in presence of a competitive mAb (Bevacizumab) that does not recognize the target cells. An equivalent amount of non-specific mAb, with respect to the starting mAb, was added to the previously prepared ADS solution and the sample was tested by FACS analysis.

Cells were incubated in 25 or 75 cm² flasks at 37°C, 5% CO₂ and 95% humidity. Then, cells (3 x 10⁵/sample) were suspended in 200 µl of cold PBS and centrifuged at 1300 rpm for 5 minutes at 4°C to create a pellet. The supernatant was removed and the cells were added of 50 µl of the sample at the proper concentration. Cells were incubated in ice for 30 minutes in the dark. Before analysis, cells were washed twice with PBS, resuspended in 300 µl of FACS buffer (0.9% NaCl solution containing 2% bovine serum albumin and 0.02% NaN₃), and finally analyzed with a flow cytometer FACS-CALIBUR (Becton Dickinson). Data analysis was performed using the FlowJo 7.6.5 data analysis software package (TreeStar, USA).

4.18 Tubulysin A-PEG-Protein G/ Trastuzumab cytotoxicity

The cytotoxicity assay of the ADS TubA-PEG-Protein G/Trastuzumab was carried out in the laboratory of Prof Antonio Rosato at Istituto Oncologico Veneto. Briefly, in vitro cytotoxicity of TubA-PEG-Protein G/Trastuzumab, and as control Trastuzumab and TubA-PEG-Protein G alone, was assessed against MDA/MB-231 (HER2-) and SKBR-3 (HER2+) cell lines using the ATPlite luminescence adenosine triphosphate (ATP) detection assay system, according to the manufacturer's instructions. Briefly, cells were resuspended in complete medium and seeded into 96-well flat-bottomed plates (8x10³/well). The day after, different drug concentrations were added (final volume, 100 µl/well) for 72 hours. At day 4, 50 µl of lysis solution were added to each well followed by addition of 50 µl of substrate solution and final counting of

luminescence by the TopCount Microplate Counter (PerkinElmer). Within each experiment, determinations were performed in triplicate and experiments were repeated two times for each cell line. The percentage of cell survival was calculated by determining the counts per second (cps) values according to the formula: $[(cps_{\text{tested}} - cps_{\text{blank}})/(cps_{\text{untreated control}} - cps_{\text{blank}})] \times 100$, with cps_{blank} referring to the cps of wells that contained only medium and ATPlite solution. IC50 values were calculated from semi-logarithmic dose-response curves by linear interpolation.

4.19 Biodistribution studies

The in vivo capacity of an ADS to target the tumour site was studied performing biodistribution experiments in animal models. The experiments were conducted in the laboratory of Prof Antonio Rosato at Istituto Oncologico Veneto.

Biodistribution of Cy5-PEG-Protein G/Trastuzumab was performed in immunodeficient NSG mice. IGROV-1 (HER2-) and SKOV-3 (HER2+) tumour cells were inoculated in two animals via subcutaneous injection. After 10 days mice were injected intravenously with Cy5-PEG-Protein G/Trastuzumab or Trastuzumab-Cy5, both containing 1.3 nmol of Cy5. In vivo biodistribution was performed at different time points post-injection: 4, 8, 24, 48 and 72 hours. Biodistribution of Trastuzumab-Cy5 (this time containing 2.4 nmol in Cy5) was also repeated and prolonged over the time (1, 2, 3, 4, 5, and 7 days).

In vivo biodistribution was analyzed by total body scanning at the selected time points on isoflurane/oxygen anesthetized animals, using the MX2 scanner (ART, Montreal, Canada).

4.20 Cellular experiments using HUVECs

Pooled human umbilical vein endothelial cells (HUVECs) were maintained in M199 medium supplemented with 15% fetal bovine serum (FBS), 2 mM glutamine, 15 µg/ml endothelial cell growth supplement (ECGS), 100 µg /ml heparin, 100 U/ml penicillin and 100 µg/ml streptomycin. For the experiments, cells were seeded onto 12 mm² gelatin coated coverslips in 24-well plates and the cultures were maintained at 37°C, 5% CO₂ and 95% relative humidity. To induce ICAM-1 expression on the surface, cells were treated with 10 ng/ml of tumor necrosis factor-α (TNF-α) for at least 16 hours (and less than 20 h to avoid cell death). TNF-α treatment was shown to increase HUVEC ICAM-1 expression ~10- fold by flow-cytometry¹⁴⁴. TNF-α was removed by washing cells in serum-free media. In order to achieve endothelium targeting, a

mouse IgG2a against human ICAM-1 receptor (aICAM) was employed as targeting antibody in ADS formation.

4.20.1 Binding experiment

TNF- α activated and quiescent HUVECs were incubated with 300 μ l of a 111.11 nM solution of Alexa488-PEG-Protein G, Alexa488-PEG-Protein G/aICAM or Alexa488-PEG-Protein G/IgG for 1 hour at 37°C. Then, cells were washed with M199 to remove the unbound fraction and fixed with a 2% paraformaldehyde (PFA), PBS solution at room temperature for 15 min. Cells were washed again using PBS, mounted onto slides with Mowiol and analyzed by fluorescence microscopy.

4.20.2 Avidity experiment

TNF- α activated HUVECs were fixed with 2% PFA to avoid internalization and incubated for 1 hour at 37°C, with different concentrations (1.11, 2.22, 11.11, 22.22, 111.11 and 222.22 nM) of ADS (Alexa488-PEG-Protein G/aICAM) solution in order to determine the avidity of the ADS for cells over-expressing ICAM-1 receptor. Then, cells were washed with M199, fixed again with 2% PFA, washed using PBS, mounted onto slides with Mowiol and analyzed by fluorescence microscopy to measure the green fluorescence given by Alexa488.

4.20.3 Kinetic of binding experiment

Fixed activated HUVECs were incubate at 37°C with a 11.11 nM solution of the ADS for various incubation times (5 min, 15 min, 30 min, 1 h, 2 h and 23 h) in order to study the kinetic of binding of the ADS. Then cells were treated and analyzed by fluorescence microscopy as previously reported.

4.20.4 Internalization mechanism of Alexa488-PEG-Protein G/aICAM

The mechanism of uptake was evaluated conducting cellular experiments in absence (control) or in presence of one of the following pharmacological inhibitors of endocytic transport: 3 mM amiloride (inhibitor of CAM-pathway), 1 μ g/ml filipin (inhibitor of caveolar endocytosis), 50 μ M monodansylcadaverine (MCD; inhibitor of clathrin endocytosis), or 0.5 μ M wortmannin

Materials & Methods

(inhibitor of phosphatidylinositol 3 kinase (PI3K), involved in macropinocytosis)¹⁴⁴. TNF- α activated HUVECs were pre-incubated with each inhibitor for 30 min at 37°C, and then 300 μ l of an 11.11 nM solution of the ADS was added to the cells in the presence of the respective inhibitor for 1 h at 37°C. After the incubation time, ADSs that did not bind to cells were eliminated by washing with M199. Then, cells were fixed with 2% PFA and incubated with a Texas Red labelled secondary goat antibody that binds to aICAM located at cell surface, but cannot access aICAM that had been internalized within cells (since cells were not permeabilized). Nuclei were stained with 4',6-diamidino-2-phenylindole (DAPI). The effect of the inhibitors on the uptake of the conjugate was evaluated using fluorescence microscopy. ADSs located on the cell surface were double-labelled with Texas Red and Alexa488 giving yellow fluorescence (red + green), while internalized ADSs appeared as single-labelled in green Alexa488. Internalization efficiency in each condition was calculated as the percentage of internalized ADS as compared to the total amount of ADSs associated per cell (where the cell borders were identified by phase-contrast) respect to the control without any inhibitor.

4.20.5 Internalization and lysosomal trafficking of Alexa488-PEG-Protein G/aICAM

Intracellular trafficking of the ADS was followed labelling lysosomes with Texas Red dextran 10 kDa, a polysaccharide that accumulates in lysosomes and allows their visualization since it cannot be enzymatically degraded in mammalian cells. Activate HUVECs were incubated with 100 μ M of this marker for 45 min at 37°C to allow dextran uptake, followed by removal of the medium. Incubation was continued with fresh medium for other 45 min at 37°C to ensure trafficking of internalized dextran to lysosomes. Cells were incubated with an 11.11 nM solution of the ADS for 1 h at 37°C and then washed with M-199 to remove unbound ADSs, followed by replacement with fresh media and additional incubation for 2 and 4 h at 37°C. Cells were washed again with M199 and fixed with 2% PFA. Cell-surface bound ADSs were counter stained with Alexa350 goat anti-mouse secondary antibody. Since fixed cells were not permeabilized, the secondary antibody bound only ADSs on the surface and did not bind ADSs that were endocytosed into the cells. To quantify the percentage of ADSs internalization and co-localization of internalized ADSs within lysosomes, cells were analysed by fluorescence microscopy. In merged micrograph, green fluorescence alone revealed endocytosed ADSs, yellow fluorescence (green + red) revealed ADSs localized to Texas Red dextran-labelled lysosomes and cyan (green + blue) indicated surface-bound ADSs. Uptake after 1, 3 and 5 h

incubation was calculated as the percentage of internalized ADSs with respect to the total number of cell-associated ADSs (cell-surface bound + internalized).

Whereas, lysosomal trafficking efficiency was calculated as the fraction of internalized ADSs that co-localized within lysosomes (i.e. the percentage of ADSs co-localized within lysosomes compared to the percentage of the internalized ADSs).

4.20.6 Statistics

Samples were imaged by fluorescence microscopy using a 60× objective, FITC and Texas Red and nDAPI filters, and Image-Pro 6.3 was used as the image analysis software.

During the analysis at least 30 cells were randomly selected through the entire cell sample of $\approx 10^5$ cells. Data were calculated as mean \pm standard error of the mean (SEM) and statistical significance was determined as $p < 0.05$ by Student's t-test.

5 RESULTS

5.1 Characterization of PDP-PEG-diethylacetal 20 kDa

In the first step of PDP-PEG-diethylacetal 20 kDa synthesis, the amino group of H₂N-PEG-COOH 20 kDa was attached to SPDP linker. SPDP derivatization was determined as 91.6, 81 and 70% according to TNBS assay, pyridine-2-thione assay and ¹H-NMR, respectively. In NMR analysis (Fig 31), the integration of aromatic protons in the pyridine ring was made using as reference the signals of the protons of the ethylene glycol chain at $\delta = 3.72$ ppm. Probably, the value of SPDP activation resulted underestimated owing to the great difference in numbers between the aromatic H and the H of PEG and also the different relaxing time. After PDP-PEG-COOH lyophilization, the yield was 90.8% w/w. The subsequent step consisted in the diethylacetal derivatisation of PEG at the carboxylic group end. The carboxylic group was activated via DCC/HOBt and then reacted with the amino group of 4-aminobutylaldehyd-diethyl-acetal. Degree of diethylacetal linkage was assessed by ¹H-NMR, resulting as 72.8% by calculating signal integration respect to the signals of PEG protons (an underestimation is also here expected). The yield of this last step of PDP-PEG_{20kDa}-diethylacetal synthesis was 55.7% w/w.

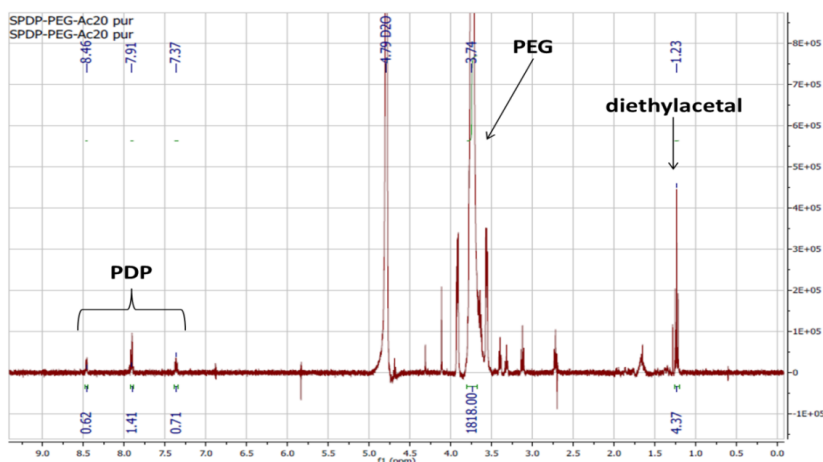
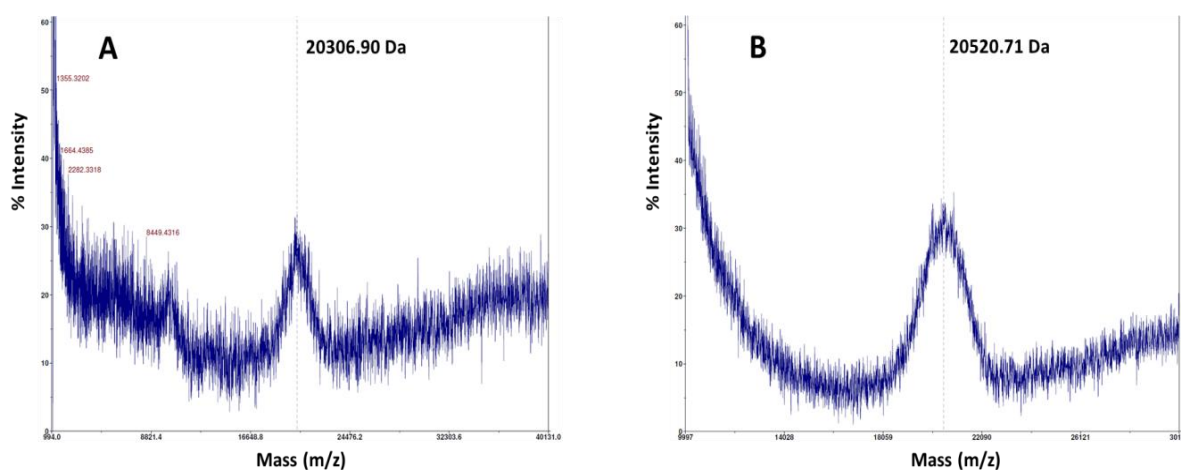


Figure 31. ¹H-NMR spectrum of PDP-PEG-diethylacetal 20 kDa.

Table 7. Signals of PDP-PEG-diethylacetal 20 kDa NMR spectrum.

δ (ppm)	Multiplicity	Theoretical integration	Real integration	Protons
8.46	dd	1	0.62	-CH in <i>ortho</i> position respect to N of pyridine ring [SPDP]
7.91	dt	2	1.41	-CH in <i>meta</i> and <i>para</i> positions respect to N pyridine ring [SPDP]
7.37	dd	1	0.71	-CH in <i>meta</i> position respect to N of pyridine ring [SPDP]
4.79	s	-	-	D ₂ O
3.72	m	1818	1818	-(CH ₂ CH ₂ O) _n - [PEG]
1.23	t	6	4.37	-(OCH ₂ CH ₃) ₂ [diethylacetal]

The final product was also characterized by MALDI-TOF (Fig 32). The molecular weight of the polymer was 20520.4 Da, showing an increment of about 200 Da respect to the starting polymer H₂N-PEG-COOH.

**Figure 32.** MALDI-TOF spectrum of A) H₂N-PEG_{20kDa}-COOH and B) PDP-PEG_{20kDa}-diethylacetal.

5.2 Protein G characterization

Molecular weight of Protein G was determined in two independent mass experiments using a MALDI-TOF and a Q-TOF spectrometer, and the resulting mass was 22768.10 and 22810.25 Da, respectively, as showed in Fig 33.

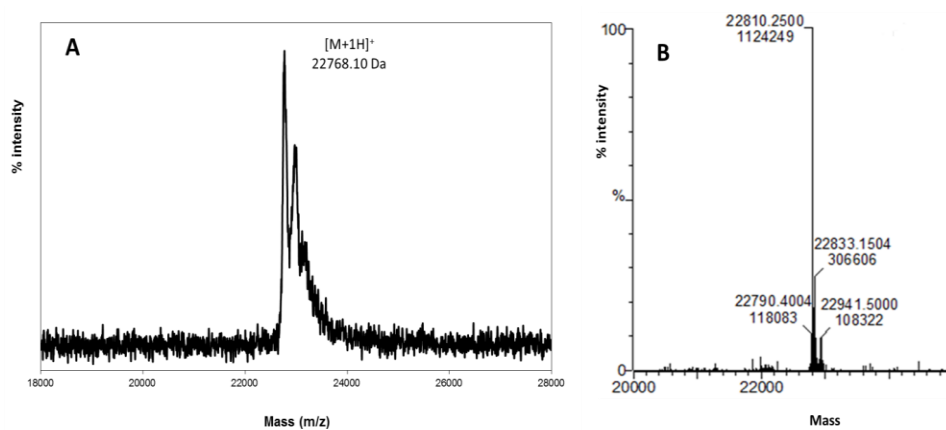


Figure 33. Determination of Protein G molecular weight by A) MALDI-TOF and 2) and ESI-TOF mass analysis.

Chromatographic runs of Protein G in RP-HPLC (Fig 34) and anion exchange (Fig 35) columns shown that the protein has a retention time of 16.4 and 83.5 minutes, respectively.

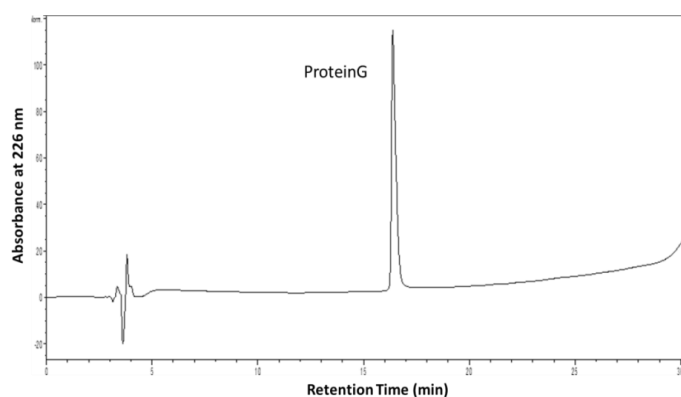


Figure 34. RP-HPLC run of Protein G (Phenomenex Jupiter C18 column 250 × 4.6 mm, 300 Å, 5 μm, 1 ml/min, 226 nm, eluting with H₂O MilliQ (eluent A) and ACN (eluent B), added of 0.1% TFA v/v, gradient B%: 0 min 10%, 25 min 60%, 28 min 90%, 30 min 10%).

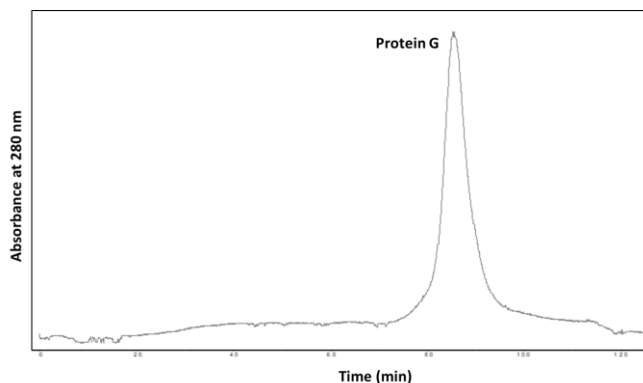


Figure 35. Elution of Protein G in anion exchange chromatography (DEAE-Toyopearl 650M 1.6 × 4.5 cm column, 1 ml/min, 280 nm, eluting with 10 mM Tris-HCl pH 8 (buffer A) and 10 mM Tris-HCl, 0.1 M NaCl pH 8 (buffer B), gradient B%: 0 min 0%, 10 min 0%, 80 min 100%, 105 min 100%, 110 min 0%).

5.3 Characterization of PEG_{20kDa}-Nter-Protein G and PDP-PEG_{20kDa}-Nter-Protein G

PEGylation of Protein G was performed as described in Section 4.3 using mPEG_{20kDa}-aldehyde and PDP-PEG_{20kDa}-aldehyde. The conjugates were purified by anion exchange chromatography as reported in Fig 36: diPEG-Protein G eluted at 59.1 min, PEG-Protein G at 68 min and free protein at 83.5 min. The presence of PDP did not change the elution profile of the conjugates.

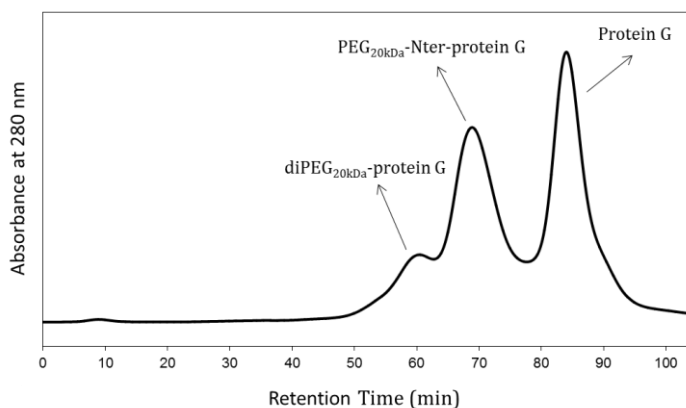


Figure 36. Purification of the solution reaction between Protein G and PEG-aldehyde 20kDa by anion exchange chromatography (DEAE-Toyopearl 650M, 1.6 × 4.5 cm column, 1 ml/min, 280 nm, eluting with 10 mM Tris-HCl pH 8 (buffer A) and 10 mM Tris-HCl, 0.1 M NaCl pH 8 (buffer B), gradient B%: 0 min 0%, 10 min 0%, 80 min 100%, 105 min 100%, 110 min 0%).

MonoPEGylated Protein G was characterized by RP-HPLC, SDS-PAGE, MALDI-TOF and circular dichroism.

Results

In RP-HPLC column, the monoconjugate displayed a retention time of 19 min (Fig 37). Moreover, RP-HPLC analysis showed that a negligible impurity of free Protein G was present at 16.4 min: 3% in the case of mPEG-Protein G and 6.89 % in case of PDP-PEG-Protein G. In the last case, the impurity was completely removed in following steps by gel filtration chromatography.

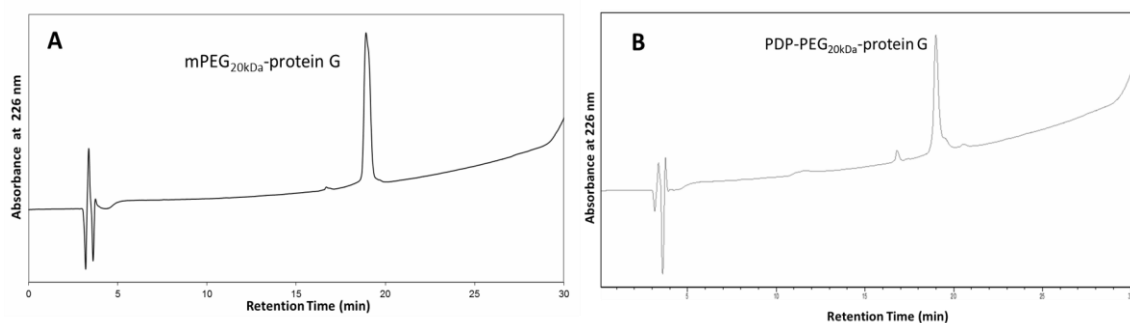


Figure 37. RP-HPLC characterization of A) mPEG_{20kDa}-Protein G and B) PDP-PEG_{20kDa}-Protein G monoconjugates (Phenomenex Jupiter C18 column, 250 × 4.6 mm, 300 Å, 5 μm, 1 ml/min, 226 nm, eluting with H₂O MilliQ (eluent A) and ACN (eluent B) added of 0.1% TFA v/v, gradient B%: 0 min 10%, 25 min 60%, 28 min 90%, 30 min 10%).

According to MALDI-TOF analysis, mPEG-Protein G had a MW 45070.0 Da (Fig 38, Panel A) and PDP-PEG-protein G of 43605.0 Da (Fig 38, Panel B), both corresponding to the MW of one molecule of protein G (22.8 kDa) linked to one chain of polymer (about 20 kDa).

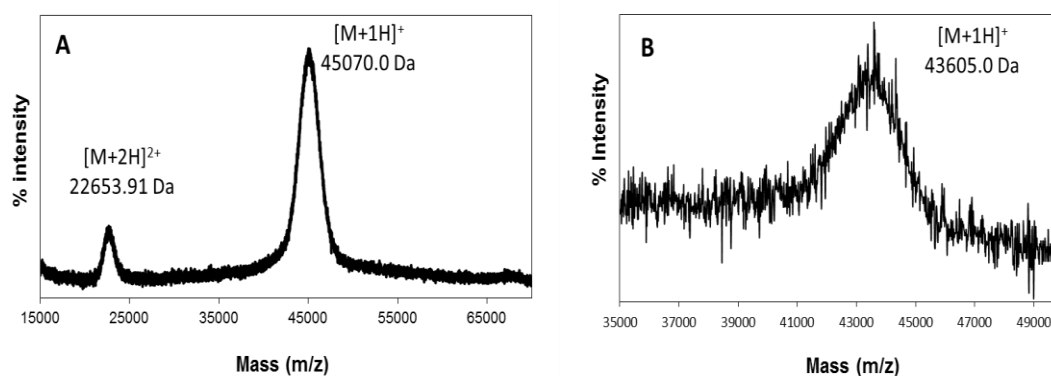


Figure 38. MALDI-TOF spectra of A) mPEG_{20kDa}-Protein G and B) PDP-PEG_{20kDa}-Protein G.

In SDS-PAGE (Fig 39), mPEG-Protein G and PDP-PEG-Protein G appeared as a band at about 70 kDa. PEG has a large hydrodynamic volume that confers to PEGylated proteins a high apparent molecular weight in SDS-PAGE that does not correspond to MW determined by mass

spectrometry. Both MALDI-TOF and SDS-PAGE analyses confirmed that the conjugates were monoPEGylated species, and that purification from unmodified protein and multiPEGylated species was successful. Trace impurities of bi- and tri- conjugates were present inside PDP-PEG-Protein G sample, but were removed in the following steps.

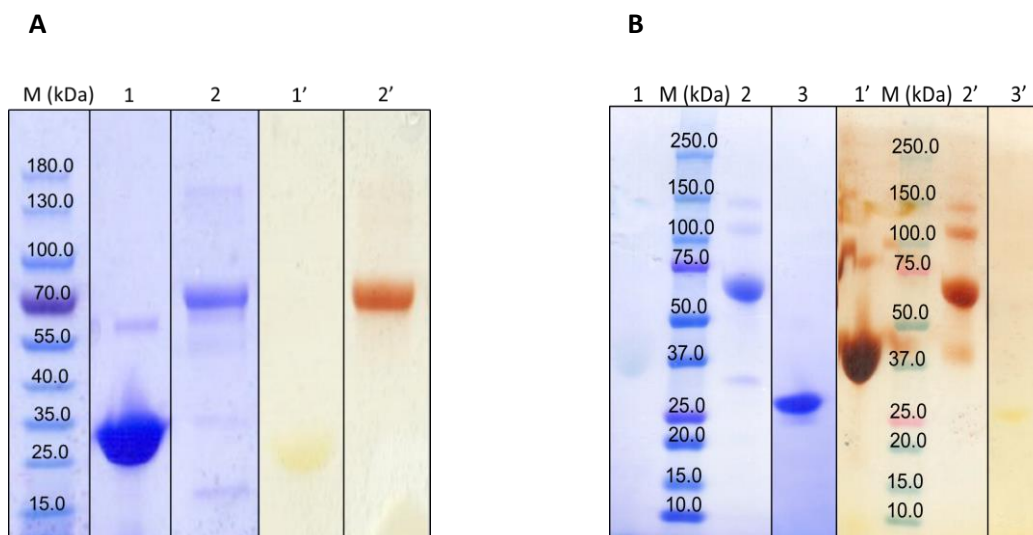


Figure 39. Characterization by SDS-PAGE (4-15%) of A) Protein G (Lane 1 and 1') and mPEG_{20kDa}-Protein G (Lane 2 and 2'); and B) PDP-PEG_{20kDa}-aldehyde (Lane 1 and 1'), PDP-PEG_{20kDa}-Protein G (Lane 2 and 2') and Protein G (Lane 3 and 3'). Markers are in Lane M. Lanes N are Coomassie stained for protein detection and Lanes N' are iodine stained for PEG detection.

5.4 Characterization of Cy5- and Alexa488-PEG_{20kDa}-Protein G

First, DTT was added to PDP-PEG-Protein G in order to obtain the free thiol of PDP linker. DTT was then removed by gel filtration chromatography and HS-PEG-Protein G (t_r 22.43 minutes) was collected (Fig 40).

Dye coupling to PDP-PEG-Protein G was performed as described in Section 4.4. The reaction occurred between the maleimide group of the dye and the new thiol generated reactive handle of PEG. The reaction and the removal of unreacted dye were monitored by gel filtration (Fig 41). Final drug loading was quantified by UV-Vis spectroscopy: Cy5/Protein G ratio was 0.72, while Alexa488/Protein G ratio was 0.75. Cy5-PEG-Protein G was also characterized by SDS-PAGE (Fig 46) in order to assess that this procedure did not cause any alteration in the conjugate structure.

Results

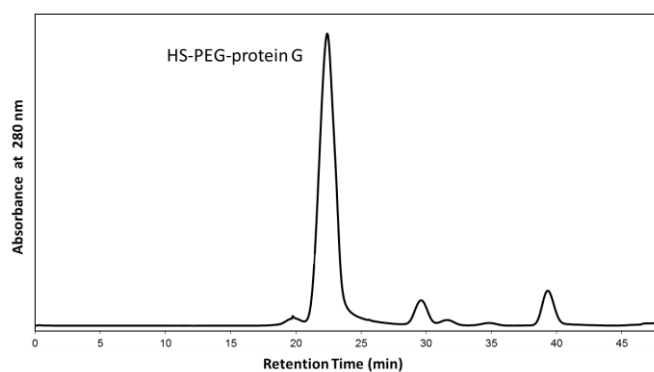


Figure 40. HS-PEG-Protein G purification by gel filtration chromatography (GE Healthcare Superdex 200 Increase 300 x 10 mm, 0.5 ml/min, 280 nm, eluting with PBS with 5mM EDTA pH 7.4).

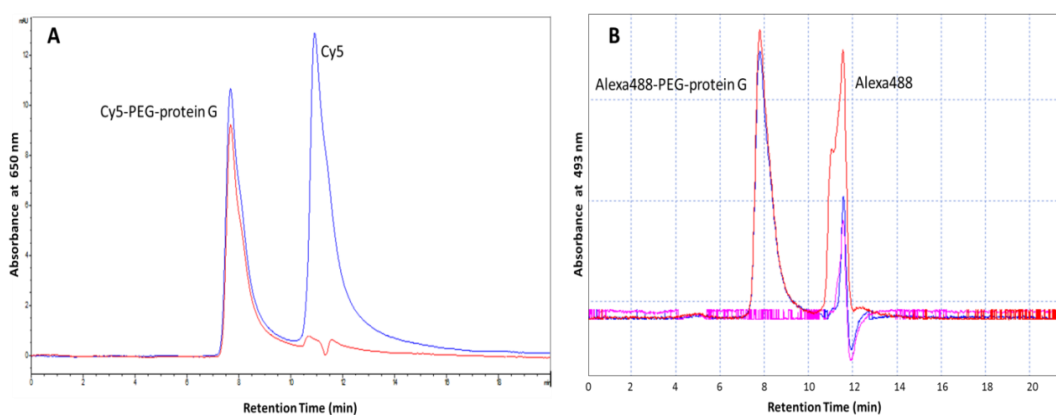


Figure 41. Analysis of A) Cy5-PEG-Protein G before (blue line) and after (red line) the removal of unreacted dye, and of B) Alexa488-PEG-Protein G (red line) and after (blue line) the removal of unreacted dye (pink line is the signal of the buffer) by gel filtration chromatography (Phenomenex BioSep-SEC-S 3000 column, 300 x 4.6 mm, 0.35 ml/min, 650 nm (A) or 493 nm (B), eluting with 20 mM sodium phosphate, 130 mM sodium chloride, 20% ACN pH 7).

5.5 Characterization of Tubulysin A-PEG_{20kDa}-Nter-Protein G

Tubulysin A mass was determined by ESI-TOF and resulted of 1012.49 Da (Fig 42). The toxin was injected in RP-HPLC column and eluted with a retention time of 19 min (Fig 43).

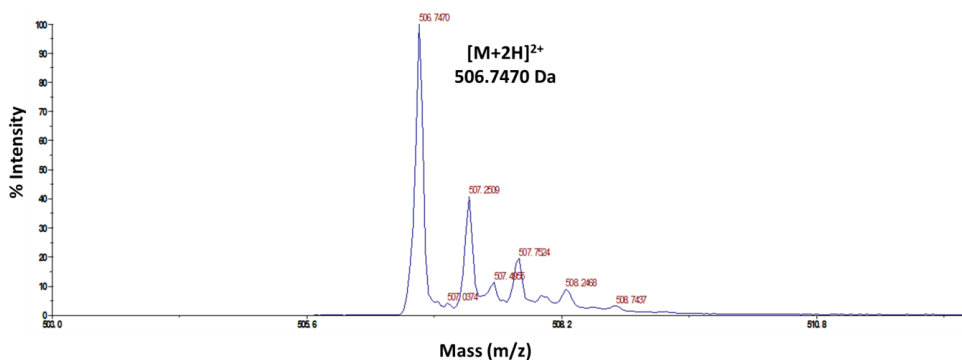


Figure 42. ESI-TOF spectrum of Tubulysin A.

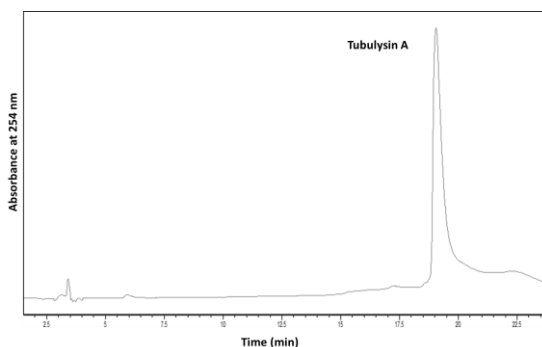


Figure 43. RP-HPLC analysis of Tubulysin A (Phenomenex Jupiter C18 column 250 × 4.6 mm, 300 Å, 5 μm, 1 ml/min, 254 nm, eluting with 10 mM ammonium bicarbonate pH 7 (eluent A) and ACN (eluent B), gradient B%: 0 min 40%, 10 min 52%, 15 min 70%, 18 min 90%, 25 min 40%).

HS-PEG-Protein G was obtained as previously reported and was reacted with Tubulysin A as described in Section 4.5. Reaction was monitored by RP-HPLC: TubA-PEG-Protein G eluted at 7.45 min and unreacted TubA at 19 min. After the removal of the excess, TubA coupled to the conjugate was quantified using a calibration curve obtained from RP-HPLC injections of toxin standards in reduced form. 10 mM DTT was added to TubA-PEG-Protein G in order to reduce the disulphide bond between the toxin and the polymer and the released reduced TubA, that eluted at 17.5 min (Fig 44, red line) was quantified. TubA/Protein G ratio was 0.41.

Results

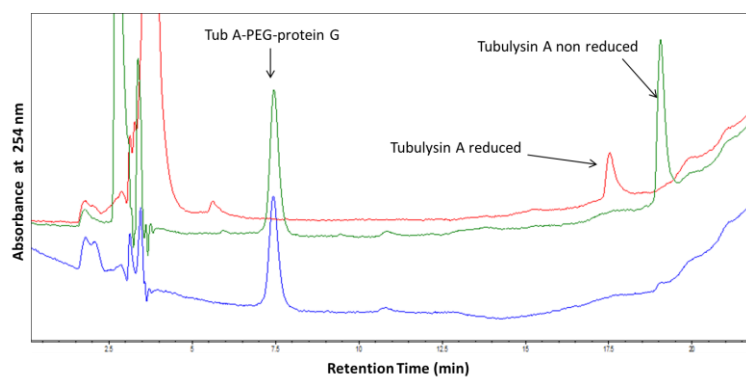


Figure 44. RP-HPLC analysis of TubA-PEG-Protein G before (green line) and after (blue line) dialysis and filtration to remove unbound toxin. Red line is the run of TubA-PEG-Protein G added of 10 mM DTT. (Phenomenex Jupiter C18 column 250×4.6 mm, 300 \AA , $5 \mu\text{m}$, 1 ml/min , 254 nm , eluting with 10 mM ammonium bicarbonate pH 7 (eluent A) and ACN (eluent B), gradient B%: 0 min 40%, 10 min 52%, 15 min 70%, 18 min 90%, 25 min 40%).

TubA-PEG-Protein G was characterized by RP-HPLC, MALDI-TOF and SDS-PAGE. The conjugate coupled to toxin eluted at 20.6 min (Fig 45, panel A). The conjugate had a molecular weight of 44170.3 Da, with an increase of 565.3 Da respect to PDP-PEG-Protein G (Fig 45, panel B).

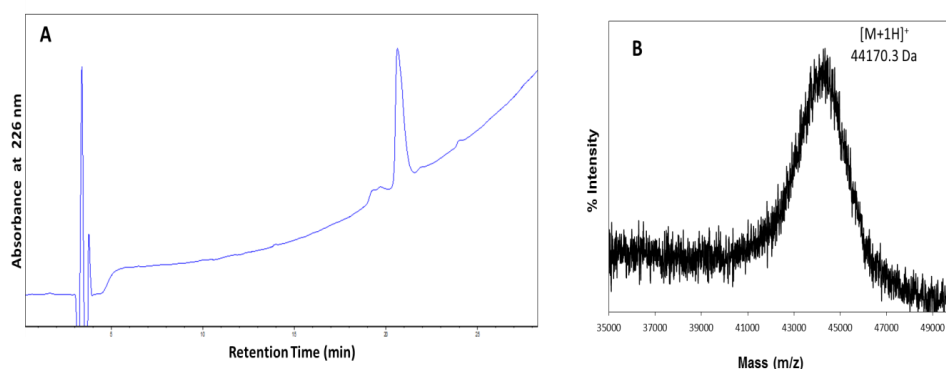


Figure 45. A) RP-HPLC characterization (Phenomenex Jupiter C18 column, 250×4.6 mm, 300 \AA , $5 \mu\text{m}$, 1 ml/min , 226 nm , eluting with H_2O MilliQ (eluent A) and ACN (eluent B) added of 0.1% TFA v/v, gradient B%: 0 min 10%, 25 min 60%, 28 min 90%, 30 min 10%) and B) MALDI-TOF spectrum of TubA-PEG-Protein G.

As expected, TubA-PEG-Protein G run as a species of about 70 kDa in SDS-PAGE (Fig 46). The product was pure and only traces of unconjugated PEG were present.

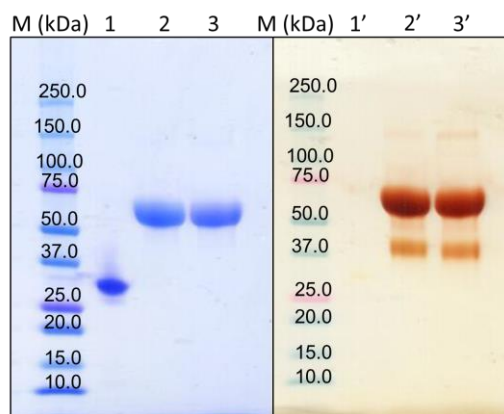


Figure 46. Characterization by SDS-PAGE (4-15%) of Protein G (Lane 1 and 1'), Cy5-PEG_{20kDa}-Protein G (Lane 2 and 2') and TubA-PEG_{20kDa}-Protein G (Lane 3 and 3'). Markers are in Lane M. Lanes N are Coomassie stained for protein detection and Lanes N' are iodine stained for PEG detection.

5.6 Characterization of Alexa647-PEG_{5kDa}-maleimide

AlexaFluor647 was attached to the activate carboxylic acid of NHS-PEG-maleimide 5 kDa as described in section 4.6 and the reaction was monitored in a gel filtration column measuring the absorbance at 650 nm as showed in Fig 47: Alexa647-PEG eluted at 8.2 min and unreacted dye at 9.8 min. Reaction yield was 63.35%. The molecular weight of the polymer was determined by MALDI-TOF and resulted of 5212.05 Da (Fig 48).

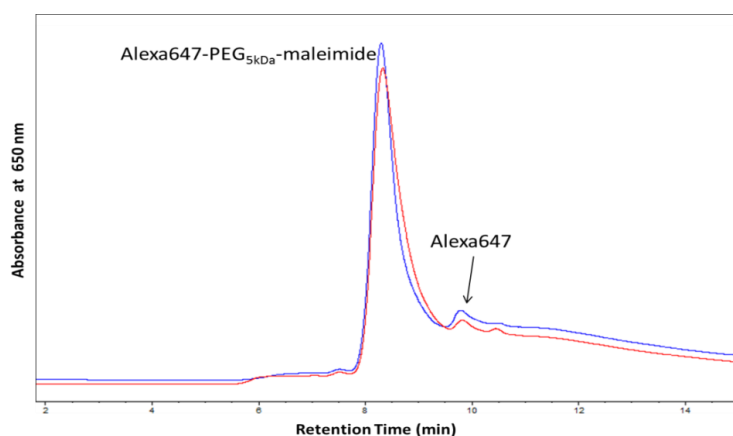


Figure 47. Analysis of Alexa647-PEG_{5kDa}-maleimide before (blue line) and after (red line) dialysis against MilliQ water by gel filtration chromatography (Agilent Zorbax GF250 column, 250 x 4.6 mm, 0.3 ml/min, 650 nm, eluting with 20 mM sodium phosphate, 130 mM sodium chloride, 20% ACN pH 7).

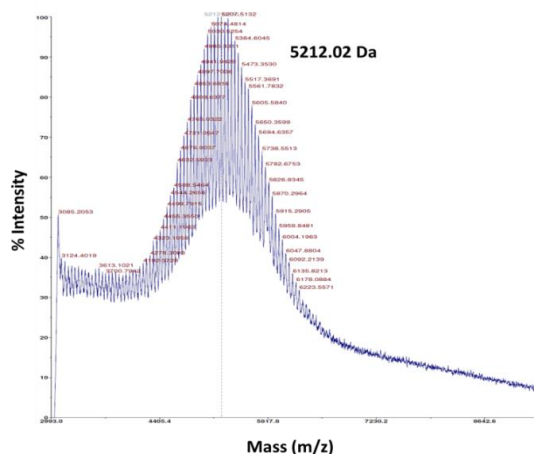


Figure 48. MALDI-TOF spectrum of Alexa647-PEG_{5kDa}-maleimide.

5.7 Characterization of goat anti-human-Fc NEM-Fab, (PEG_{5kDa})_n-Fab and (Alexa647-PEG_{5kDa})_n-Fab

Goat anti-human F(ab')₂ against the Fc region of human immunoglobulins G had a molecular weight of 96132.47 Da, as assessed by MALDI-TOF spectrometry (Fig 49). In gel filtration chromatography, the protein had a retention volume of 13.2 ml (Fig 50, blue line).

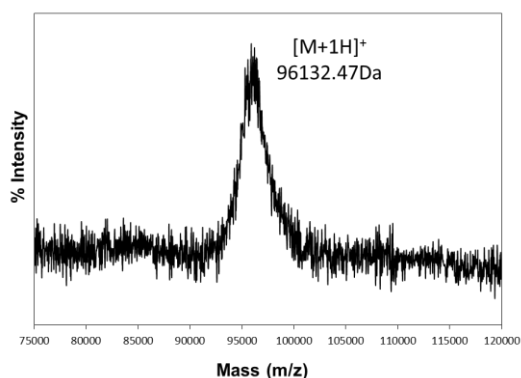


Figure 49. MALDI-TOF spectrum of goat anti-human-Fc F(ab')₂.

Fab' was obtained by the reduction of F(ab')₂ with cysteamine as described in section 4.7. The reducing agent was removed by gel filtration chromatography (Fig 50): Fab' eluted at 15.2 ml and cysteamine at 21.2 ml. Fab' was pooled and immediately added of NEM or polymers.

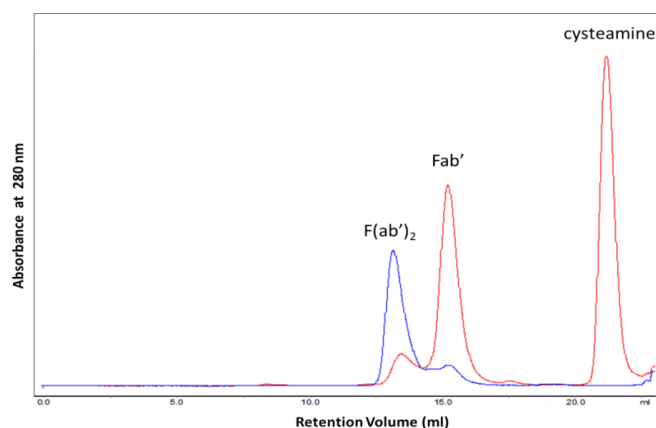


Figure 50. Gel filtration chromatography of goat anti-human-Fc $F(ab')_2$ (blue line) and its Fab' fragment with cysteamine (red line) (GE Healthcare Superdex 200 Increase 300 x 10 mm, 0.5 ml/min, 280 nm, eluting with 50 mM sodium phosphate, 150 mM sodium chloride, 10 mM EDTA pH 5).

NEM was used to block the free sulfhydryl groups and to obtain the non PEGylated Fab' . In absence of a blocking agent, thiol groups of Fab' re-formed disulphide bridges producing again $F(ab')_2$. In fact, after overnight dialysis of Fab' and cysteamine solution, gel filtration chromatography showed the formation of a 40% amount of $F(ab')_2$ (Fig 51, blue line) because the removal of the reducing allowed sulphidryl groups reoxidation.

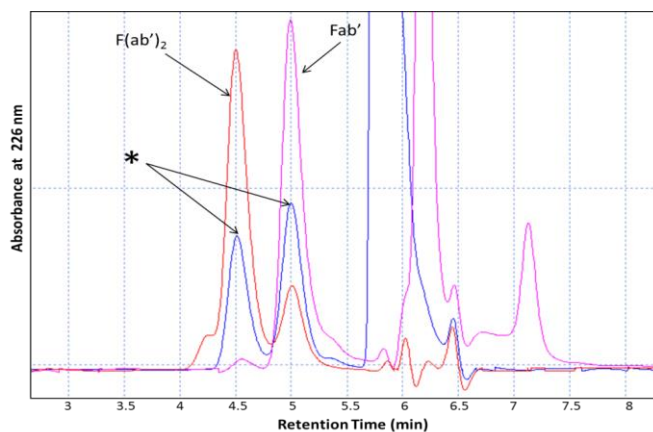


Figure 51. Gel filtration chromatography (Phenomenex Yarra SEC3000, 150 x 7.8 mm, 1 ml/min, 226 nm, eluting with sodium phosphate, 0.3 M sodium chloride, 20% ACN pH 6.8) of $F(ab')_2$ (red line), Fab' with cysteamine (pink line) and Fab' after dialysis (blue line).

Unreacted NEM was removed by gel filtration chromatography and NEM-Fab eluted at 15.2 ml was collected (Fig 52, panel A). NEM-Fab MW was 48367.9 Da as determined by MALDI-TOF (Fig 52, panel B), and in SDS-PAGE (Fig 56) the protein run as a species of about 45 kDa.

Results

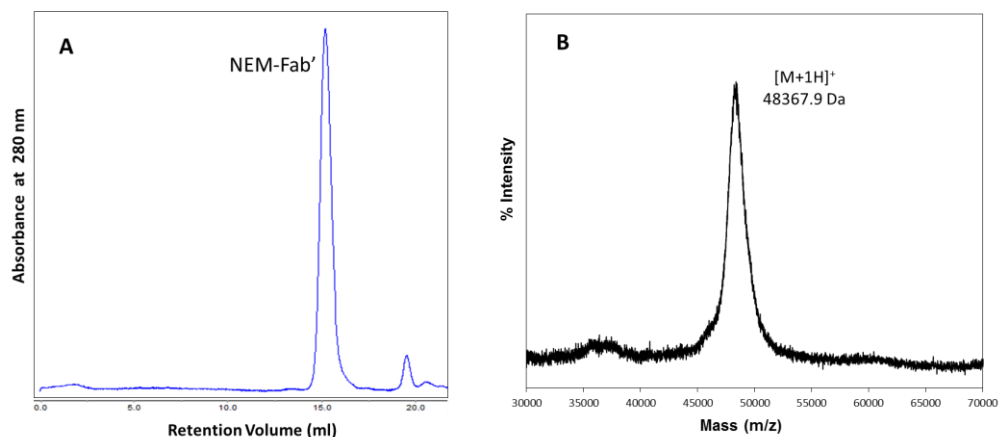


Figure 52. A) Gel filtration chromatography (GE Healthcare Superdex 200 Increase 300 x 10 mm, 0.5 ml/min, 280 nm, eluting with PBS pH 7.4) and B) MALDI-TOF spectrum of goat anti-human-Fc NEM-Fab.

The reaction solutions between Fab' and mPEG_{5kDa}-maleimide or Alexa647-PEG_{5kDa}-maleimide were purified by gel filtration chromatography (Fig 53 and 54, respectively). The eluting peaks were collected and characterized by MALDI-TOF, gel filtration chromatography and SDS-PAGE. Regarding the reaction between Fab' and mPEG-maleimide, MALDI-TOF analysis assessed that peak at 12 ml had a MW of 65563.09 Da (Fig 55, panel A) corresponding to triPEGylated Fab, peak at 12.60 ml had a MW of 59276.34 Da (Fig 55, panel B) corresponding to diPEGylated Fab and peak at 13.70 ml had a MW of 54068.70 Da (Fig 55, panel C) corresponding to monoPEGylated Fab. Peak at 15.70 ml included both unconjugated Fab and free polymer. The collected species were characterized in SDS-PAGE (Fig 56) confirming the results obtained by mass spectrometry.

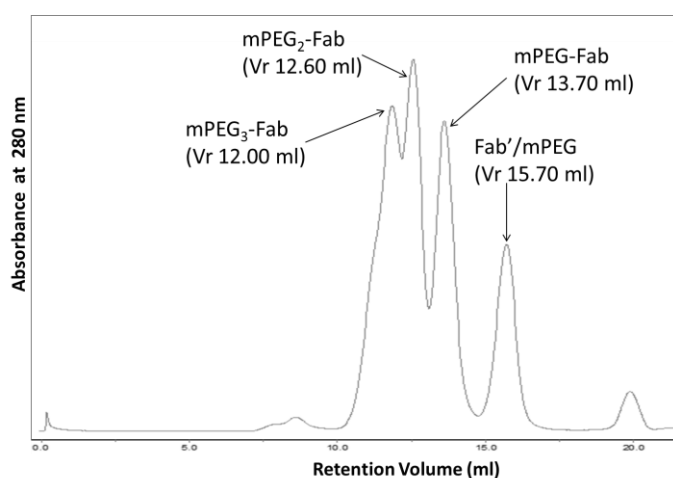


Figure 53. Purification of the reaction solution between goat anti-human-Fc Fab' and mPEG_{5kDa}-maleimide by gel filtration chromatography (GE Healthcare Superdex 200 Increase 300 x 10 mm, 0.5 ml/min, 280 nm, eluting with PBS pH 7.4).

Elution profile of the reaction solution between Fab' and Alexa647-PEG-maleimide was similar to the previous one and two peaks of PEGylated species were pooled: peak at 12 ml that was not detected by MALDI-TOF and peak at 13.70 ml that had a MW of 54247.88 Da (Fig 55, panel D) corresponding to the monoconjugate. SDS-PAGE analysis (Fig 57) confirmed that peak at 12 ml was monoPEGylated protein and peak at 13.70 ml appeared as a mixture of di and triPEGylated Fab. Since the latter exhibited an elution profile in analytical gel filtration column (Fig 58) almost superimposable to the profile of mPEG₃-Fab, we assumed that it contained prevalently the triPEGylated species (Tr Fab 9.80 min, Tr mPEG-Fab 9.12 min, Tr mPEG₂-Fab 8.72 min, Tr mPEG₃-Fab 8.38 min, Tr Alexa647-PEG-Fab 8.92 min, Tr (Alexa647-PEG)₂₋₃-Fab 8.35 min).

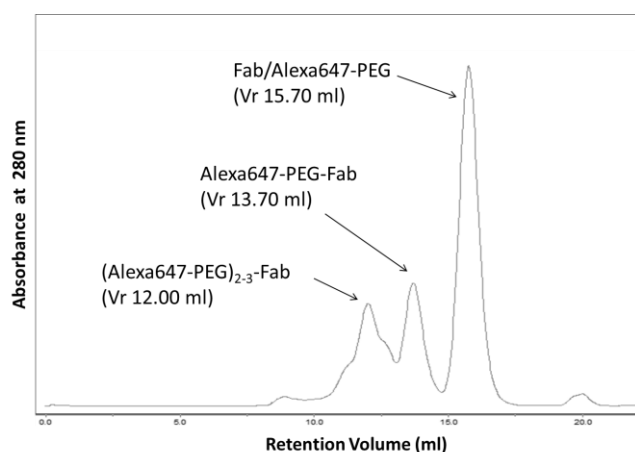
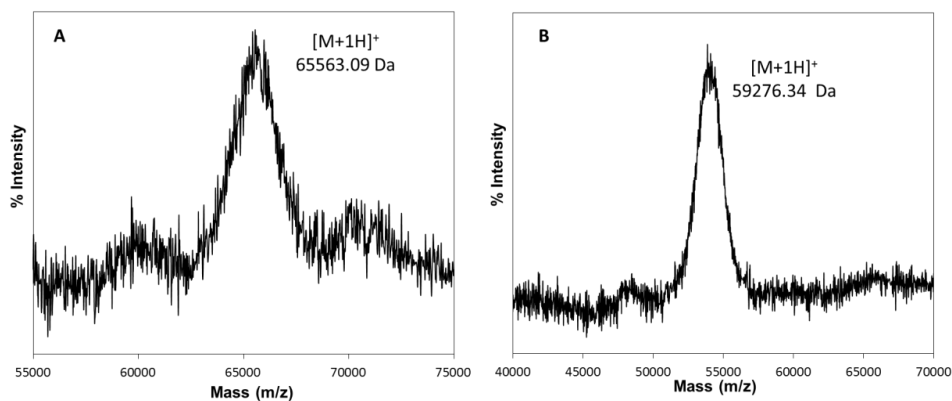


Figure 54. Purification of the reaction solution between goat anti-human-Fc Fab' and Alexa647-PEG_{5kDa}-maleimide by gel filtration chromatography (GE Healthcare Superdex 200 Increase 300 x 10 mm, 0.5 ml/min, 280 nm, eluting with PBS pH 7.4).



Results

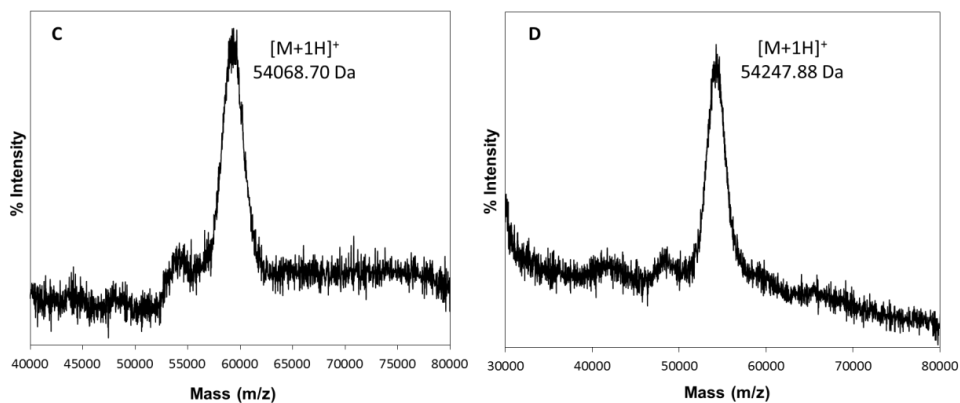


Figure 55. MALDI-TOF spectra of A) mPEG₃-Fab (peak at 12 ml, Fig 53), B) mPEG₂-Fab (peak at 12.60 ml, Fig 53), C) mPEG-Fab (peak at 13.70 ml, Fig 53), and D) Alexa647-PEG-Fab (peak at 13.70 ml, Fig 54).

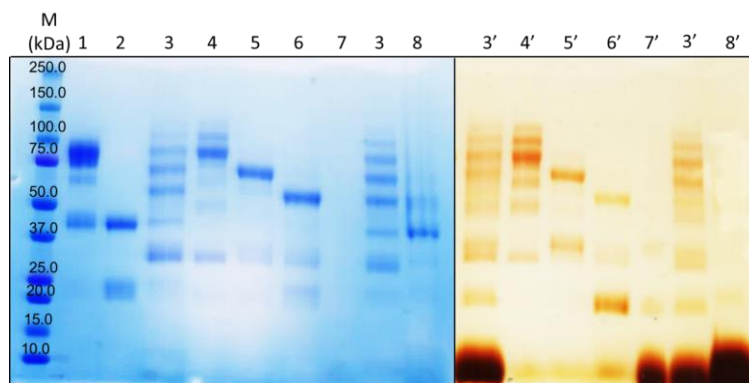


Figure 56. Characterization by SDS-PAGE (4-15%) of goat anti-human-Fc F(ab')₂ (Lane 1), NEM-Fab (Lane 2), reaction solution between Fab' and mPEG_{5kDa}-maleimide (Lane 3 and 3'), (mPEG_{5kDa})₃-Fab (Lane 4 and 4'), (mPEG_{5kDa})₂-Fab (Lane 5 and 5'), mPEG_{5kDa}-Fab (Lane 6 and 6'), mPEG_{5kDa}-maleimide (Lane 7 and 7'), peak at 15.70 ml of the chromatogram in Fig 53 (Lane 8 and 8'). Markers are in Lane M. Lanes N are Coomassie stained for protein detection and Lanes N' are iodine stained for PEG detection.

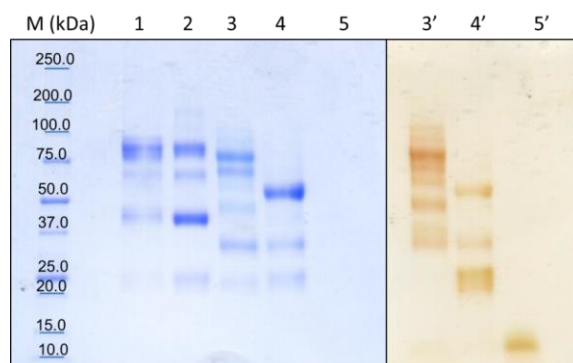


Figure 57. Characterization by SDS-PAGE (4-15%) of goat anti-human-Fc F(ab')₂ (Lane 1), Fab' with F(ab')₂ impurity (Lane 2), (Alexa647-PEG_{5kDa})₂₋₃-Fab (Lane 3 and 3'), Alexa647-PEG_{5kDa}-Fab (Lane 4 and 4'), peak at 15.70 ml of the chromatogram in Fig 54 (Lane 5 and 5'). Markers are in Lane M. Lanes N are Coomassie stained for protein detection and Lanes N' are iodine stained for PEG detection.

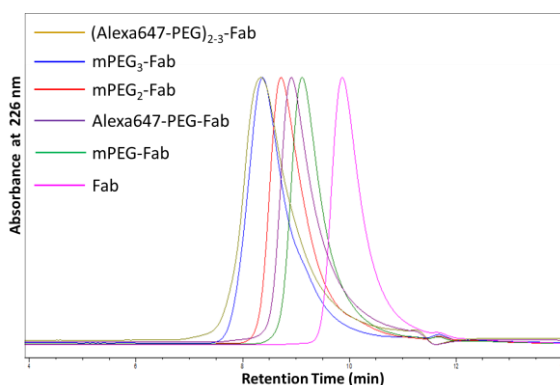


Figure 58. Gel filtration chromatography of (Alexa647-PEG)₂₋₃-Fab (yellow line), mPEG₃-Fab (blue line), mPEG₂-Fab (red line), Alexa647-PEG-Fab (violet line), mPEG-Fab (green line) and Fab' (pink line) (Phenomenex BioSep-SEC-S 3000 column, 300 x 4.6 mm, 0.35 ml/min, 226 nm, eluting with 20 mM sodium phosphate, 130 mM sodium chloride, 20% ACN pH 7).

5.8 Fab PEGylation pattern of Rituximab Fab

Rituximab was digested by pepsin as described in section 4.8 to obtain F(ab')₂ that was purified by gel filtration chromatography (Vr 14.1 ml, Fig 59, red line). MALDI-TOF analysis (Fig 61, panel A) assessed that F(ab')₂ had a MW of 96806.49 Da and SDS-PAGE gel showed that entire IgG was completely removed. F(ab')₂ was then reduced adding cysteamine and, again, Fab' was purified by gel filtration (Vr 16.0, Fig 59, blue line). MW of Fab' was 48515.25 Da (Fig 61, panel B) and in SDS-PAGE gel (Fig 62) traces of separated light and heavy chains appeared with an apparent volume of 15-25 kDa.

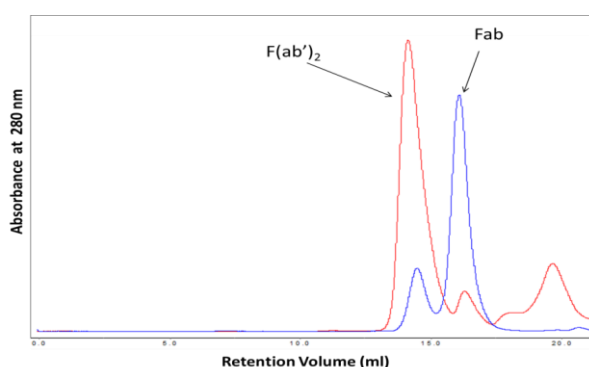


Figure 59. Gel filtration chromatography of rituximab F(ab')₂ (red line) and its Fab' fragment with cysteamine (blue line) (GE Healthcare Superdex 200 Increase 300 x 10 mm, 0.5 ml/min, 280 nm, eluting with 50 mM sodium phosphate, 150 mM sodium chloride, 10 mM EDTA pH 5).

Results

Fab' peak was immediately added of mPEG-maleimide 5kDa and let react overnight. The reaction solution was purified by gel filtration chromatography and the diPEGylated conjugate at 12.50 ml was collected (Fig 60) and characterized by MALDI-TOF and SDS-PAGE.

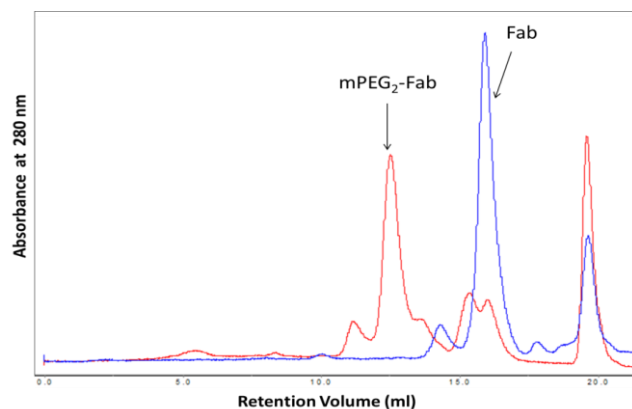


Figure 60. Purification of the reaction solution between Rituximab Fab' and mPEG_{5kDa}-maleimide by gel filtration chromatography (GE Healthcare Superdex 200 Increase 300 x 10 mm, 0.5 ml/min, 280 nm, eluting with PBS pH 7.4).

The diPEGylated Fab of Rituximab had a MW of 59842.54 Da (Fig 61, panel C) and in SDS-PAGE appeared as a band slightly above 75 kDa (trace impurities of PEGylated heavy and light chains were also present at 30-37 kDa).

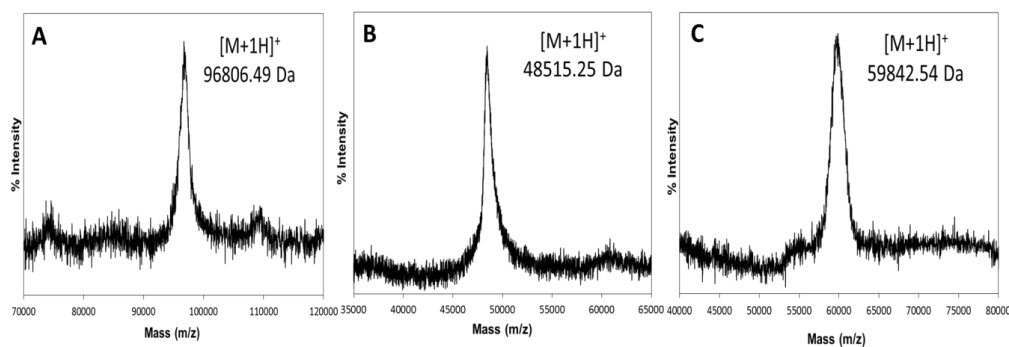


Figure 61. MALDI-TOF spectra of A) Rituximab F(ab')₂, B) Rituximab Fab' and C) Rituximab mPEG₂-Fab.

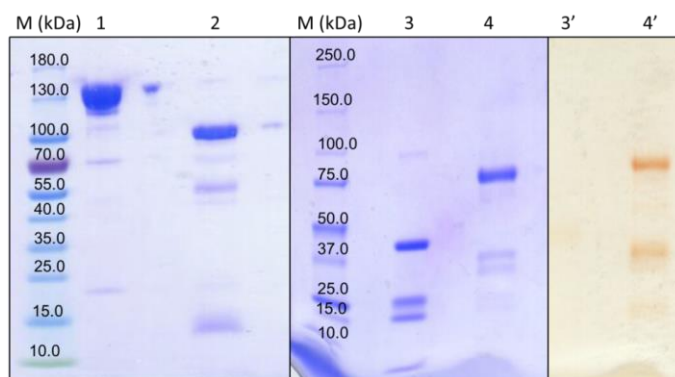


Figure 62. Characterization by SDS-PAGE (4-15%) of rituximab (Lane 1), F(ab')₂ (Lane 2), Fab' (Lane 3 and 3') and mPEG₂-Fab (Lane 4 and 4'). Markers are in Lane M. Lanes N are Coomassie stained for protein detection and Lanes N' are iodine stained for PEG detection.

5.9 Dye conjugation to monoclonal antibodies

Dye molecules were tethered to antibodies through lysine residues. Dye/antibody ratio values ranged from 1 to 3.6. In gel filtration, labeled antibody eluted at 8.60 minutes (Fig 63), whereas unconjugated dye at 11.5 min.

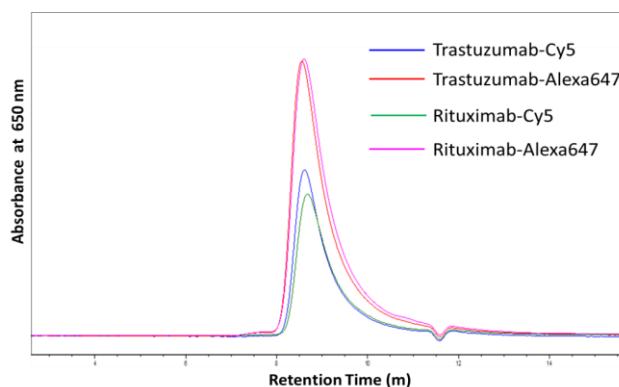


Figure 63. Gel filtration chromatography of Trastuzumab-Cy5 (blue line), Trastuzumab-Alexa647 (red line), Rituximab-Cy5 (green line) and Rituximab-Alexa647 (pink line) (Phenomenex BioSep-SEC-S 3000 column, 300 x 4.6 mm, 0.35 ml/min, 650 nm, eluting with 20 mM sodium phosphate, 130 mM sodium chloride, 20% ACN pH 7).

5.10 Circular dichroism

FUV-CD data are expressed in mean residue ellipticity. CD experiments were performed in order to verify if PEGylation had caused a modification in protein secondary structure that could potentially alter the biological activity.

Protein G had predominantly an α -helical structure in physiological conditions as showed by the two characteristic bands at 222 and 208 nm in FUV-CD spectra (Fig 64). The conjugates exhibited the same ellipticity and the profiles were almost superimposable with that of the unmodified form, although PDP-PEG-Protein G spectrum presented a reduction in the intensity of the dichroic signal, which may be due to the underestimation of PDP-PEG-Protein G concentration owing to the presence of PDP group that absorb at 280 nm. Protein G is a highly stable bacterial receptor and a thermal analysis was conducted to assess if after thermal denaturation it was able to regain its secondary structure. During the experiment, temperature was gradually brought to 90°C registering the spectra at 208 nm and, then, temperature was decreased to 25°C and FUV-CD spectrum was registered again. Protein G and the PEGylated conjugates had a melting temperature of 77°C (Fig 65), meaning that the polymer had not changed the thermal stability. After denaturation, the species almost regained the secondary structure, especially in the case of mPEG-Protein G (Fig 66, 67 and 68).

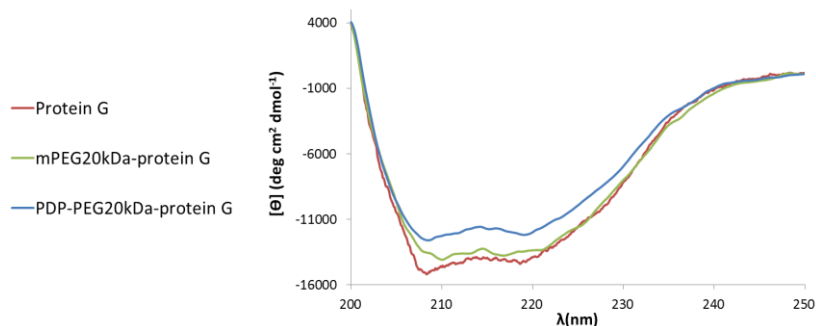


Figure 64. Comparison of FUV-CD spectra of Protein G (red line), mPEG_{20kDa}-Protein G (green line) and PDP-PEG_{20kDa}-Protein G (blue line).

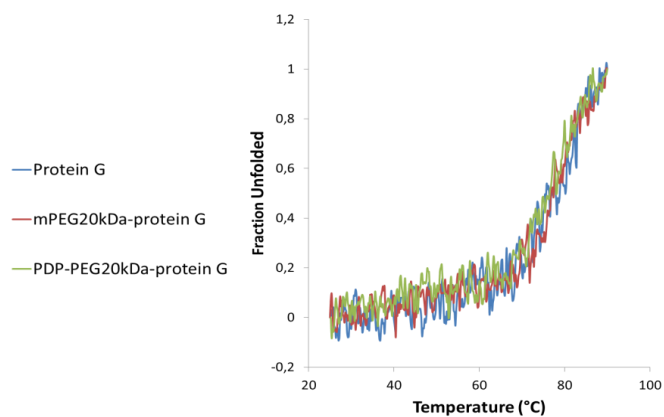


Figure 65. Thermal stability studies of Protein G (blue line), mPEG_{20kDa}-PEG-Protein G (red line) and PDP-PEG_{20kDa}-Protein G (green line).

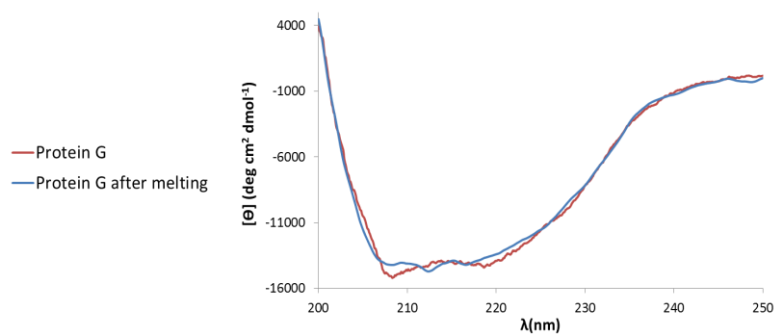


Figure 66. Comparison of FUV-CD spectra of Protein G before (red line) and after (blue line) melting.

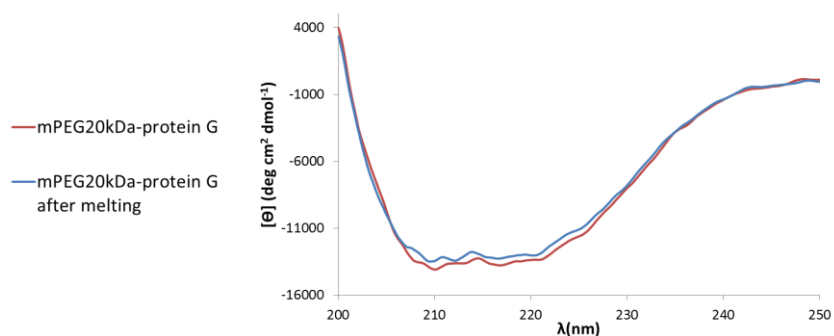


Figure 67. Comparison of FUV-CD spectra of mPEG_{20kDa}-Protein G before (red line) and after (blue line) melting.

Results

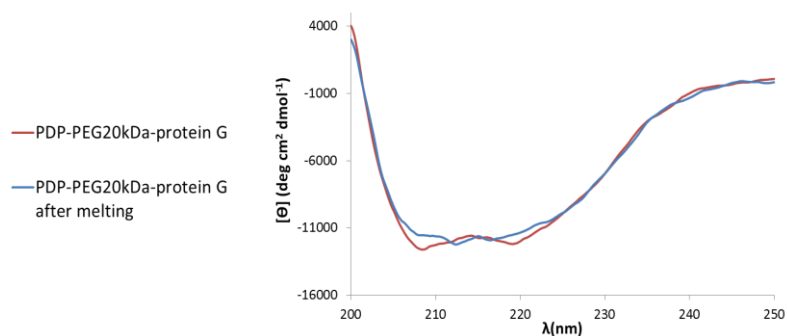


Figure 68. Comparison of FUV-CD spectra of PDP-PEG_{20kDa}-Protein G before (red line) and after (blue line) melting.

FUV-CD spectra of Fab and its mono-, di- and tri-PEGylated form exhibited a negative band centered around 218-220 nm, that is characteristic of the β -sheet structure. Immunoglobulins contain a large quantity of aromatic amino acids (especially Trp and Tyr), that are mostly localized in the variable region, in and around the binding site¹⁴⁸. Electronic transitions of aromatic residues can contribute to the FUV-CD spectrum, affecting the shape and the intensity of the signal and distorting the relatively weak CD signal originating from the β -sheet. According to X-ray spectroscopy, the amount of β - and α - structure in a Fab fragment is 47% and 2%, respectively¹⁴⁹. Moreover, the spectra showed a positive maximum at about 204 nm.

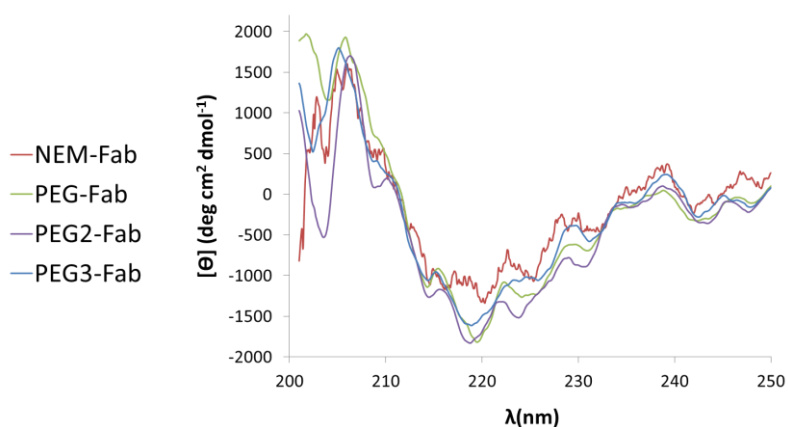


Figure 69. Comparison of FUV-CD spectra of NEM-Fab (red line), mPEG_{5kDa}-Fab (green line), (mPEG_{5kDa})₂-Fab (violet line) and (mPEG_{5kDa})₃-Fab (blue line).

5.11 Dynamic light scattering

DLS was exploited for size determination of the single biomolecules and of the FcBM/antibody complexes in solution.

Average diameters of Protein G and goat Fab were 3.62 ± 1.38 and 8.72 ± 3.35 nm, respectively, while the PEGylated forms are, as expected, bigger due to polymer contribution to dimensions: PEG-Protein G and PEG₂-Fab were 16.51 ± 3.26 and 13.54 ± 5.35 nm, respectively (Table 8). Rituximab and Trastuzumab diameters were about 11 nm, while mouse IgG2a was about 13.5 nm. This technique was used to determine the average diameter of complexes in solution at increasing FcBM/antibody ratio (Table 8). The maximum complexes size was reached at FcBM/antibody ratio similar to the binding stoichiometry determined by ITC analysis (i.e. 1 for both Protein G/antibody and Fab/antibody). For all other ratio, the sizes were reduced because the instrument reported a size that was an average of the complex size and the size of the compound in excess, the Fc-binding protein or the antibody. This investigation confirmed the binding stoichiometry determined by ITC.

Table 8. Dynamic light scattering analysis of the FcBMs, the antibodies, and their complexes at different FcBM/antibody molar ratios.

Species	MAb/protein molar ratio	Diameter (nm)	PdI
Rituximab (0.19 mg/ml)	-	11.08 ± 4.05	0.276
Trastuzumab (0.84 mg/ml)	-	10.96 ± 3.73	0.195
Protein G (2 mg/ml)	-	3.62 ± 1.38	0.523
Mouse anti-ICAM1 IgG2a (0.84 mg/ml)	-	14.74 ± 4.04	0.313
mPEG _{20kDa} -Protein G (0.456 mg/ml)	-	16.51 ± 3.26	0.562
PDP-PEG _{20kDa} -Protein G (1.2 mg/ml)	-	13.53 ± 2.56	0.657
NEM-Fab (1.3 mg/ml)	-	8.72 ± 3.35	0.595
(mPEG _{5kDa}) ₂ -Fab (1 mg/ml)	-	13.54 ± 5.35	0.421

Results

Complex	MAb/protein molar ratio	Diameter (nm)	Pdl
Trastuzumab / PDP-PEG _{20kDa} -Protein G	1:0.25	13.87 ± 7.123	0.252
	1:0.5	25.15 ± 11.68	0.196
	1:1	66.11 ± 22.82	0.113
	1:2	35.45 ± 10.00	0.116
	1:4	27.97 ± 7.522	0.155
Trastuzumab / mPEG _{20kDa} -Protein G	1:0.25	12.52 ± 4.102	0.383
	1:0.5	31.49 ± 11.59	0.192
	1:1	55.81 ± 17.60	0.090
	1:2	28.01 ± 11.52	0.201
	1:4	22.59 ± 9.171	0.186
Mouse aICAM-1 / mPEG _{20kDa} -Protein G	1:0.25	32.38 ± 11.43	0.232
	1:0.5	45.66 ± 15.25	0.204
	1:1	45.44 ± 13.84	0.250
	1:2	34.47 ± 10.98	0.304
	1:4	32.44 ± 10.05	0.348
Trastuzumab / Goat (mPEG _{5kDa}) ₂ -Fab	1:0.5	21.04 ± 11.72	0.214
	1:1	24.36 ± 15.06	0.234
	1:4	15.69 ± 7.44	0.172

5.12 Isothermal titration calorimetry

ITC was used to determine K_a and binding stoichiometry between antibodies and FcBM. All titrations were carried out in PBS, which has a relatively small and negligible heat of ionization. The binding properties of Protein G and goat Fab were evaluated against Trastuzumab and Rituximab, respectively. The thermodynamic parameters of complex formation are reported in Table 9.

The binding parameters of Protein G against Trastuzumab were not determined because the Protein G/Trastuzumab complex precipitated during the experiment, likely due to the formation of a highly cross-linked non-covalent aggregate because Protein G can interact also with Fab moieties beside the Fc. This phenomenon did not occur when the PEGylated version was used. In this case, a soluble complex was formed and the ITC analysis showed a molar ratio of one molecule of PEG-Protein G per Trastuzumab ($FcBM/antibody = 1.05 \pm 0.0155$) and a K_a of $5.76 \times 10^7 \pm 1.27 \text{ M}^{-1}$. Previous studies have shown that Protein G monoPEGylated with PEG 5kDa at the N-terminus induces complex precipitation, as well as unconjugated Protein G, while multiPEGylated Protein G at lysine using a PEG 2kDa does not give precipitation when

added of antibody solution, as well as Protein G monoPEGylated at the N-terminus with PEG 20kDa. Lund and coworkers used a variant of Protein G that did not crosslink IgGs giving precipitation and were able to performed an ITC experiment determining an affinity of 10^8 M^{-1} for both the entire antibody and the isolated Fc fragment⁷⁹. Therefore, despite having three IgG-binding domains, unmodified Protein G was reported to be capable to bind only 1 molecule of antibody. Interestingly, PEGylation did not greatly affected the binding affinity even in the case of conjugation with a 20kDa PEG.

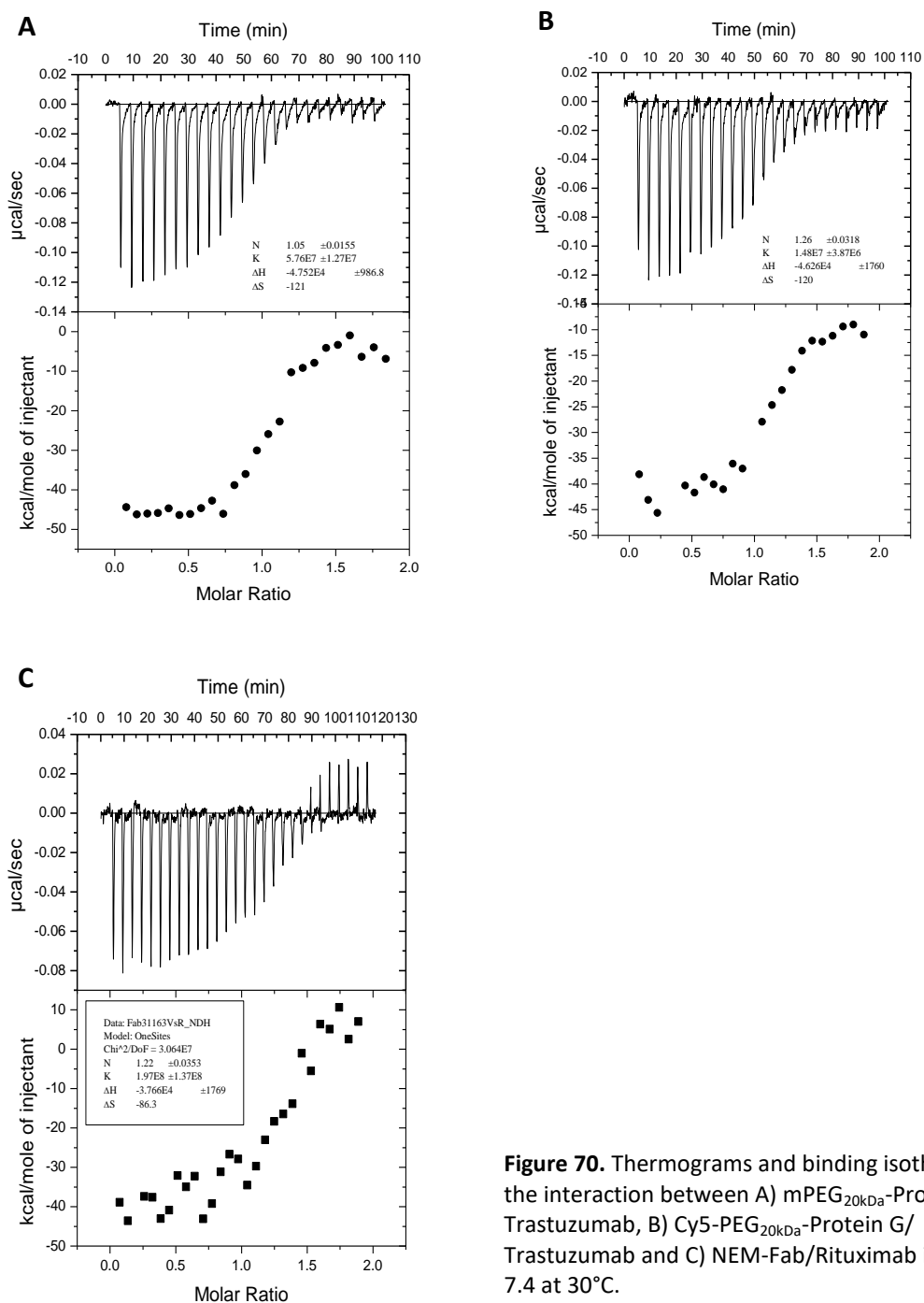


Figure 70. Thermograms and binding isotherms for the interaction between A) mPEG_{20kDa}-Protein G/Trastuzumab, B) Cy5-PEG_{20kDa}-Protein G/Trastuzumab and C) NEM-Fab/Rituximab in PBS pH 7.4 at 30°C.

Results

Table 9. Thermodynamic parameters for binding of mPEG_{20kDa}-Protein G, Cy5-PEG_{20kDa}-Protein G and goat NEM-Fab to human antibodies at 30°C in PBS pH 7.4.

Complex	K _a (M ⁻¹)	ΔH° (cal/mol)	ΔS° [cal/(K mol)]	N
mPEG _{20kDa} -Protein G/ Trastuzumab	(5.76 ± 1.27) × 10 ⁷	-4.752 × 10 ⁴ ± 986.8	-121	1.05 ± 0.0105
Cy5-PEG _{20kDa} -Protein G/ Trastuzumab	(1.48 ± 0.39) × 10 ⁷	-4.626 × 10 ⁴ ± 1760	-120	1.26 ± 0.0318
Goat NEM-Fab/ Rituximab	(1.97 ± 1.37) × 10 ⁸	-3.766 × 10 ⁴ ± 1769	-86.3	1.22 ± 0.0353

Fab-NEM displayed a K_a for Rituximab of 1.97×10⁸ ± 1.37 and a Fab/antibody binding stoichiometry of 1.22 ± 0.0353, meaning that on average one molecule of Fab bound one molecule of antibody. PEGylated Fab were also tested but the measured heat generated by the interaction between the conjugate and the antibody was too low to obtain a thermogram and probably a higher amount of sample was needed.

5.13 Analysis of interaction of ADS with target cancer cell lines

To assess the capacity of a PEG-protein/mAb ADS to bind the target antigen expressed on cell surface, the polymer moiety was labelled with the Cy5 or the Alexa647 fluorophore. Cy5-PEG-Protein G/Trastuzumab was tested on SKOV-3 and SKBR-3 HER2 positive cell lines, Alexa647-PEG_n-Fab/Trastuzumab on SKOV-3 cell line and Alexa647-PEG_n-Fab/Rituximab on LCL CD20 positive cell line. In all the cases, cells not expressing the proper antigen (HER2 or CD20), recognized by the mAb in the ADS, served as negative controls. Instead, the respective targeting antibody directly linked to the dye through lysine residues, likewise the classical ADCs, was used as positive control and a non specific antibody, prepared in the same way, was used as negative control. Furthermore, other two controls were the non targeted PEG-FcBM (i.e. the conjugate alone) and the non specific ADS between PEG-FcBM and an antibody that did not recognize the antigen. Each sample was added to 300000 cells and three different antibody amounts were tested: 0.1, 5 and 10 μg dissolved in 50 μl of PBS. PEG-FcBM amounts were calculated on the bases of the targeting antibody used.

Results disclosed that all the tested ADSs bound to antigen target cancer cells as well as the free control antibody. Indeed, the geo mean of positive cells was significantly high compared to the non-specific mAb, both for the ADS and the free mAb form (Fig 71, 72, 73 and 74). Non targeted PEG-Fab showed a certain degree of non-specific binding to LCL (CD20⁺) cells, that was eliminated in the presence of the non-specific mAb (Trastuzumab) because the mAb blocked the interactions between the Fab and the cell membrane. These results were similar between all the tested antibody concentrations. In this conditions, ADSs proved to be selective for antigen expressing cells.

Results

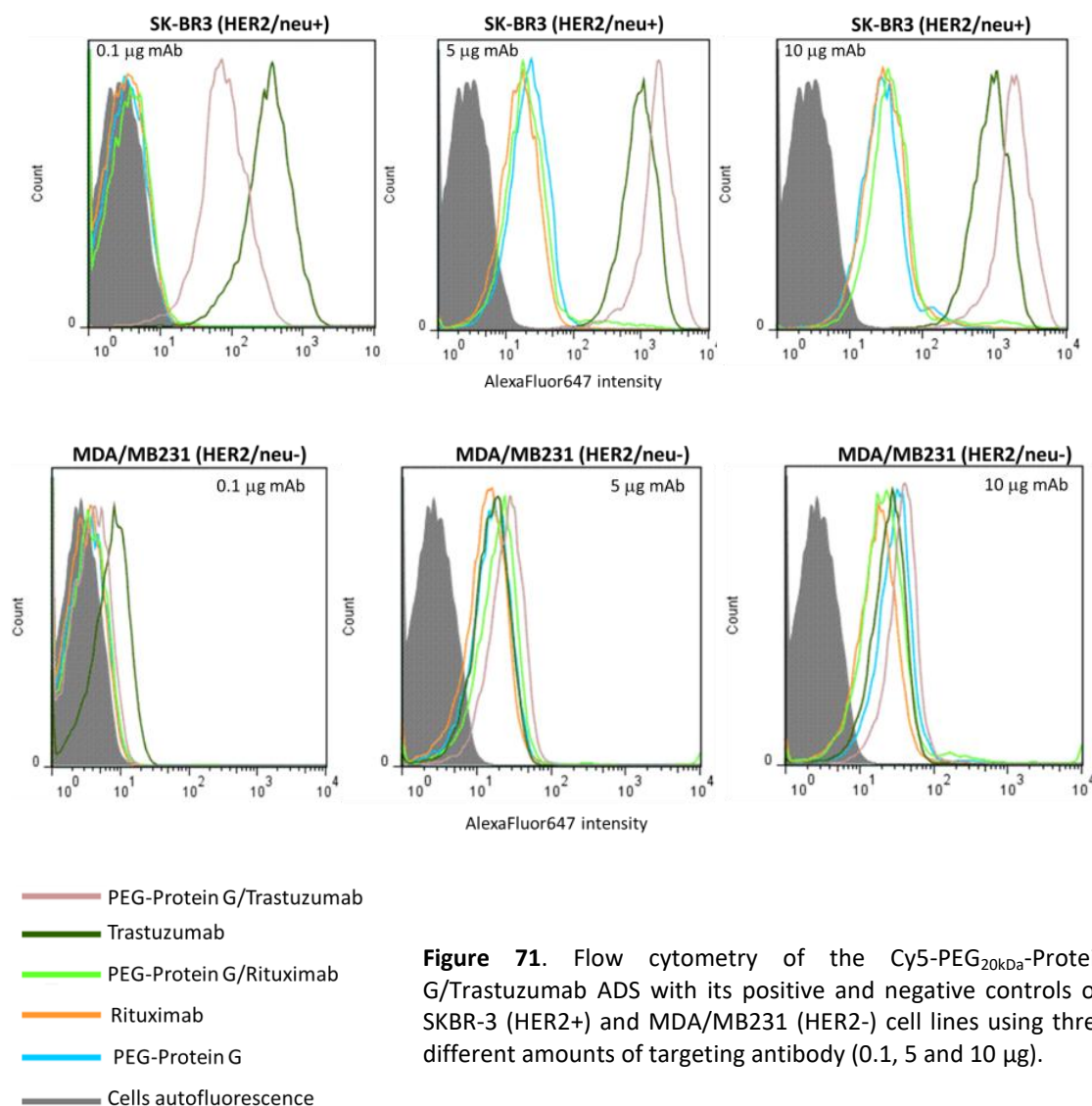


Figure 71. Flow cytometry of the Cy5-PEG_{20kDa}-Protein G/Trastuzumab ADS with its positive and negative controls on SKBR-3 (HER2+) and MDA/MB231 (HER2-) cell lines using three different amounts of targeting antibody (0.1, 5 and 10 µg).

Table 10. Geometrical Mean values of the previous flow cytometry experiment (Fig 71) with the Cy5-PEG_{20kDa}-Protein G/Trastuzumab ADS.

Sample	Geometrical Mean					
	SKBR-3 (HER2+)			MDA/MB231 (HER2-)		
	Amount of antibody			Amount of antibody		
	0.1 µg	5 µg	10 µg	0.1 µg	5 µg	10 µg
PEG-Protein G/Trastuzumab	74.9	1607	1735	3.24	23.5	37.0
Trastuzumab	308	868	840	6.69	15.0	23.2
PEG-Protein G/ Rituximab	3.25	20.8	39.2	3.04	19.1	22.4
Rituximab	2.81	15.6	30.1	2.62	12.6	16.8
PEG-Protein G	2.90	21.2	27.3	2.77	14.7	28.3
Cells autofluorescence	2.33	2.33	2.33	2.16	2.16	2.16

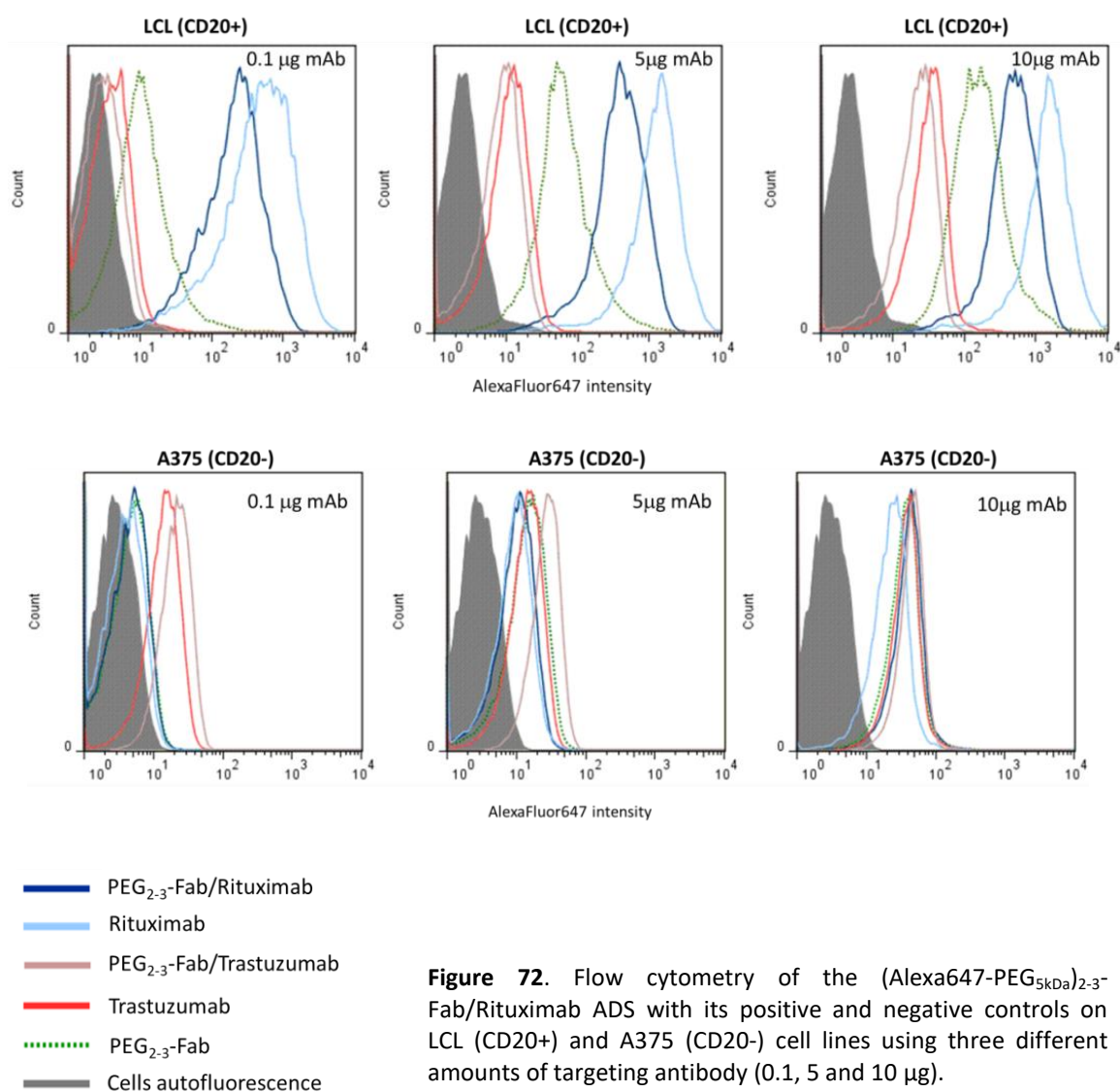


Figure 72. Flow cytometry of the (Alexa647-PEG_{5kDa})₂₋₃-Fab/Rituximab ADS with its positive and negative controls on LCL (CD20+) and A375 (CD20-) cell lines using three different amounts of targeting antibody (0.1, 5 and 10 µg).

Table 11. Geometrical Mean values of the previous flow cytometry experiment (Fig 72) with the (AlexaFluor647-PEG_{5kDa})₂₋₃-Fab/Rituximab ADS.

Sample	Geometrical Mean					
	LCL (CD20+)			A375 (CD20-)		
	Amount of antibody			Amount of antibody		
	0.1 µg	5 µg	10 µg	0.1 µg	5 µg	10 µg
PEG ₂₋₃ -Fab/Rituximab	180	358	447	3.88	9.02	37.8
Rituximab	405	1120	1301	3.39	8.43	21.2
PEG ₂₋₃ -Fab/Trastuzumab	3.32	10.1	29.0	12.9	12.9	35.1
Trastuzumab	2.52	7.54	19.7	20.1	25.6	42.9
PEG ₂₋₃ -Fab	10	62.2	162	3.94	12.7	32.9
Cells autofluorescence	1.76	1.76	1.76	2.26	2.26	2.26

Results

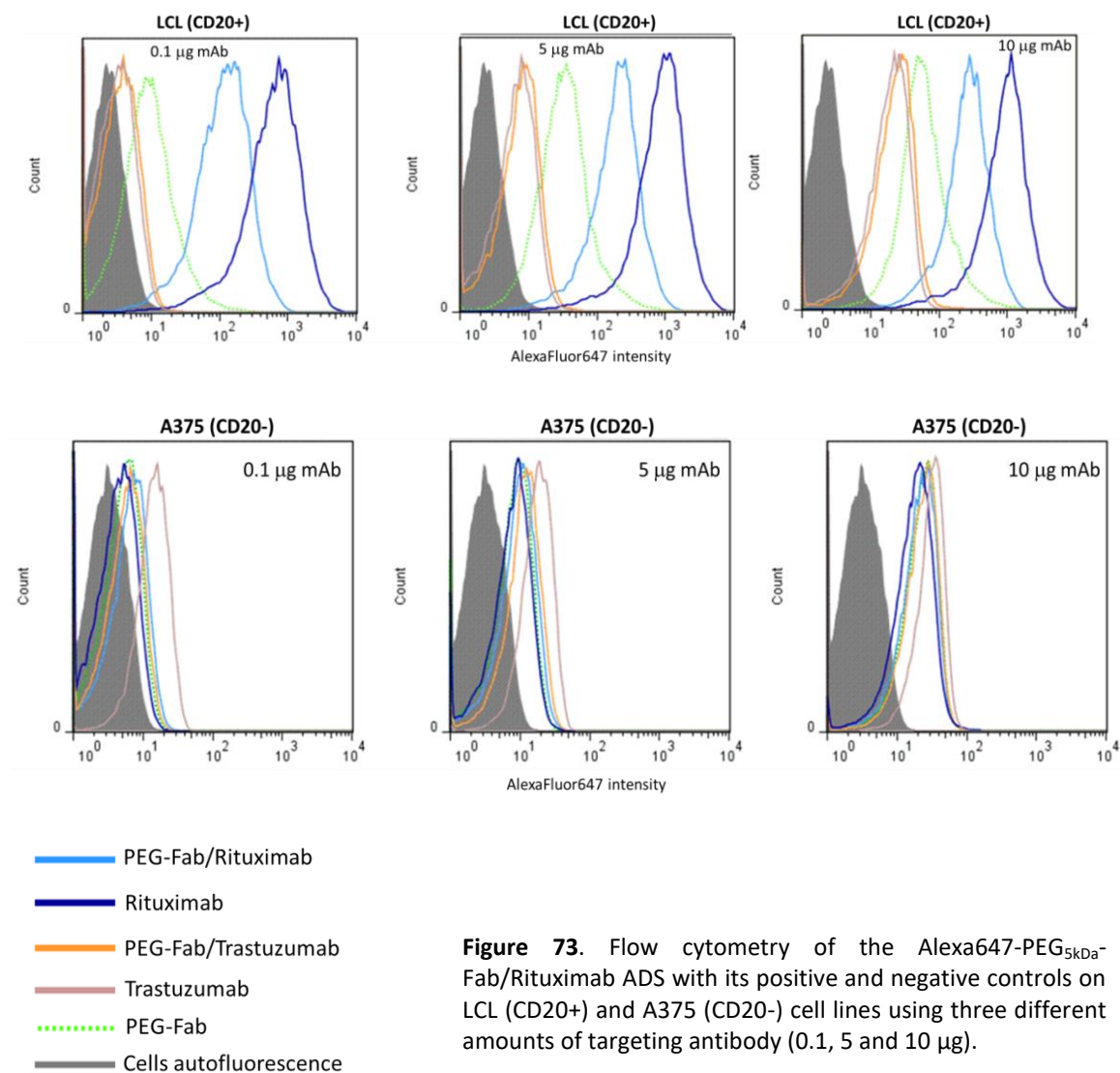


Figure 73. Flow cytometry of the Alexa647-PEG_{5kDa}-Fab/Rituximab ADS with its positive and negative controls on LCL (CD20+) and A375 (CD20-) cell lines using three different amounts of targeting antibody (0.1, 5 and 10 µg).

Table 12. Geometrical Mean values of the previous flow cytometry experiment (Fig 73) with the Alexa647-PEG_{5kDa}-Fab/Rituximab ADS.

Sample	Geometrical Mean					
	LCL (CD20+)			A375 (CD20-)		
	Amount of antibody			Amount of antibody		
	0.1 µg	5 µg	10 µg	0.1 µg	5 µg	10 µg
PEG-Fab/Rituximab	104	173	241	5.62	8.47	19.1
Rituximab	528	778	824	3.85	7.13	16.4
PEG-Fab/Trastuzumab	2.99	6.64	20.0	5.10	10.3	20.7
Trastuzumab	2.66	5.71	16.9	13.3	16.7	28.7
PEG-Fab	8.75	32.5	58.3	4.46	7.33	20.2
Cells autofluorescence	1.62	1.62	1.62	2.46	2.46	2.46

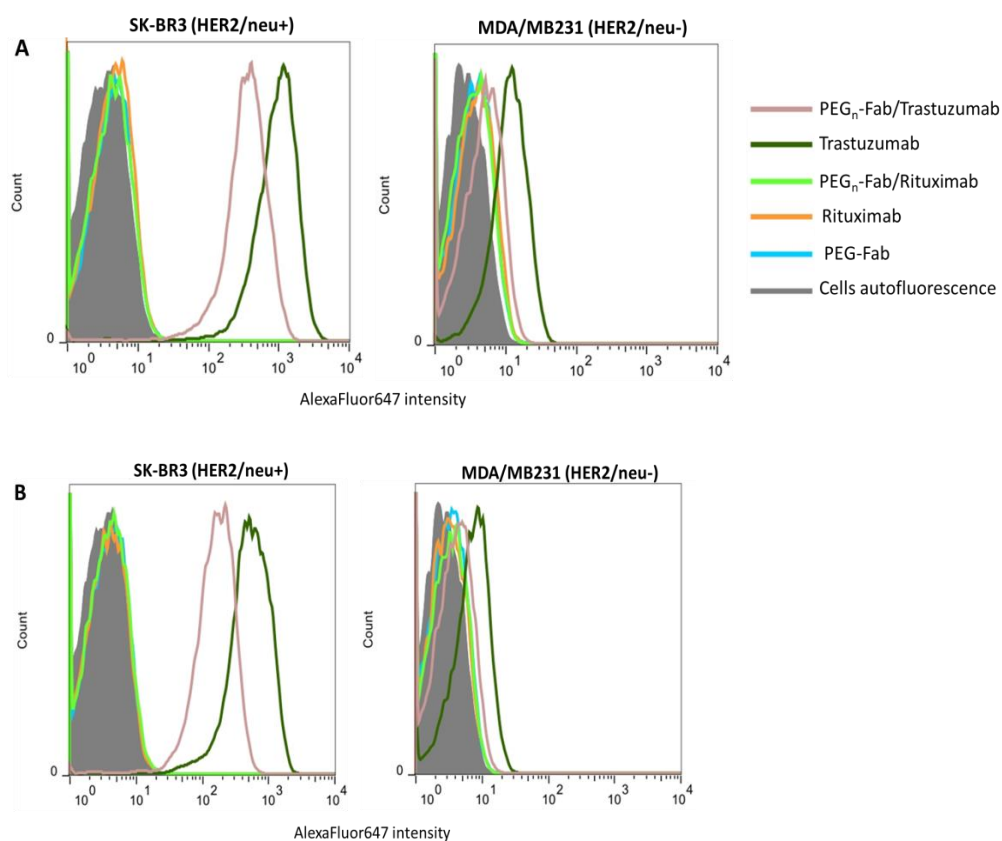


Figure 74. Flow cytometry of the ADSs: A) (Alexa647-PEG_{5kDa})₂₋₃-Fab/Trastuzumab and B) Alexa647-PEG_{5kDa}-Fab/Trastuzumab with their positive and negative controls on SKBR3- (HER2+) and MDA/MB231 (HER2-) cell lines using 0.1 μ g of targeting antibody.

Table 13. Geometrical Mean values of the previous flow cytometry experiment (Fig 74) with the ADSs: A) (Alexa647-PEG_{5kDa})₂₋₃-Fab/Trastuzumab and B) Alexa647-PEG_{5kDa}-Fab/Trastuzumab.

Sample	Geometrical Mean	
	SKBR-3 (HER2+)	MDA/MB231 (HER2-)
Exp A		
PEG ₂₋₃ -Fab/Trastuzumab	320	4.48
Trastuzumab	839	11.1
PEG-Fab/Rituximab	3.72	2.96
Rituximab	3.92	3.29
PEG ₂₋₃ -Fab	3.86	3.13
Cells autofluorescence	2.76	2.14
Exp B		
PEG-Fab/Trastuzumab	148	3.53
Trastuzumab	474	6.59
PEG-Fab/Rituximab	3.42	2.81
Rituximab	3.29	2.62
PEG-Fab	3.38	2.74
Cells autofluorescence	2.76	2.14

Results

A further competition experiment was performed to assess the stability of the Cy5-PEG-Protein G/Trastuzumab ADS after incubation with a competitive mAb, equimolar to Trastuzumab, not recognizing the target cancer cells, to evaluate whether the mAb in the starting ADS was displaced by another mAb. For such evaluation the incubation was performed with a non-specific mAb, Bevacizumab, a humanized anti-VEGF monoclonal IgG1 antibody not able to recognize the cell-lines. The cytofluorimetric analysis disclosed that the non-specific mAb did not perturb the strong and specific binding of the preformed ADS (Fig 75). Indeed, the geo mean values were comparable between Cy5-PEG-Protein G/Trastuzumab alone and Cy5-PEG-Protein G/Trastuzumab incubated with Bevacizumab (524 and 475, respectively). In parallel, the preformed non specific Cy5-PEG-Protein G/Bevacizumab ADS was tested in presence of an equimolar amount of Trastuzumab. In this case if a displacement occurs, as Trastuzumab replaces Bevacizumab in the ADS, the geo mean value is expected to increase because the new formed ADS with Trastuzumab is able to bind HER2 expressing cells. The geo mean values of Cy5-PEG-Protein G/Bevacizumab alone and Cy5-PEG-Protein G/Bevacizumab incubated with Trastuzumab were 31.6 and 107, respectively, showing that a certain degree of displacement had taken place.

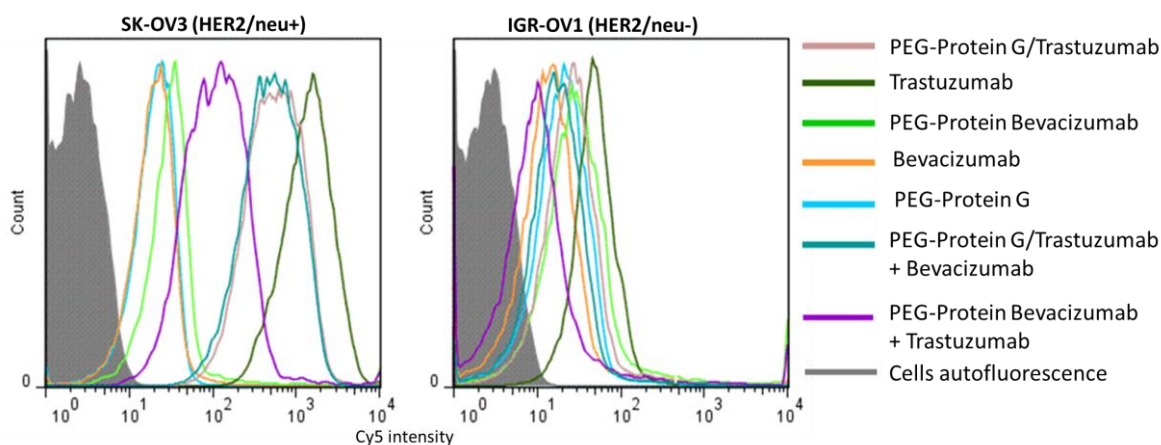


Figure 75. Flow cytometry of preformed ADSs incubated in presence of a competitive antibody. Preformed Cy5-PEG_{20kDa}-Protein G/Trastuzumab was incubated with Bevacizumab (blue line) and preformed Cy5-PEG_{20kDa}-Protein G/Bevacizumab with Trastuzumab (violet line). SKOV-3 (HER2+) and IGROV-1 (HER2-) cell lines were used.

Table 14. Geometrical Mean values of the previous flow cytometry experiment (Fig 75) with the Cy5-PEG_{20kDa}-Protein G/Trastuzumab ADS.

Sample	Geometrical Mean	
	SKOV-3 (HER2+)	IGROV-1 (HER2-)
PEG-Protein G/Trastuzumab	524	24.9
Trastuzumab	1309	48.5
PEG-Protein G/Bevacizumab	31.6	31.8
Bevacizumab	18.9	14.1
PEG-Protein G	18.7	18.6
PEG-Protein G/Trastuzumab + Bevacizumab	475	17
PEG-Protein G/Bevacizumab + Trastuzumab	107	10.9
Cells autofluorescence	2.02	2.03

To resemble physiological conditions, the ADSs were incubated in human plasma and tested again on cells. The plasma concentration of the ADS was chosen on the basis of the calculated plasma concentration reached during the therapy with Kadcyła (about 0.044 mg/ml). In this experiment, Cy5-PEG-Protein G/Trastuzumab was tested on SKOV-3 HER2 positive cells, PEG_n-Fab/Rituximab on LCL cells, and PEG_n-Fab/Trastuzumab on SKBR-3 cells. After plasma incubation, the ADS with Protein G showed a great reduction in the affinity for the HER2

Results

positive cell line (Fig 76), whereas the ADSs with the Fab exhibited only a slight affinity reduction for antigen expressing cells (Fig 77 and 78). This different behavior of the two FcBM, Protein G and Fab, could be explained as a difference in the affinity for the Fc of the antibody. Fab/antibody complex appeared to be more stable and the presence of IgGs contained in the plasma did not disrupt its stability. On the opposite, in the case of Protein G/antibody complex, the endogenous IgGs probably displaced the targeting antibody binding Protein G and the targeting effect was lost. This means that preformed Protein G/antibody complex can be perturbed in presence of high concentrations of competitive antibodies.

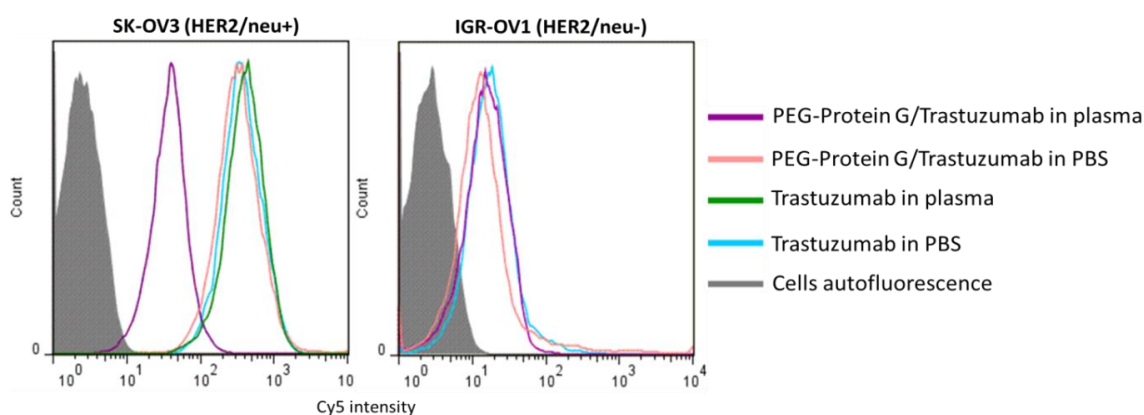


Figure 76. Flow cytometry of the Cy5-PEG_{20kDa}-Protein G/Trastuzumab ADS after plasma incubation on SKOV-3 (HER2+) and IGROV-1 (HER2-) cell lines using 10 µg of targeting antibody.

Table 15. Geometrical Mean values of the previous flow cytometry experiment (Fig 76) with the Cy5-PEG_{20kDa}-Protein G/Trastuzumab ADS.

Sample	Geometrical Mean	
	SKOV-3 (HER2+)	IGROV-1 (HER2-)
PEG-Protein G/Trastuzumab in plasma	36.3	14.5
PEG-Protein G/Trastuzumab in PBS	317	14.6
Trastuzumab in plasma	379	-
Trastuzumab in PBS	349	17.4
Cells autofluorescence	1.90	2.05

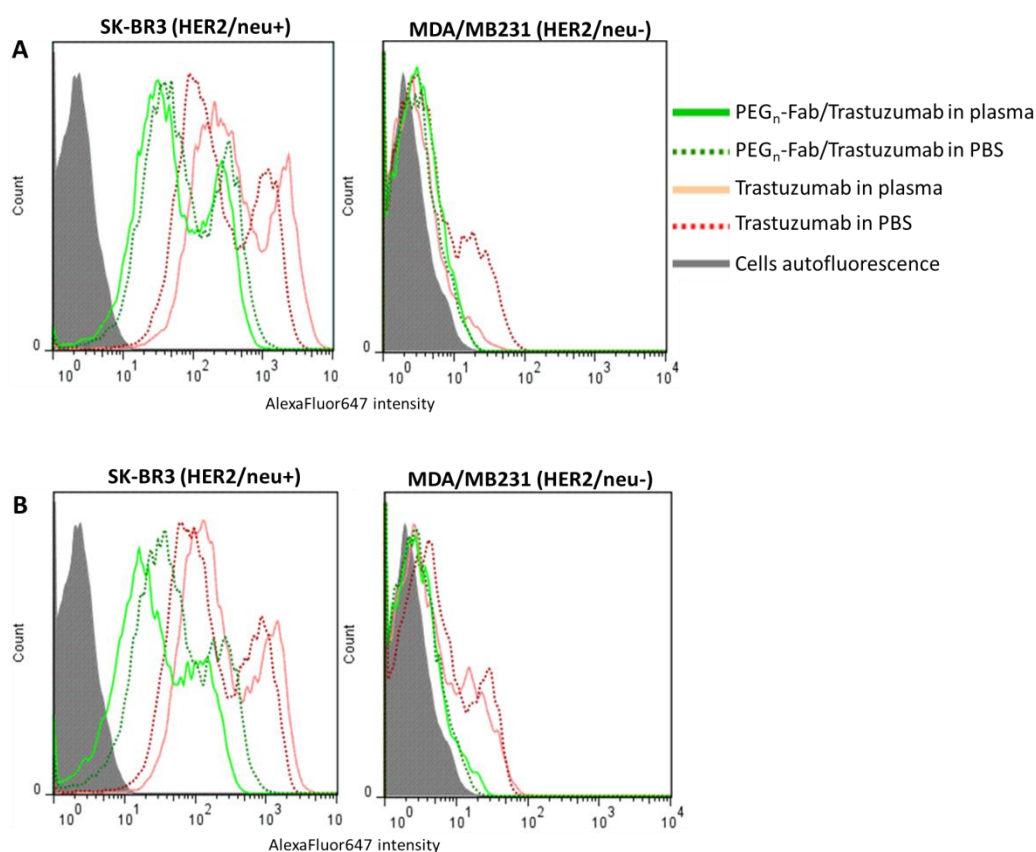


Figure 77. Flow cytometry of the ADSs: A) (Alexa647-PEG_{5kDa})₂₋₃-Fab/Trastuzumab and B) Alexa647-PEG_{5kDa}-Fab/Trastuzumab after plasma incubation on SKBR-3 (HER2+) and MDA/MB231 (HER2-) cell lines using 0.1 µg of targeting antibody.

Table 16. Geometrical Mean values of the previous flow cytometry experiment (Fig 77) with the ADSs: A) (Alexa647-PEG_{5kDa})₂₋₃-Fab/Trastuzumab and B) Alexa647-PEG_{5kDa}-Fab/Trastuzumab after incubation in human plasma.

Sample	Geometrical Mean	
Exp A	SKBR-3 (HER2+)	MDA/MB231 (HER2-)
PEG ₂₋₃ -Fab/Trastuzumab in plasma	53.3	2.50
PEG ₂₋₃ -Fab /Trastuzumab in PBS	72.2	2.27
Trastuzumab in plasma	389	2.31
Trastuzumab in PBS	227	3.77
Cells autofluorescence	1.58	1.66
Exp B	SKBR-3 (HER2+)	MDA/MB231 (HER2-)
PEG-Fab/Trastuzumab in plasma	26.3	2.27
PEG-Fab /Trastuzumab in PBS	50.1	2.17
Trastuzumab in plasma	229	3.54
Trastuzumab in PBS	158	4.33
Cells autofluorescence	1.58	1.66

Results

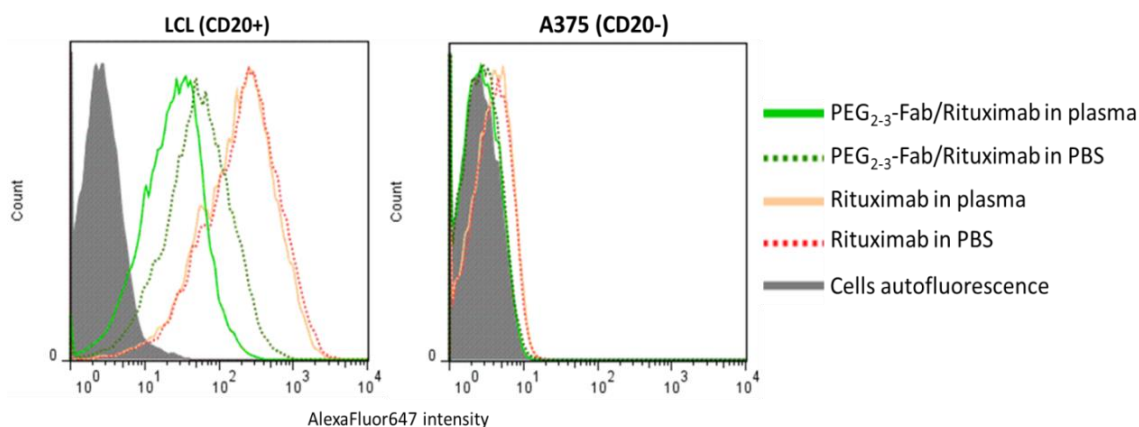


Figure 78. Flow cytometry of the (Alexa647-PEG_{5kDa})₂₋₃-Fab/Rituximab ADS after plasma incubation on LCL (CD20+) and A375 (CD20-) cell lines using 0.1 µg of targeting antibody.

Table 17. Geometrical Mean values of the previous flow cytometry experiment (Fig 78) with the (Alexa647-PEG_{5kDa})₂₋₃-Fab/Rituximab ADS after incubation in human plasma.

Sample	Geometrical Mean	
	LCL (CD20+)	A375 (CD20-)
PEG ₂₋₃ -Fab/Rituximab in plasma	22.5	3.02
PEG ₂₋₃ -Fab/Rituximab in PBS	48.7	2.99
Rituximab in plasma	169	2.12
Rituximab in PBS	189	2.72
Cells autofluorescence	1.98	2.08

5.14 Evaluation of *in vitro* tumor growth inhibition activity of ADS

To test TubA-PEG-Protein G/Trastuzumab *in vitro* efficacy against target cancer line, cells were incubated with escalating doses of the ADS, non targeted TubA-PEG-Protein G, and Trastuzumab alone (Fig 79).

In the HER2 negative MDA/MB-231 human breast cancer cells, the cytotoxicity of TubA-PEG-Protein G was almost constant in presence (IC₅₀ 0.017 µg/ml ± 0.006) or in absence (IC₅₀ 0.02 µg/ml ± 0.006) of the targeting antibody (Trastuzumab), as expected, because any active targeting occurred. On the other hand, when tested in the HER2 positive cell line (SKBR-3), TubA-PEG-Protein G cytotoxicity shown a 2.75 fold increase in presence of Trastuzumab (IC₅₀ 0.004 µg/ml ± 0.0002), compared to TubA-PEG-Protein G alone (IC₅₀ 0.011 µg/ml ± 0.001),

proving that Trastuzumab achieved a specific targeting of the whole system that resulted in a selective cytotoxicity. Overall, TubA-PEG-Protein G exhibited a similar cytotoxic efficacy in either cell lines, while Trastuzumab had no cytotoxic effect in any culture.

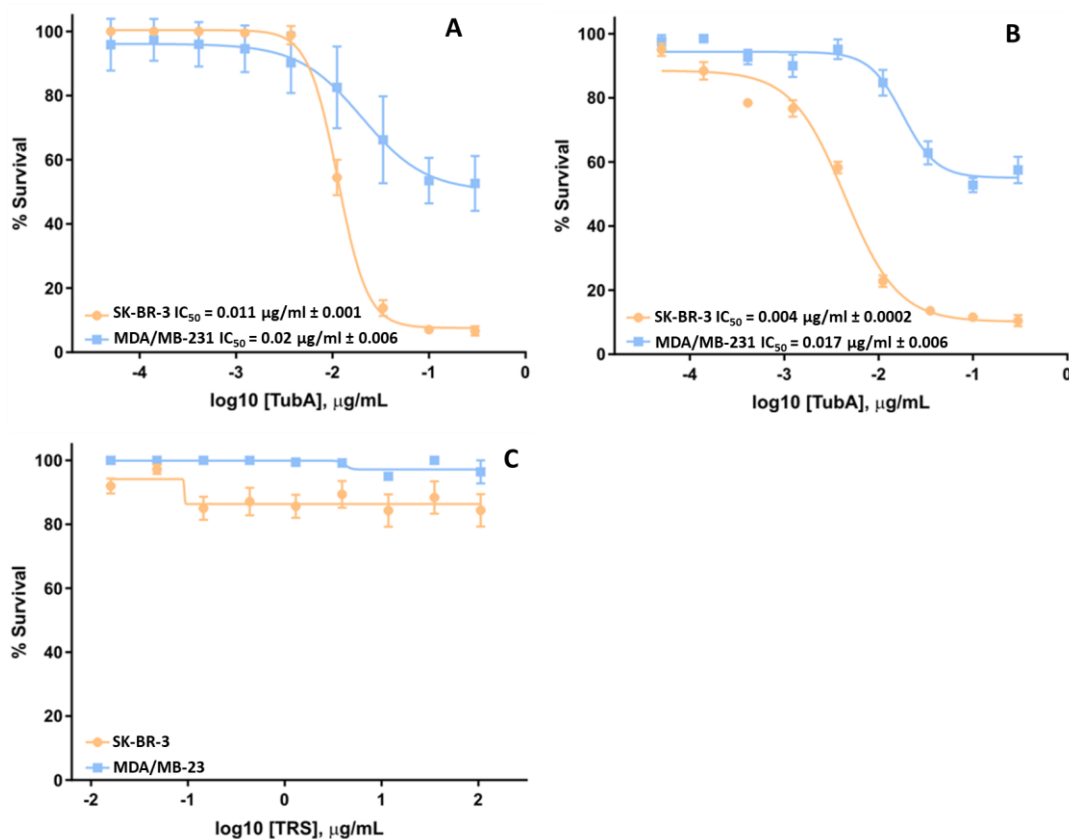


Figure 79. Survival curves of human breast cancer cell lines in response to A) TubA-PEG-Protein G, B) TubA-PEG-Protein G/Trastuzumab and C) Trastuzumab. The growth inhibition effect of ADS in SKBR-3 (orange line) and MDA/MB-231 (blue line) cell line was evaluated by ATPlite assay. Figure shows mean \pm SD of two independent experiments. For each experiment, the IC₅₀ was calculated from each single semi-logarithmic dose-response curve by linear interpolation, and obtained values were then averaged. Values are reported in $\mu\text{g/ml}$ in free drug equivalents.

The observed significant reduction in cytotoxic sensitivity of MDA/MB-231 to ADS is likely to reflect the lack of HER2 expression in this cell line and indicate HER2 mediated binding and internalisation of ADS in the SKBR-3 cell line. Moreover, SKBR-3 cell line appeared more sensitive to the drug than MDA/MB-231 cells: at the higher concentration of Tubulysin A in the assay, the % survival of SKBR-3 cells was reduced to $\approx 7\%$ while that of MDA/MB-231 cells to $\approx 55\%$, with or without the targeting antibody.

5.15 Evaluation of ADS biodistribution in an animal model

Biodistribution studies were performed in NSG mice to evaluate ADS localization at the target tumour. Xenografts tumours were induced by inoculation of cancer cells through subcutaneous injection. IGROV-1 (HER2-) and SKOV-3 (HER2+) were injected in different locations of mice body in order to verify the selective accumulation of the ADS at the target tumour respect to the non target tumour. After tumour growth, the mice were intravenously injected with Cy5-PEG-Protein G/Trastuzumab and Cy5-Trastuzumab, as positive control, and underwent tracking with a fluorescent optical imager to collect fluorescent data and gain anatomical information, at different time points. Cy5-PEG-Protein G/Trastuzumab and Cy5-Trastuzumab were expected to accumulate at HER2 positive tumour if antibody-mediate active targeting occurred.

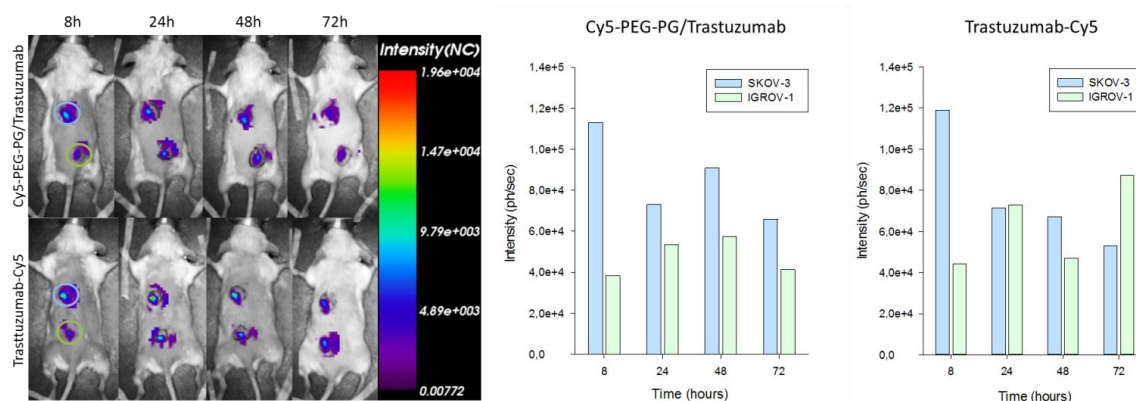


Figure 80. In vivo biodistribution of Cy5-PEG-Protein G/Trastuzumab and Cy5-Trastuzumab. Mice were subcutaneously injected with HER2 positive SKOV-3 (blue bars) and HER2 negative IGROV-1 (green bars) tumour cells. Fluorescence at the tumour masses were detected with a fluorescence optical imager at different time points.

As showed in Fig 80, both Cy5-PEG-protein G/Trastuzumab and Cy5-Trastuzumab accumulated rapidly at the HER2 positive tumour in SKOV-3, reaching the maximum accumulation within 8 hours. After that, selective localization of Cy5-PEG-Protein G/Trastuzumab at the targeted tumour decreased, but still ADS concentration in SKOV-3 tumour remained higher than in non targeted IGROV-1 tumour. This not happened for Cy5-Trastuzumab: the antibody did not show any preferential accumulation at HER2 positive site after 24 h.

To clarify Trastuzumab in vivo behaviour, the biodistribution was repeated and prolonged over the time till 7 days (Fig 81). In this case, slightly higher levels of antibody were found at SKOV-3 tumour till day 4.

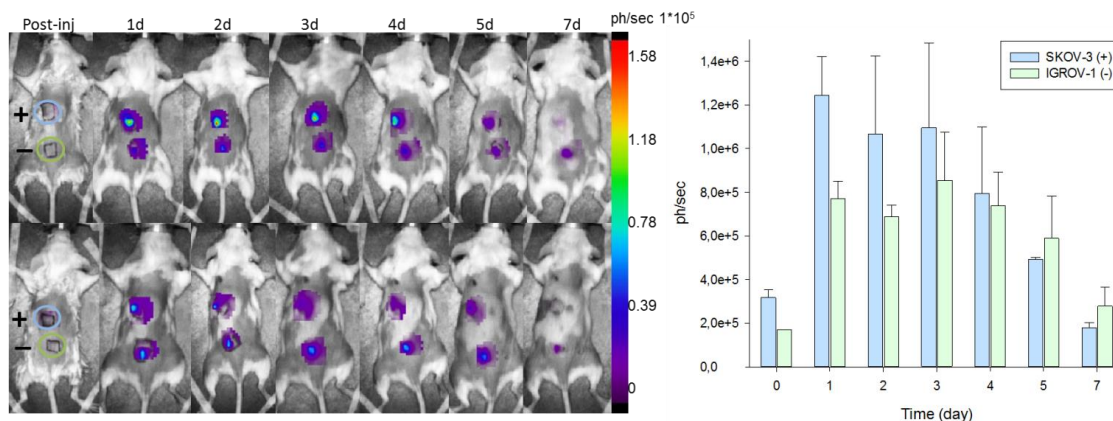


Figure 81. In vivo biodistribution of Cy5-Trastuzumab. Mice were subcutaneously injected with HER2 positive SKOV-3 (blue bars) and HER2 negative IGROV-1 (green bars) tumour cells. Fluorescence at the tumour masses were detected with a fluorescence optical imager at different time points.

5.16 Binding of Alexa488-PEG-Protein G/ICAM ADS to HUVECs

In the initial binding study, the specificity and efficacy of the Alexa488-PEG-Protein G/ICAM ADS to bind TNF α stimulated living HUVECs were tested and compared to non-targeted Alexa488-PEG-Protein G and to the ADS with a non specific mouse IgG. Both TNF α activated ECs, to mimic a pathological condition, and quiescent ECs were used. Samples were analyzed by fluorescence microscopy (Fig 82) to measure fluorescence intensity for binding quantification (Fig 83). The results showed that the ICAM-1 targeted ADS bound specifically activate HUVECs that over-expressed the receptor, while it did not bind to non stimulated HUVECs. On the contrary, the IgG mock ADS control and Protein G alone did not show any specific binding.

Results

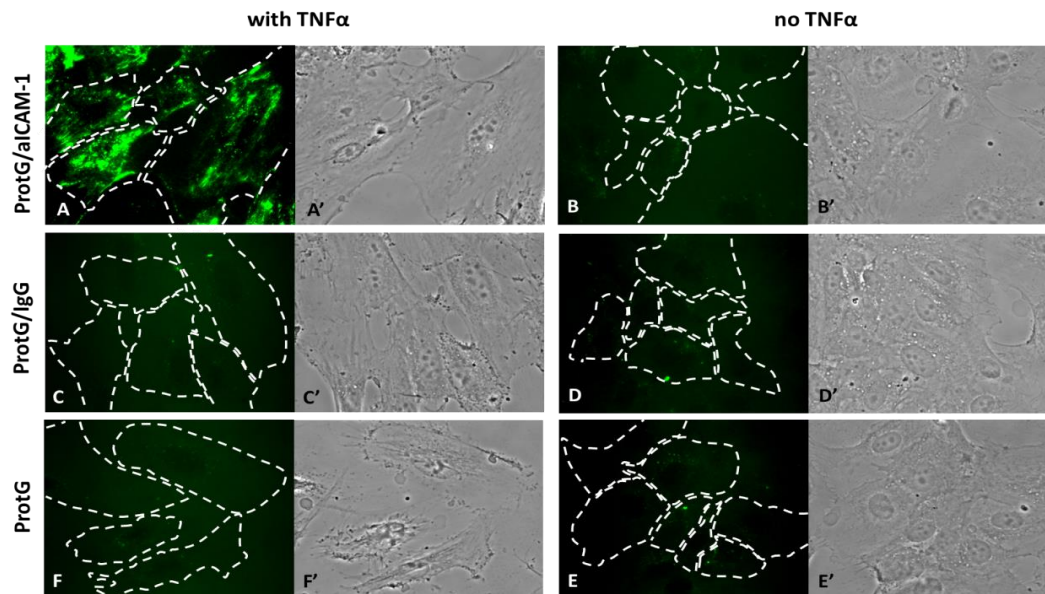


Figure 82. Binding of Alexa488-PEG-Protein G/aICAM-1 (A and B), Alexa488-PEG-Protein G/IgG (C and D) and Alexa488-PEG-Protein G (F and E) to TNF α stimulated (A, C and F) and non stimulated (B, D and E) HUVECs. Samples were incubated for 1h at 37°C. Dashed lines represent the cell borders. X letters indicate the images observed using FITC filter, X' letters indicate the images observed by phase-contrast.

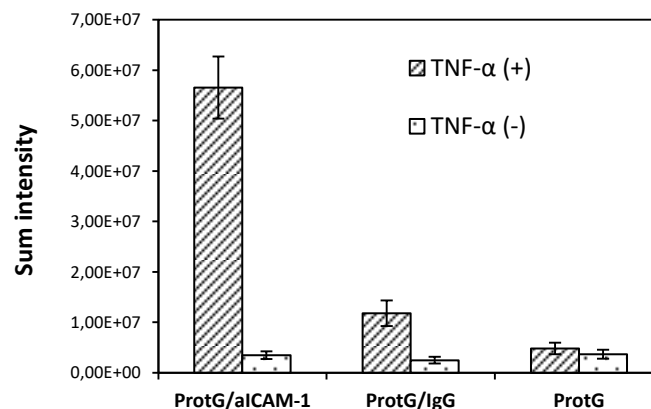


Figure 83. Sum intensity of Alexa488 fluorescence obtained from the cellular images of the binding experiment (an average of 30-45 cells were analyzed). * $p \leq 0.05$ compare to all other conditions, by Student's t-test. Data are the mean \pm S.E.M.

In the following avidity study, the effect of ADS concentration on binding was investigated incubating cells with different concentrations of the ADS for 1 hour at 37°C (Fig 85). In this case, fixed cells were used to avoid ADS internalization and focused the attention only on its surface binding properties. Cell fixation was achieved by incubating cells with 2% PFA in PBS for 15 min. To validate fixation method and verify that the procedure did not cause any cells alteration that could prevent surface binding, a comparison of fluorescence response between living and fixed cells, incubated for 1h at 37°C with the same ADS amount (11.11 nM), was

made. Any significant difference in fluorescence sum intensity was detected between fixed and non fixed HUVECs, establishing that fixative protocol did not alter cell membranes (Fig 84).

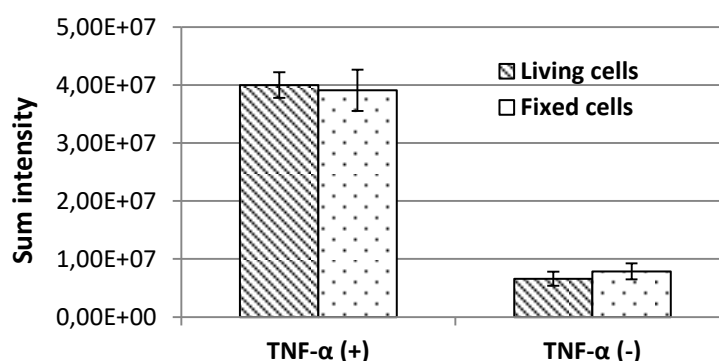


Figure 84. Sum intensity comparison between living and fixed cells incubated with the Alexa488-PEG-Protein G/aICAM ADS for 1 h at 37°C.

In the avidity experiment, as expected, the ADS bound to the surface receptor in a concentration dependent manner without reaching the saturation even at the highest concentration tested, 222.22 nM that corresponds to 10 μ g of aICAM antibody for each well. The obtained data were fitted using SigmaPlot 11.0 according to the “one site saturation” model to calculate the affinity of the ADS for HUVECs. Sum intensity data were used for affinity calculation, giving a K_d of the ADS for HUVECs of 54.34 nM.

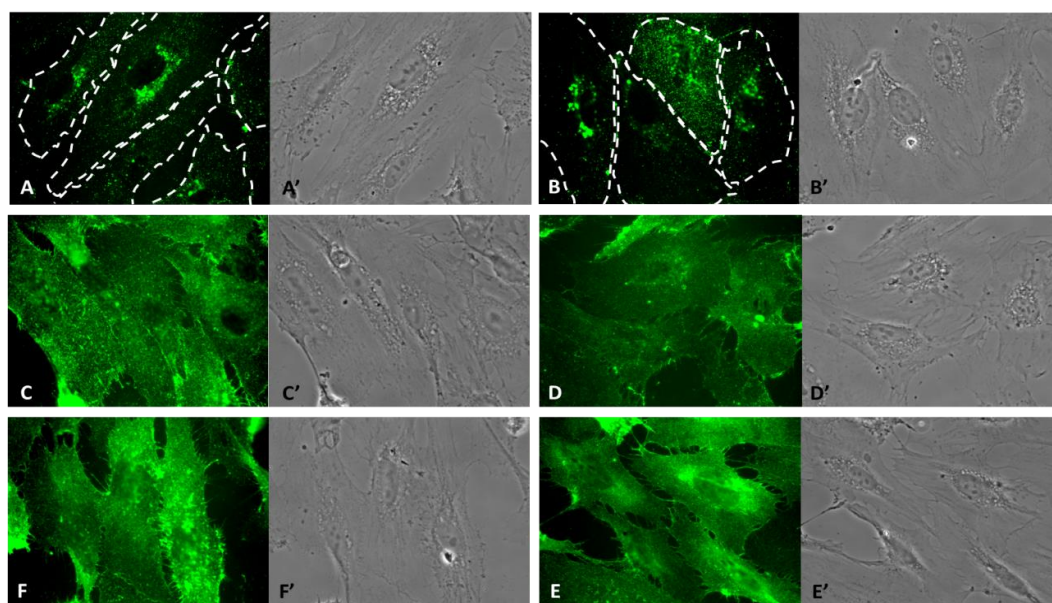


Figure 85. TNF α stimulated HUVECs were incubated with different Alexa488-PEG-Protein G/aICAM concentrations: A) 1.11, B) 2.22, C) 11.11, D) 22.22, E) 111.11 and F) 222.22 nM. Samples were incubated for 1h at 37°C. Dashed lines represent the cell borders. X letters indicate the images observed using FITC filter, X' letters indicate the images observed by phase-contrast.

Results

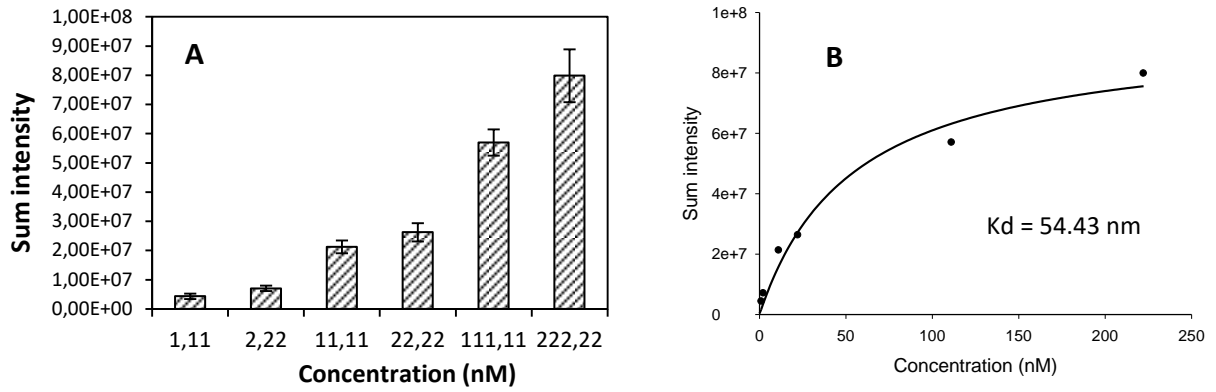


Figure 86. A) Sum intensity of TNF α stimulated HUVECs that were incubated with different concentrations of Alexa488-PEG-Protein G/aICAM. Data are mean \pm S.E.M. ($n > 50$). B) Kd value for the affinity between the ADS and the cells calculated using SigmaPlot 11.0.

To evaluate the kinetic of binding, HUVECs were incubated with the same ADS concentration for different periods of time (Fig 87). The obtained fluorescent data were fitted using SigmaPlot 11.0 calculating a $t_{1/2}$ of 40 min (Fig 88).

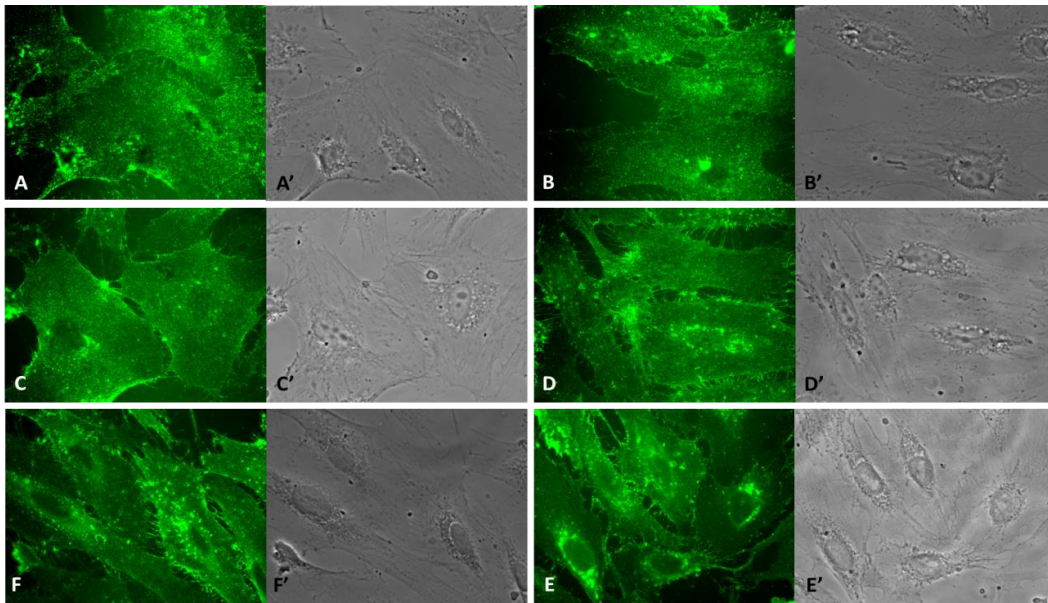


Figure 87. TNF α stimulated HUVECs were incubated at 37°C with a 11.11 nM solution of Alexa488-PEG-Protein G/aICAM for A) 5 min, B) 15 min, C) 30 min, D) 1 h, E) 2 h and E) 23 h. X letters indicate the images observed using FITC filter, X' letters indicate the images observed by phase-contrast.

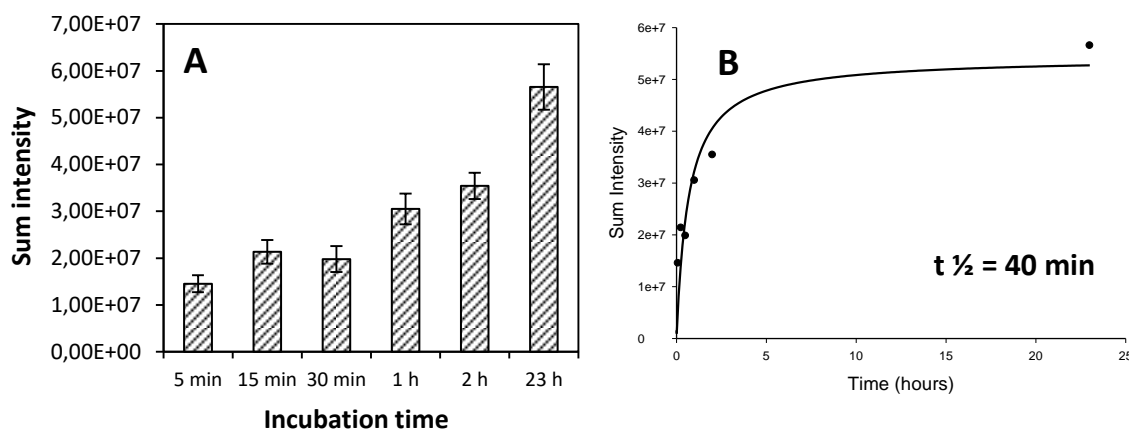


Figure 88. A) Sum intensity of HUVECs incubated with Alexa488-PEG-Protein G/aICAM 11.11 nM for different periods of time. Data are mean \pm S.E.M. ($n > 30$). B) $t_{1/2}$ value for the binding between the ADS and the cells calculated using SigmaPlot 11.0.

5.17 Internalization mechanism of Alexa488-PEG-Protein G/aICAM

To elucidate ADS mechanism of uptake, HUVECs were incubated with different inhibitors of the endocytic transport (Fig 89). When cells were in presence of amiloride, a pharmacological agent known to inhibit Na^+/H^+ exchanger involved in CAM-mediated endocytosis, internalization of ADSs was significantly reduced by $39.47 \pm 4.20\%$, very similar to incubation at 4°C ($46.44 \pm 6.05\%$), condition in which cellular activity is extremely reduced (Fig 90). The binding to ICAM-1 leads to CAM-mediated endocytosis which is an independent process not related to the common endocytic pathways such as clathrin- and caveolae-mediated endocytosis. On the other hand, endocytosis in cells treated with filipin, MDC or wortmannin was not significantly affected ($91.39 \pm 6.42\%$, $87.05 \pm 5.59\%$ and $112.00 \pm 6.18\%$ respect to control at 37°C). These results demonstrated that ADSs internalization was mediated by the CAM-pathway, a non classical route of endocytosis that relied on the interaction between the targeting antibody (aICAM) and the receptor (ICAM-1 on cells surface). Since the labelling dye was tethered to Protein G through PEG linker, these results proved that during receptor binding and subsequent uptake by cells, the protein-antibody system maintained its stability acting like a unique structure.

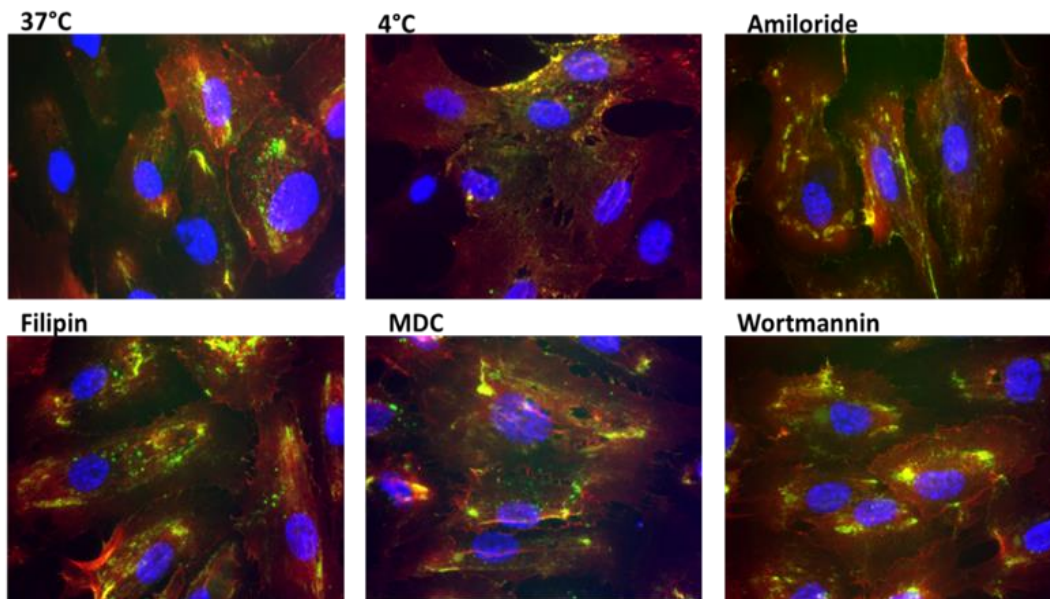


Figure 89. Representative images of TNF α stimulated HUVECs that were incubated with inhibitors of the endocytic transport and their control at 37° and 4°C (in absence of inhibitors).

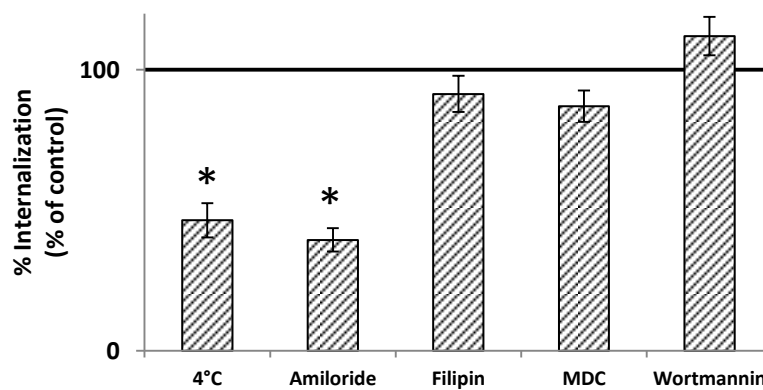


Figure 90. Endocytosis mechanism of ADSs into TNF α stimulated HUVECs, percent internalization relative to control cells at 37°C is shown. *p \leq 0.05 compares the various inhibitors to control cells. Data are mean \pm S.E.M. (n > 50).

5.18 Kinetic of internalization and lysosomal trafficking

Previous works using ICAM-1 targeted nanoparticles have showed that CAM-mediated endocytosis results in nanoparticles trafficking to lysosomes¹⁴⁴. In this study, we aimed to evaluate whether also ADSs were transported to lysosome vesicles. Intracellular trafficking was followed staining lysosomes with Texas Red dextran 10 kDa, and the Alexa488-labelled ADS over time via fluorescence microscopy (after 1, 3 and 5 hours of incubation) (Fig 91). The

results showed that ADSs internalization increased over the time, as well as the percentage of the internalized Alexa488-PEG-Protein G that co-localized within lysosomes, revealing that proteins were moved from endocytic vesicles to lysosomes for degradation (Fig 92).

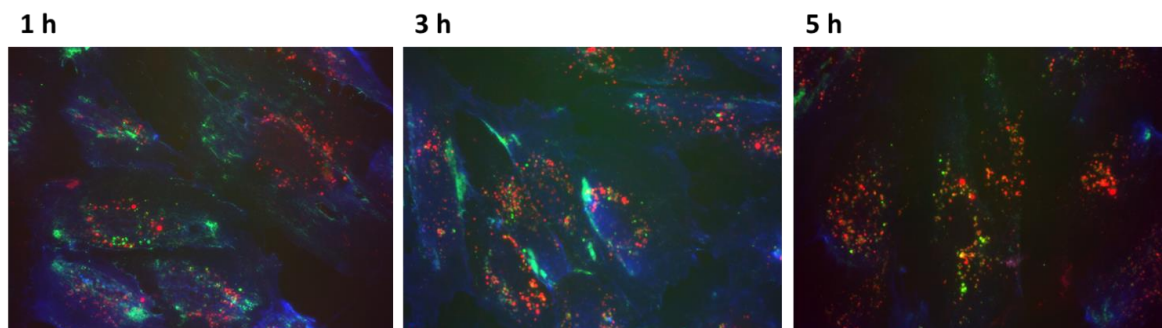


Figure 91. Representative images of TNF α activated HUVECs incubated with the Alexa488-PEG-Protein G/ α ICAM ADS for different times to determine %internalization and %lysosomal co-localization.

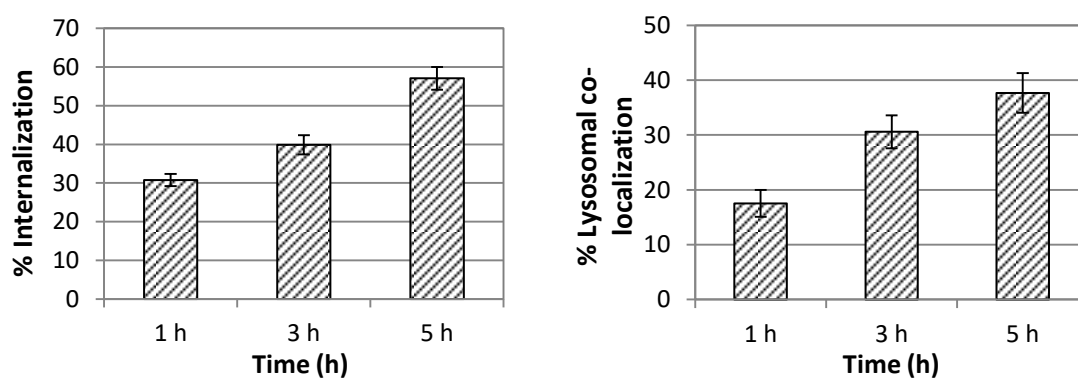


Figure 92. % Internalization and % Lysosomal co-localization of ADSs in HUVECs over time.

6 DISCUSSION

The primary goal of target therapy is pursuing a selective cytotoxicity to the diseased tissue, sparing healthy cells, in order to reduce side toxic effects, ameliorate the therapeutic index and, overall, improve therapy outcomes. Undesired toxicities and narrow therapeutic index are issues of particularly relevance in anticancer treatments, that considerably reduce the quality of life of patients. To date various approaches of drug targeted delivery have been explored and proposed. One of this consist in the direct conjugation of cytotoxic drugs to antibodies as targeting agents, generating the biopharmaceutical class of antibody-drug conjugates (ADCs). In an ADC, a potent cytotoxic drugs become a cargo delivered by a monoclonal antibody to the target tissue. Monoclonal antibodies are characterized by an incredible affinity for their antigen that can be identified with specific markers on cell surface, that typically play an important role in the pathological status (such as proteins, glycoproteins or carbohydrates). Ideally, these markers are selectively expressed on the surface of diseased cells with minimal expression in normal human tissues. Despite the great selectivity, monoclonal antibodies are generally employed in combination therapy since they are not enough potent to be therapeutically active as single agent. Thus, in an ADC, the antibody is “armed” with cytotoxic drugs that are conjugated through a specific linker. The conjugation chemistry and the linker are the key points in the development of an ADC. The first generation of ADC was obtained using non specific conjugation techniques, that exploited the reactivity of cysteine and lysine residues. The most common antibody format used in therapy is the IgG1 that contains 4 interchain disulphide bridges and up to 80 lysines. It is obvious that the resulting product was a heterogeneous mixture of ADC with different DAR (drug-antibody ratio) and isomers. Product characterization and batch to batch reproducibility of such products are difficult and, above all, different antibodies bearing a different number of drugs or/and different conjugation sites can display dissimilar pharmacokinetic and stability profiles, resulting in dissimilar clinical outcomes. For example, it is well known that a high DAR makes the system more hydrophobic and more subjected to elimination from blood circulation, resulting in a short pharmacokinetic.

Moreover, today drugs agency are demanding highly homogeneous products. For all these reasons, research is now directed to promote ADC evolution into a new generation in which site specific coupling methodologies are applied. Following this need, we are here proposing an alternative approach to covalent conjugation in order to achieve control over site of conjugation and DAR. This drug delivery system can be defined as antibody-drug system (ADS) and is formed by the targeting antibody not covalently bound to a molecule that is characterized by unique affinity for the Fc region of the antibody. This molecule, called Fc binding molecule (FcBM), also bears the drug/drugs through a linker. In an ADS, the Fab regions of the antibody, deputed to antigen recognition, remain free and DAR is well defined. An ADS is obtained by simply mixing the two components, the FcBM-drug and the antibody. In addition, being the Fc region common among the immunoglobulins, the system is very versatile because the same FcBM can be coupled to different antibodies on the basis of the disease to be treated and there is no need to adapt the coupling chemistry. Firstly, Protein A was tested as possible candidate for the role of FcBM. Protein A is a well-known surface receptor from *Staphylococcus aureus* constituted of five highly homogeneous Fc binding domains for a total MW of about 42 kDa. Its properties have been extensively studied and Protein A is now largely employed in industrial purification of antibodies by affinity chromatography showing a K_a of about 10^8 M^{-1} . The protein was site-specifically PEGylated at the N-terminus and at one glutamine residue via TGase-mediated PEGylation with a 5 kDa polymer chain in order to reduce its immunogenicity and have a unique linker for the drug molecule. Monoconjugates were complexed with monoclonal antibodies to create ADSs. Unfortunately, in vitro studies established that Protein A based ADSs were not enough stable and the protein was rejected as possible FcBM. The research of a proper FcBM have prosecuted in this work testing another bacterial Fc receptor: Protein G from some *Streptococci C* and *G* strains. Protein G has a high affinity for all human IgGs and for the IgGs of a variety of mammalian species, included mouse IgGs. As Protein A, it is often used for antibodies purification, especially in the case of human IgG3 that are not bound by Protein A. To date, different genes of Protein G have been identified producing protein of various MW. In its entire form, Protein G is a 60 kDa protein containing also a albumin binding site, however, we used a reduced form of about 23 kDa that contains the three IgG binding domains and lacks albumin binding properties. Protein G was site-specifically PEGylated at the N-terminal using a PEG-aldehyde 20 kDa. In addition to the Fc binding capacity, Protein G is able to bind also the Fab with a lower affinity. For this reason, when antibody is added to Protein G solution, a precipitate is formed because the protein crosslinks the antibody, thus giving aggregation on the complexes that become insoluble. Two PEGylated variant of Protein G have been tested to

Discussion

verify if the polymer can inhibit complex aggregation by sterically preventing the binding to the Fab moieties. In one conjugate PEG 5kDa was selectively attached to the N terminal amino acid, whereas the second conjugate was randomly PEGylated at the lysine residues using a PEG_{2kDa} (the average number of polymer chain per protein was 2). PEG_{2kDa}-Lys-Protein G did not give precipitation in presence of an antibody, but the complexes between PEG_{5kDa}-Nter-Protein G and the antibodies were insoluble. To avoid random PEGylation, a higher MW PEG chain (20 kDa) was used for N-terminus conjugation. The conjugate obtained did not crosslink antibodies. We decided to continue the studies using PEG_{20kDa}-Nter-Protein G conjugate. The monoPEGylated Protein G was successfully purified from unmodified protein and multiPEGylated protein by anion exchange chromatography, and had a MW of about 45 kDa given by one molecule of Protein G (23 kDa) plus one molecule of polymer (20 kDa). PEGylation had not changed the secondary structure of Protein G, as assessed by FUV-CD spectra. The conjugate had an alpha helix structure with the two minima at 208 and 222 nm, as the unmodified protein. Preservation of secondary structure is important to avoid a loss in the biological functionality of proteins. In addition, Protein G is a very stable receptor and could partially regain its secondary structure after thermal denaturation. Melting temperature remained constant around 77°C among unmodified protein and the conjugate.

To study the binding between FcBM and antibodies, ITC was chosen because affinity constant and binding stoichiometry are calculated in solution without the necessity of further modification of the species (for example immobilization on a chip as in SPR). Trastuzumab and Rituximab were selected as model antibodies for the preparation of the ADSs because they bind to two of the most validated cancer targets, are on the market from many years and Trastuzumab is also part of an FDA approved ADC (Kadcyla). PEGylated Protein G was found to bind one molecule of Trastuzumab with an affinity of 10^7 M^{-1} . Binding stoichiometry was confirmed by DLS experiments analysing solutions of the complexes between the FcBM and the antibody with different FcBM/antibody ratios. At 1:1 ratio the size of the complex reached the maximum. In the other cases, if an excess of FcBM or antibody was present, the free molecules contributed to reduce the average size measured by the instrument. Therefore, the maximum size was detected when the majority of the molecules was interested in complex formation.

In vitro cell investigations using FACS proved ADS's binding specificity and affinity towards target cell antigens. NIR labelled PEGylated Protein G was prepared conjugating the dye to the free end of the polymer. Cy5-PEG-Protein G was complexed to Trastuzumab and the resulting ADS selectively recognized HER2 positive cells (SK-OV3 and SK-BR3), while non targeted FcBM did not retain any specificity. The preformed ADS proved to be stable also in presence of a

competitive antibody (Bevacizumab), added at equimolar concentration to Trastuzumab. The preformed ADS was not perturbed by the competitor antibody preserving unchanged the affinity for the antigen. However, after incubation in human plasma, the ADS affinity for the antigen expressing cells greatly decreased probably because of the displacement of the targeting antibody (Trastuzumab) mediated by the IgG of the plasma.

The binding to the surface receptor was the essential pre-requisite for achieving the active targeting of the system. In the following step, the dye was substituted with a cytotoxic drug to evaluate the *in vitro* tumour growth inhibition activity of the ADS. Tubulysin A (TubA), a potent inhibitor of tubulin polymerization, was selective as active cargo. Tubulysins are a class of pharmacological agents that is actually considered one of the most suitable payload in an ADC development because of the very high activity (nano and sub nanomolar range). TubA presents a 3-pyridyldithio propionate reactive group that permitted to tether the toxin to the PEG end of conjugated Protein G via a disulphide bond. Disulphide bridges have been largely exploited in drug delivery systems to promote the release of the drug after cellular internalization. In fact, the cytoplasm is a reducing environment due to the high concentrations of reduced glutathione that prevents sulfhydryl bridges formation. TubA-PEG-Protein G was complexed to Trastuzumab to verify the selective cytotoxicity of the ADS on HER2 positive cells (SK-BR3) respect to HER2 negative cells (MDA/MB-231). The presence of the antibody increased TubA IC50 of about 2.75 in antigen expressing cells. Differently, TubA-PEG-Protein G had the same activity in presence or in absence of the targeting antibody on HER2- cells since any specific targeting occurred. The ADS demonstrated to selectively inhibit the growth of HER2+ tumour cells. We are planning to repeat the experiment by reducing the incubation time in view to mimic a more real *in vivo* situation. In this case, a higher cytotoxicity of the conjugate is expected for antigen expressing cells.

In vivo targeting activity of the Cy5-PEG-Protein G ADS was evaluated in xenograft mice. The animals present subcutaneous tumour masses, one HER2+ (SKOV-3) and the other HER2- (IGROV-1) in order to verify if the drug delivery system selectively accumulate to the tumour that expresses the antigen recognized by the targeting antibody. Trastuzumab directly conjugated to Cy5 through lysine residues (as a classical ADC) was used as positive control. Total body scanning was made to detect the intensity of Cy5 fluorescence and, then, the intensity of the two tumour masses were compared. A selective accumulation of ADS at HER2+ site was rapidly reached after 8 h. Then, the relative accumulation decreased, even if ADS concentration at SKOV-3 remained slightly higher. Also the biodistribution profile of Trastuzumab showed a very rapid accumulation at HER2+ tumour, but it was not preserved over the time. This was a preliminary experiment and further investigation are necessary. In

Discussion

particular, other animal model will be considered since subcutaneous tumour present a low amount of blood vessels and are reached with difficulty, especially by antibodies that scarcely extravasate.

The second FcBM investigated in order to overcome the limiting issues of Protein G stability in plasma was a Fab' against the Fc region of human IgGs. Fab' was obtained by partial reduction of a goat F(ab')₂ that led to the reduction of the disulphide bridges of the hinge region. The reactive thiol groups were then exploited for the reaction with PEG-maleimide 5 kDa via a Michael addition reaction. The conjugates were purified by gel filtration and the subsequent characterization showed that up to three polymer chains were conjugated. In order to elucidate goat Fab' PEGylation pattern, Rituximab was used as model for antibody fragmentation and Fab' PEGylation. Rituximab is a chimeric IgG1 containing a human hinge region. It is well known that IgG1 present two disulphide bridge at the hinge region that give two reactive thiol groups for each Fab' molecule yielding the obtainment of biPEGylated form. This was confirmed by our results: we isolated a Fab conjugate having a MW of almost 60 kDa, that corresponds to one molecule of Fab' (48.5 kDa) plus two molecules of PEG (5 kDa x 2). We can assume that the different reactivity between human and goat Fab' derives from a difference in the hinge region or from the presence of more disulphide bridges in goat Fab' that are susceptible to reduction. According to Strausbauch et al., in the hinge region of a goat IgG there is only one interchain disulphide bond, and in close proximity there is a intrachain bridge located in the heavy chain. We can suppose that after hinge opening mediated by cysteamine, also the intracellular bridge becomes exposed and can be reduced giving other two possible reactive site for PEG attachment (Fig 93).

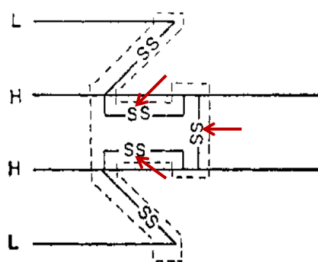


Figure 93. Arrangments of disulphide bonds in a goat IgG. Red arrows indicate the bridges that are proposed to undergo reduction.

PEGylated Fab was characterized and analysed as previously described for Protein G. Secondary structure was assessed by FUV-CD. Dichroic signal of Fab and its PEGylated forms was very weak, but we could still identified the minimum around 218 nm that is typical of β -

sheet motifs. It is known that IgGs structure is prevalently β -sheet and that IgGs contain a lot of aromatic residues (especially in Fab region) that can give a contribution to the spectrum. Also in this case secondary structure was preserved after PEGylation, even in the case of triPEGylated conjugate. ITC binding studies disclosed that Fab affinity for Rituximab was about 10^8 M^{-1} and that Fab/antibody stoichiometry was 1. Unfortunately, we could not determine the affinity of the PEGylated forms for Rituximab because of the amount of PEG-Fab was not enough to conduct the experiment. For FACS experiments, two PEGylated batches of Fab were prepared: the first containing only the monoconjugate, and the second containing a mixture of bi- and tri-conjugate (with a prevalence of triPEG-Fab). Both the purified batches were complexed with Trastuzumab and with Rituximab to prove the versatility of the system: we can potentially use the same FcBM with different antibodies depending on the target tissue. This is possible because the Fc region is shared between all IgGs. When FACS experiment was conducted after ADS incubation in human plasma to resemble a more physiological condition, PEGylated Fab preserved their affinity for antigen expressing cells and showed only a little reduction compare to incubation in PBS. It is reasonable that Fab interaction with the Fc of antibodies is stronger than Protein G, therefore the stability of the preformed ADS is enough strong to be not disturbed by the presence of plasma antibodies. In the next steps, we are planning to perform in vivo biodistribution in animal models to assess PEG-Fac/antibody in vivo stability and targeting capacity.

Until now, the ADS approach was applied to the field of cancer therapy, as the majority of the ADCs currently under development. However, in the last part of this work we focused our attention on another tissue, the endothelium. Using human endothelial cells we investigate the possibility to achieve intracellular delivery of our ADS. Moreover this constitutes a proof of concept for ADS applicability to different therapeutic needs. Nowadays, endothelium targeting of therapeutic and diagnostic agents is an expanding field of research due to the involvement of this tissue in a variety of pathological conditions, including inflammation, ischemia-reperfusion, atherosclerosis, thrombosis. Among endothelial cells (EC) surface determinants, the intercellular adhesion molecule-1 (ICAM-1) constitutes a good candidate target for this purpose because it is a receptor exposed primarily by ECs, it is readily accessible to the circulation, and it is up-regulated by pathological factors such as $\text{TNF}\alpha$, $\text{INF}\gamma$ and IL-1. Antibodies directed to ICAM-1 have been investigated as therapeutic agents and delivery vehicles for drug carriers. The block of ICAM-1 receptor gives by itself a benefit response providing an anti-inflammatory effect. In the present study, we characterized receptor binding, internalization and intracellular trafficking of Cy-PEG-protein G complexed to a mouse IgG2a against the human ICAM-1 receptor. ICAM-1 targeting offers the possibility of intracellular

Discussion

drug delivery, via a unique pathway called cell adhesion molecule (CAM)-mediated endocytosis. In this study, we used fluorescence microscopy to determine and visualize EC targeting of Alexa488-PEG-Protein G mediated by anti ICAM-1 (aICAM-1) antibodies. As the classical endocytic receptors, also CAM-mediated endocytosis follows intracellular trafficking from endocytic vesicles to lysosomes, and the internalized receptor can be recycled to the cell surface. The experiments were performed in human umbilical vein endothelial cells (HUVECs) that were seeded on gelatin coated coverslips. To induce ICAM-1 overexpression on cell surface, HUVECs were treated with TNF α for at least 16 h. Alexa488-PEG-Protein G/aICAM-1 ADS selectively bound activated HUVECs. This binding was specific since aICAM-1 substitution with a non specific mouse IgG created an ADS that did not have any binding capacity, as well as non targeted Alexa-PEG-Protein G. The affinity of the ADS for the system was estimated to be 54 nM and the $t_{1/2}$ of binding was around 40 min. The subsequent studies aimed to define the internalization process. Mechanism of uptake was evaluated in presence of different inhibitors of the endocytic transport: amiloride (that inhibits CAM-pathway), filipin (that inhibits caveolar endocytosis), MDC (that inhibits clathrin endocytosis) and wortmannin (that inhibits macropinocytosis). Only amiloride significantly reduced ADS internalization by almost 40%, compared to the control without any inhibitors, proving that the uptake relies on the interaction with ICAM-1 receptors. Moreover, the result disclosed that during receptor binding and following uptake process, the ADS preserved its integrity acting like a whole structure (since the dye was tethered to protein G through the PEG). Following the intracellular trafficking of the ADS demonstrated that ADS were moved from the endocytic vesicle to lysosomes for degradation.

In conclusion, ADS approach has proven the possibility to create a non covalent drug delivery system using an antibody, as targeting moiety, that preserved a great in vitro affinity for antigen presenting cells. In a ADS the number of drug molecules delivered by a single antibody can be strictly controlled and only the Fc region is involved in complex formation with the FcBM ensuring that the Fab region are free to interact with the antigen. The system is also very versatile since different antibodies can be used with the same FcBM construct. However a possible issue is the displacement of the targeting antibody mediate by plasma IgGs once the ADS is injected in vivo. This focus the attention on the importance of the FcBM –in particularly in its Fc affinity- that emerges as the core of the entire ADS. Indeed, the affinity of the FcBM must be enough high to avoid premature dissociation that would result in systemic toxicity. Moreover, in human endothelial cellular models, it was proven the possibility to achieve an active delivery of cytotoxic drugs inside cells through ADS approach. This underline how during

the binding and the uptake process the ADS maintains its integrity and behave as a unique molecular entity.

7 REFERENCES

1. Chari, R. V. J., Miller, M. L. & Widdison, W. C. Antibody-drug conjugates: An emerging concept in cancer therapy. *Angew. Chemie - Int. Ed.* 53, 3796–3827 (2014).
2. Siegel, R., Miller, K. & Jemal, A. Cancer statistics, 2017. *CA Cancer J Clin* 67, 7–30 (2017).
3. Ross, J. S. *et al.* Targeted therapies for cancer 2004. *Am J Clin Pathol.* 122, 598–609 (2004).
4. Perez, H. L. *et al.* Antibody-drug conjugates: current status and future directions. *Drug Discov. Today.* 19, 869–881 (2014).
5. Tsuchikama, K. & An, Z. Antibody-drug conjugates: recent advances in conjugation and linker chemistries. *Protein Cell.* 1–14 (2016).
6. Gébleux, R. & Casi, G. Antibody-drug conjugates: Current status and future perspectives. *Pharmacol. Ther.* 167, 48-58 (2016).
7. Yao, H., Jiang, F., Lu, A. & Zhang, G. Methods to design and synthesize antibody-drug conjugates (ADCs). *Int. J. Mol. Sci.* 17, (2016).
8. Ford, C. H. *et al.* Localisation and toxicity study of a vindesine-anti-CEA conjugate in patients with advanced cancer. *Br. J. Cancer* 47, 35–42 (1983).
9. Roboz, G. J. *et al.* Efficacy and safety of Gemtuzumab Ozogamicin in patients with poor-prognosis acute myeloid leukemia. *Leuk. Lymphoma* 43, 1951–1955 (2002).
10. Van Der Velden, V. H. J. *et al.* Targeting of the CD33-calicheamicin immunoconjugate Mylotarg (CMA-676) in acute myeloid leukemia: In vivo and in vitro saturation and internalization by leukemic and normal myeloid cells. *Blood* 97, 3197–3204 (2001).
11. Younes, A. *et al.* Brentuximab vedotin (SGN-35) for relapsed CD30-positive lymphomas. *N. Engl. J. Med.* 363, 1812–1821 (2010).
12. Verma, S. *et al.* Trastuzumab emtansine for HER2-positive advanced breast cancer. *N. Engl. J. Med.* 367, 1783–91 (2012).
13. Diamantis, N. & Banerji, U. Antibody-drug conjugates—an emerging class of cancer treatment. *Br. J. Cancer* 114, 362–367 (2016).
14. Vidarsson, G., Dekkers, G. & Rispens, T. IgG subclasses and allotypes: From structure to effector functions. *Front. Immunol.* 5, 1–17 (2014).
15. Wang, W., Singh, S., Zeng, D. L., King, K. & Nema, S. Antibody structure, instability, and

- formulation. *Journal of Pharmaceutical Sciences* 96, 1–26 (2007).
16. Lobo, E. D., Hansen, R. J. & Balthasar, J. P. Antibody pharmacokinetics and pharmacodynamics. *J. Pharm. Sci.* 93, 2645–2668 (2004).
 17. Natsume, A., Niwa, R. & Satoh, M. Improving effector functions of antibodies for cancer treatment: Enhancing ADCC and CDC. *Drug Des. Devel. Ther.* 3, 7–16 (2009).
 18. Shakib, F. & Stanworth, D. R. Human IgG subclasses in health and disease. (A review). Part I. *Ric. Clin. Lab.* 10, 463–479
 19. Stiehm, E. R. & Fudenberg, H. H. Serum levels of immune globulin in health and disease: a survey. *Pediatrics*, Vol 37, No 5, Part I (1966).
 20. Weir, A. N. *et al.* Formatting antibody fragments to mediate specific therapeutic functions. *Biochem. Soc. Trans.* 30, 512–516 (2002).
 21. Moore, G. L., Chen, H., Karki, S. & Lazar, G. A. Engineered Fc variant antibodies with enhanced ability to recruit complement and mediate effector functions. *MAbs* 2, 181–189 (2010).
 22. Gelderman, K. A., Tomlinson, S., Ross, G. D. & Gorter, A. Complement function in mAb-mediated cancer immunotherapy. *Trends Immunol.* 25, 158–164 (2004).
 23. Peters, C. & Brown, S. Antibody-drug conjugates as novel anti-cancer chemotherapeutics. *Biosci. Rep.* 35, e00225 (2015).
 24. Köhler, G. & Milstein, C. Continuous cultures of fused cells secreting antibody of predefined specificity. *Nature* 256, 495–497 (1975).
 25. Brekke, O. H. & Sandlie, I. Therapeutic antibodies for human diseases at the dawn of the twenty-first century. *Nat. Rev. Drug Discov.* 2, 52–62 (2003).
 26. Van Wauwe, J. P., De May, J. R. & Goossens, J. G. OKT3 : a monoclonal anti-human T lymphocyte antibody with potent mitogenic properties. *J. Immunol.* 124, 2708-2013.
 27. Morrison, S. L., Johnson, M. J., Herzenberg, L. A. & Oi, V. T. Chimeric human antibody molecules: mouse antigen-binding domains with human constant region domains. *Proc. Natl. Acad. Sci. U. S. A.* 81, 6851–6855 (1984).
 28. Green, L. L. Antibody engineering via genetic engineering of the mouse: XenoMouse strains are a vehicle for the facile generation of therapeutic human monoclonal antibodies. *J. Immunol. Methods* 231, 11–23 (1999).
 29. Fujimori, K., Covell, D. G., Fletcher, J. E. & Weinstein, J. N. A modeling analysis of monoclonal antibody percolation through tumors: a binding-site barrier. *J. Nucl. Med.* 31, 1191–1198 (1990).
 30. Ackerman, M. E., Pawlowski, D. & Wittrup, K. D. Effect of antigen turnover rate and expression level on antibody penetration into tumor spheroids. *Mol. Cancer Ther.* 7,

References

- 2233–2240 (2008).
31. Owen, S. C. *et al.* Targeting HER2 + breast cancer cells: Lysosomal accumulation of anti-HER2 antibodies is influenced by antibody binding site and conjugation to polymeric nanoparticles. *J. Control. Release* 172, 395–404 (2013).
 32. Kovtun, Y. V. *et al.* Antibody-drug conjugates designed to eradicate tumors with homogeneous and heterogeneous expression of the target antigen. *Cancer Res.* 66, 3214–3221 (2006).
 33. Junttila, T. T., Li, G., Parsons, K., Phillips, G. L. & Sliwkowski, M. X. Trastuzumab-DM1 (T-DM1) retains all the mechanisms of action of trastuzumab and efficiently inhibits growth of lapatinib insensitive breast cancer. *Breast Cancer Res. Treat.* 128, 347–356 (2011).
 34. McDonagh, C. F. *et al.* Engineered anti-CD70 antibody-drug conjugate with increased therapeutic index. *Mol. Cancer Ther.* 7, 2913–2923 (2008).
 35. Schroff, R. W. *et al.* Human anti-murine immunoglobulin responses in patients receiving monoclonal antibody therapy. *Cancer Res.* 45, 879–885 (1985).
 36. Scott, A. M., Wolchok, J. D. & Old, L. J. Antibody therapy of cancer. *Nat. Rev.* 12, 278–287 (2012).
 37. Teicher, B. A. & Chari, R. V. J. Antibody conjugate therapeutics: Challenges and potential. *Clin. Cancer Res.* 17, 6389–6397 (2011).
 38. Doronina, S. O. *et al.* Development of potent monoclonal antibody auristatin conjugates for cancer therapy. *Nat. Biotech.* 21, 778–784 (2003).
 39. Chari, R. V. J. *et al.* Immunoconjugates containing novel maytansinoids: promising anticancer drugs. *Cancer Res.* 52, 127–131 (1992).
 40. Hinman, L. M. *et al.* Preparation and characterization of monoclonal antibody conjugates of the calicheamicins: a novel and potent family of antitumor antibiotics. *Cancer Res.* 53, 3336–3342 (1993).
 41. Hamblett, K. J. *et al.* Effects of drug loading on the antitumor activity of a monoclonal antibody drug conjugate. *Cancer Res.* 10, 7063–7070 (2004).
 42. Bakhtiar, R. Antibody drug conjugates. *Biotechnol. Lett.* 38, 1655–1664 (2016).
 43. Adem, Y. T. *et al.* Auristatin antibody drug conjugate physical instability and the role of drug payload. *Bioconjug. Chem.* 25, 656–664 (2014).
 44. Polakis, P. Antibody Drug Conjugates for Cancer Therapy. *Pharmacol. Rev.* 68, 3–19 (2016).
 45. Ducry, L. & Stump, B. Antibody-drug conjugates: linking cytotoxic payloads to monoclonal antibodies. *Bioconjug Chem.* 21, 5–13 (2010).

46. Dubowchik, G. M. & Firestone, R. A. Cathepsin B-sensitive dipeptide prodrugs. 1. A model study of structural requirements for efficient release of doxorubicin. *Bioorg. Med. Chem. Lett.* 8, 3341–3346 (1998).
47. Saito, G., Swanson, J. A. & Lee, K. D. Drug delivery strategy utilizing conjugation via reversible disulfide linkages: Role and site of cellular reducing activities. *Adv. Drug Deliv. Rev.* 55, 199–215 (2003).
48. Hamilton, G. S. Antibody-drug conjugates for cancer therapy: The technological and regulatory challenges of developing drug-biologic hybrids. *Biologicals.* 43, 318–332 (2015).
49. Lambert, J. M. & Chari, R. V. J. Ado-trastuzumab Emtansine (T-DM1): an antibody-drug conjugate (ADC) for HER2-positive breast cancer. *J. Med. Chem.* 57, 6949–6964 (2014).
50. Mueller, B. M., Wrasidlo, W. A. & Reisfeld, R. A. Determination of the number of e-amino groups available for conjugation of effector molecules to monoclonal antibodies. *Hybridoma* 7, 453–456 (1988).
51. Shen, B. Q. *et al.* Conjugation site modulates the in vivo stability and therapeutic activity of antibody-drug conjugates. *Nat. Biotechnol.* 30, 184–189 (2012).
52. Tian, F. *et al.* A general approach to site-specific antibody drug conjugates. *Proc. Natl. Acad. Sci. U. S. A.* 111, 1766–71 (2014).
53. Zimmerman, E. S. *et al.* Production of site-specific antibody–drug conjugates using optimized non-natural amino acids in a cell-free expression system. *Bioconjug. Chem.* 25, 351–361 (2014).
54. Sochaj, A. M., Świdorska, K. W. & Otlewski, J. Current methods for the synthesis of homogeneous antibody-drug conjugates. *Biotechnol. Adv.* 33, 775–784 (2015).
55. Junutula, J. R. J. R. *et al.* Site-specific conjugation of a cytotoxic drug to an antibody improves the therapeutic index. *Nat. Biotechnol.* 26, 925–32 (2008).
56. McDonagh, C. F. *et al.* Engineered antibody-drug conjugates with defined sites and stoichiometries of drug attachment. *Protein Eng. Des. Sel.* 19, 299–307 (2006).
57. Jeger, S. *et al.* Site-specific and stoichiometric modification of antibodies by bacterial transglutaminase. *Angew. Chemie - Int. Ed.* 49, 9995–9997 (2010).
58. Strop, P. *et al.* Location matters: Site of conjugation modulates stability and pharmacokinetics of antibody drug conjugates. *Chem. Biol.* 20, 161–167 (2013).
59. Madej, M. P. *et al.* Engineering of an anti-epidermal growth factor receptor antibody to single chain format and labeling by sortase A-mediated protein ligation. *Biotechnol. Bioeng.* 109, 1461–1470 (2012).
60. Drake, P. M. *et al.* Aldehyde tag coupled with HIPS chemistry enables the production of

References

- ADCs conjugated site-specifically to different antibody regions with distinct in vivo efficacy and PK outcomes. *Bioconjug. Chem.* 25, 1331–1341 (2014).
61. Qasba, P. K. Glycans of antibodies as a specific site for drug conjugation using glycosyltransferases. *Bioconjug. Chem.* 26, 2170–2175 (2015).
 62. Boeggeman, E. *et al.* Site specific conjugation of fluoroprobes to the remodeled Fc N-glycans of monoclonal antibodies using mutant glycosyltransferases: Application for cell surface antigen detection. *Bioconjug. Chem.* 20, 1228–1236 (2009).
 63. Lin, K. & Tibbitts, J. Pharmacokinetic considerations for antibody drug conjugates. *Pharm. Res.* 29, 2354–2366 (2012).
 64. Dudley, A. C. Tumor Endothelial Cells. *Cold Spring Harb Perspect Med.* 2, a006536 (2012)
 65. Henderson, L. A., Baynes, J. W. & Thorpe, S. R. Identification of the sites of IgG catabolism in the rat. *Arch. Biochem. Biophys.* 215, 1–11 (1982).
 66. Levêque, D., Wisniewski, S. & Jehl, F. Pharmacokinetics of therapeutic monoclonal antibodies used in oncology. *Anticancer Res.* 25, 2327–2343 (2005).
 67. Roopenian, D. C. & Akilesh, S. FcRn: the neonatal Fc receptor comes of age. *Nat. Rev. Immunol.* 7, 715–25 (2007).
 68. Keizer, R., Huitema, A., Schellens, J. & Beijnen, J. Clinical pharmacokinetics of therapeutic monoclonal antibodies. *Clin Pharmacokinet* 49, 493–507 (2010).
 69. Loganzo, F., Sung, M. & Gerber, H.P. Mechanisms of resistance to antibody-drug conjugates. *Mol. Cancer Ther.* 15, 2825-2834 (2016).
 70. Bross, P. F. *et al.* Approval summary: gemtuzumab ozogamicin in relapsed acute myeloid leukemia. *Clin Cancer Res* 7, 1490–6 (2001).
 71. Tsimberidou, A. M. *et al.* The role of gemtuzumab ozogamicin in acute leukaemia therapy. *Br. J. Haematol.* 132, 398–409 (2006).
 72. Lo Coco, F., Ammatuna, E. & Noguera, N. Treatment of acute promyelocytic leukemia with gemtuzumab ozogamicin. *Clin. Adv. Hematol. Oncol.* 4, 57–77 (2006).
 73. Deng, C., Pan, B. & O'Connor, O. A. Brentuximab Vedotin. *Clin. Cancer Res.* 19, 22–27 (2013).
 74. Senter, P. D. & Sievers, E. L. The discovery and development of brentuximab vedotin for use in relapsed Hodgkin lymphoma and systemic anaplastic large cell lymphoma. *Nat. Biotechnol.* 30, 631–637 (2012).
 75. De Claro, R. A. *et al.* U.S. Food and Drug Administration approval summary: Brentuximab vedotin for the treatment of relapsed Hodgkin lymphoma or relapsed systemic anaplastic large-cell lymphoma. *Clin. Cancer Res.* 18, 5845–5849 (2012).

76. Peddi, P. F. & Hurvitz, S. A. Ado-trastuzumab emtansine (T-DM1) in human epidermal growth factor receptor 2 (HER2)-positive metastatic breast cancer: latest evidence and clinical potential. *Ther. Adv. Med. Oncol.* 6, 202–9 (2014).
77. Denizli, A. Purification of Antibodies by Affinity Chromatography. *Hacettepe J. Biol. Chem.* 39, 18 (2011).
78. Akerstrom, B. & Bjorck, L. A physicochemical study of protein G, a molecule with unique immunoglobulin G-binding properties. *J. Biol. Chem.* 261, 10240–10247 (1986).
79. Lund, L. N. *et al.* Exploring variation in binding of Protein A and Protein G to immunoglobulin type G by isothermal titration calorimetry. *J. Mol. Recognit.* 24, 945–952 (2011).
80. Akerström, B., Nielsen, E. & Björck, L. Definition of IgG- and albumin-binding regions of streptococcal protein G. *J. Biol. Chem.* 262, 13388–13391 (1987).
81. Fahnstock, S. R., Alexander, P., Nagle, J. & Filpula, D. Gene for an immunoglobulin-binding protein from a group G streptococcus. *J. Bacteriol.* 167, 870–880 (1986).
82. Sjöbring, U., Björck, L. & Kastern, W. Streptococcal Protein G. *J. Biol. Chem.* 266, 399–405 (1991).
83. Olsson, A. *et al.* Structure and evolution of the repetitive gene encoding streptococcal protein G. *Eur. J. Biochem.* 168, 319–324 (1987).
84. Guss, B. *et al.* Structure of the IgG-binding regions of streptococcal protein G. *EMBO J.* 5, 1567–1575 (1986).
85. Akerstrom, B., Brodin, T., Reis, K. & Bjorck, L. Protein G : a powerful tool for binding and detection of monoclonal and polyclonal antibodies. *J. Immunol.* 135, 2589-2592 (1985).
86. Linhult, M., Binz, H. K., Uhlén, M. & Hober, S. Mutational analysis of the interaction between albumin-binding domain from streptococcal protein G and human serum albumin. *Protein Sci.* 11, 206–213 (2002).
87. Sauer-Eriksson, A. E., Kleywegt, G. J., Uhlén, M. & Jones, T. A. Crystal structure of the C2 fragment of streptococcal protein G in complex with the Fc domain of human IgG. *Structure.* 3, 265–278 (1995).
88. Gallagher, T., Alexander, P., Bryan, P. & Gilliland, G. L. Two crystal structures of the B1 immunoglobulin-binding domain of streptococcal protein G and comparison with NMR. *Biochemistry.* 33, 4721–4729 (1994).
89. Achari, A. *et al.* 1.67 Å X-ray structure of the B2 immunoglobulin-binding domain of streptococcal protein G and comparison to the NMR structure of the B1 domain. *Biochemistry.* 31, 10449–10457 (1992).
90. Gronenborn, A. M., Clore, M. G. & Clore, G. M. Identification of the contact surface of a

References

- streptococcal protein G domain complexed with a human Fc Fragment. *J. Mol. Biol.* 233, 331–335 (1993).
91. Lian, L. Y. *et al.* Sequential ^1H NMR assignments and secondary structure of an IgG-binding domain from protein G. *Biochemistry.* 30, 5335–5340 (1991).
 92. Derrick, J. P. & Wigley, D. B. Crystal structure of a streptococcal protein G domain bound to an Fab fragment. *Nature.* 359, 752–754 (1992).
 93. Micusan, V. V & Borduas, A. G. Biological properties of goat immunoglobulins G. *Immunology.* 32, 373–381 (1977).
 94. Strausbauch, P. H., Hurwitz, E. & Givol, D. Interchain disulfide bonds of goat immunoglobulin G. *Biochemistry.* 10, 2231–7 (1971).
 95. O'Donnell, I. J., Frangione, B. & Porter, R. R. The disulphide bonds of the heavy chain of rabbit immunoglobulin G. *Biochem. J.* 116, 261–268 (1970).
 96. Covell, D. G. *et al.* Pharmacokinetics of monoclonal immunoglobulin G1, F(ab')₂, and Fab' in mice. *Cancer Res.* 46, 3969–3978 (1986).
 97. Chapman, A. P. PEGylated antibodies and antibody fragments for improved therapy: A review. *Adv. Drug Deliv. Rev.* 54, 531–545 (2002).
 98. Chapman, A. P. *et al.* Therapeutic antibody fragments with prolonged in vivo half-lives. *Nat. Biotechnol.* 17, 780–783 (1999).
 99. Kitamura, K. *et al.* Chemical engineering of the monoclonal antibody A7 by polyethylene glycol for targeting cancer chemotherapy. *Cancer Res.* 51, 4310–4315 (1991).
 100. Humphreys, D. P. *et al.* Alternative antibody Fab fragment PEGylation strategies: Combination of strong reducing agents, disruption of the interchain disulphide bond and disulphide engineering. *Protein Eng. Des. Sel.* 20, 227–234 (2007).
 101. Schlesselman, L. S. Certolizumab pegol. *Formulary* 43, 22–28 (2008).
 102. Bourne, T., Fossati, G. & Nesbitt, A. A PEGylated Fab' fragment against tumor necrosis factor for the treatment of Crohn disease: exploring a new mechanism of action. *BioDrugs* 22, 331–337 (2008).
 103. Andrew, S. M. & Titus, J. A. Fragmentation of immunoglobulin G. *Curr. Protoc. Immunol.* Unit 2.8, Chapter 2 (2001).
 104. Crivianu-Gaita, V., Romaschin, A. & Thompson, M. High efficiency reduction capability for the formation of Fab' antibody fragments from F(ab)₂ units. *Biochem. Biophys. Reports* 2, 23–28 (2015).
 105. Roberts, M. J., Bentley, M. D. & Harris, J. M. Chemistry for peptide and protein PEGylation. *Adv. Drug Deliv. Rev.* 64, 116–127 (2012).
 106. Harris, J. M. Poly(ethylene glycol) chemistry Biotechnical and Biomedical Applications.

- Journal of Chemical Information and Modeling*. 53, (1992).
107. Knop, K., Hoogenboom, R., Fischer, D. & Schubert, U. S. Poly(ethylene glycol) in drug delivery: Pros and cons as well as potential alternatives. *Angew. Chemie - Int. Ed.* 49, 6288–6308 (2010).
 108. Abuchowski, A., Mccoy, J. R., Palczuk, N. C., Van Es, T. & Davis, F. F. Effect of Covalent Attachment of Polyethylene Glycol on Immunogenicity and Circulating Life of Bovine Liver Catalase. *J. Biol. Chem.* 252, 3582–3586 (1976).
 109. Abuchowski, A., Es, T. V., Palczuk, N. C. & Davis, F. F. Alteration of immunological properties of bovine serum albumin by covalent attachment of poly(ethylene glycol). *J. Control. Rel.* 252, 3578–3581 (1977).
 110. Pasut, G. & Veronese, F. M. Polymer-drug conjugation, recent achievements and general strategies. *Prog. Polym. Sci.* 32, 933–961 (2007).
 111. Dozier, J. K. & Distefano, M. D. Site-specific pegylation of therapeutic proteins. *Int. J. Mol. Sci.* 16, 25831–25864 (2015).
 112. Verhoef, J. J. F., Carpenter, J. F., Anchordoquy, T. J. & Schellekens, H. Potential induction of anti-PEG antibodies and complement activation toward PEGylated therapeutics. *Drug Discov. Today* 19, 1945–1952 (2014).
 113. Pasut, G. & Veronese, F. M. State of the art in PEGylation: The great versatility achieved after forty years of research. *J. Control. Release* 161, 461–472 (2012).
 114. Veronese, F. M. & Pasut, G. PEGylation, successful approach to drug delivery. *Drug Discov. Today* 10, 1451–1458 (2005).
 115. Kinstler, O., Molineux, G., Treuheit, M., Ladd, D. & Gegg, C. Mono-N-terminal poly(ethylene glycol)-protein conjugates. *Adv. Drug Deliv. Rev.* 54, 477–485 (2002).
 116. Baldwin, A. D. & Kiick, K. L. Tunable degradation of maleimide-Thiol adducts in reducing environments. *Bioconjug. Chem.* 22, 1946–1953 (2011).
 117. Sasse, F. *et al.* Tubulysins, new cytostatic peptides from myxobacteria acting on microtubuli. Production, isolation, physico-chemical and biological properties. *J. Antibiot. (Tokyo)*. 53, 879–885 (2000).
 118. Steinmetz, H. *et al.* Isolation, crystal and solution structure determination, and biosynthesis of tubulysins - Powerful inhibitors of tubulin polymerization from myxobacteria. *Angew. Chemie - Int. Ed.* 43, 4888–4892 (2004).
 119. Bai, R., Petit, G. R. & Hamel, E. Dolastatin 10, a powerful cytostatic peptide derived from a marine animal. *Biochem. Pharmacol.* 39, 1941–1949 (1990).
 120. Khalil, M. W., Sasse, F., Lünsdorf, H., Elnakady, Y. A. & Reichenbach, H. Mechanism of action of tubulysin, an antimetabolic peptide from myxobacteria. *ChemBioChem.* 7, 678–

References

- 683 (2006).
121. Kaur, G. *et al.* Biological evaluation of tubulysin A: a potential anticancer and antiangiogenic natural product. *Biochem. J.* 396, 235–242 (2006).
 122. Cohen, R. *et al.* Development of novel ADCs: Conjugation of tubulysin analogues to trastuzumab monitored by dual radiolabeling. *Cancer Res.* 74, 5700–5710 (2014).
 123. Nathan Tumej, L. *et al.* Optimization of tubulysin antibody-drug conjugates: a case study in addressing ADC metabolism. *ACS Med. Chem. Lett.* 7, 977–982 (2016).
 124. Leverett, C. A. *et al.* Design, synthesis, and cytotoxic evaluation of novel tubulysin analogs as ADC payloads. *ACS Med. Chem. Lett.* 7, 999–1004 (2016).
 125. Saito, G., Swanson, J. A. & Lee, K. Drug delivery strategy utilizing conjugation via reversible disulfide linkages role and site of cellular reducing activities. *Adv. Drug Deliv. Rev.* 55, 199–215 (2003).
 126. Feener, E. P., Shen, W. C. & Ryser, H. J. P. Cleavage of disulfide bonds in endocytosed macromolecules. A processing not associated with lysosomes or endosomes. *J. Biol. Chem.* 265, 18780–18785 (1990).
 127. Pillay, C. S., Elliott, E. & Dennison, C. Endolysosomal proteolysis and its regulation. *Biochem. J.* 363, 417–429 (2002).
 128. Hudis, C. A. Trastuzumab — Mechanism of Action and Use in Clinical Practice. *N. Engl. J. Med.* 357, 39–51 (2007).
 129. Goldenberg, M. M. Trastuzumab, a recombinant DNA-derived humanised monoclonal antibody, a novel agent for the treatment of metastatic breast cancer. *Clin. Ther.* 21, 309–18 (1999).
 130. Brennan, P. J., Kumogai, T., Berezov, A., Murali, R. & Greene, M. I. HER2/Neu: mechanisms of dimerization/oligomerization. *Oncogene.* 19, 6093–6101 (2000).
 131. Rubin, I. & Yarden, Y. The basic biology of Her2. *Ann. Oncol.* 17, 15–23 (2006).
 132. Valabrega, G., Montemurro, F. & Aglietta, M. Trastuzumab: Mechanism of action, resistance and future perspectives in HER2-overexpressing breast cancer. *Ann. Oncol.* 18, 977–984 (2007).
 133. Nahta, R. & Esteva, F. J. HER2 therapy: molecular mechanisms of trastuzumab resistance. *Breast Cancer Res.* 8, 215 (2006).
 134. Leyland-Jones, B. Trastuzumab: Hopes and realities. *Lancet Oncol.* 3, 137–144 (2002).
 135. Maloney, D. G. *et al.* IDEC-C2B8 (Rituximab) anti-CD20 monoclonal antibody therapy in patients with relapsed low-grade non-Hodgkin's lymphoma. *Blood.* 90, 2188–2195 (2013).
 136. Cheson, B. D. & Leonard, J. P. Monoclonal antibody therapy for B-Cell non-Hodgkin's

- lymphoma. *N. Engl. J. Med.* 359, 613–626 (2008).
137. Pescovitz, M. D. Rituximab, an anti-CD20 monoclonal antibody: History and mechanism of action. *Am. J. Transplant.* 6, 859–866 (2006).
 138. Smith, M. R. Rituximab (monoclonal anti-CD20 antibody): mechanisms of action and resistance. *Oncogene* 22, 7359–7368 (2003).
 139. Teeling, J. L. *et al.* The biological activity of human CD20 monoclonal antibodies is linked to unique epitopes on CD20. *J. Immunol.* 177, 362–71 (2006).
 140. Ding, B., Dziubla, T., Shuvaev, V. V, Muro, S. & Muzykantov, V. R. Advanced drug delivery systems that target the vascular endothelium. *Mol. Interv.* 6, 98–112 (2006).
 141. Rothlein, R., Dustin, M. L., Marlin, S. D. & Springer, T. A. A human intercellular adhesion molecule (ICAM-1) distinct from LFA-1. *J. Immunol.* 137, 1270–1274 (1986).
 142. Hubbard, A. K. & Rothlein, R. Intercellular adhesion molecule-1 (ICAM-1) expression and cell signaling cascades. *Free Radic. Biol. Med.* 28, 1379–1386 (2000).
 143. Carpén, O., Pallai, P., Staunton, D. E. & Springer, T. A. Association of intercellular adhesion molecule-1 (ICAM-1) with actin-containing cytoskeleton and alpha-actinin. *J. Cell Biol.* 118, 1223–34 (1992).
 144. Muro, S. *et al.* A novel endocytic pathway induced by clustering endothelial ICAM-1 or PECAM-1. *J. Cell Sci.* 116, 1599–1609 (2003).
 145. Snyder, S. L. & Sobocinski, P. Z. An improved 2,4,6-trinitrobenzenesulfonic acid method for the determination of amines. *Anal. Biochem.* 64, 284–288 (1975).
 146. Carlsson, J., Drevin, H. & Axén, R. Protein thiolation and reversible protein-protein conjugation. N-Succinimidyl 3-(2-pyridyldithio)propionate, a new heterobifunctional reagent. *Biochem. J.* 173, 723–737 (1978).
 147. Laemmli, U. K. (1970): Cleavage of structural proteins during assembly of head of bacteriophage-T4. *Nature* 227, 680–685 (1970).
 148. Tetin, S. Y., Prendergast, F. G. & Venyaminov, S. Y. Accuracy of protein secondary structure determination from circular dichroism spectra based on immunoglobulin examples. *Anal. Biochem.* 321, 183–187 (2003).
 149. Vermeer, A. W. P., Bremer, M. G. E. G. & Norde, W. Structural changes of IgG induced by heat treatment and by adsorption onto a hydrophobic Te £ on surface studied by circular dichroism spectroscopy. *Biochim Biophys Acta* 1425, 1–12 (1998).